Understanding flow of solids in continuous flow reactors

Thesis Submitted to AcSIR For the Award of
the Degree of
DOCTOR OF PHILOSOPHY
In Engineering Sciences

By
Sayan Pal
20EE13A26044

Under the guidance of
Dr. Amol Kulkarni (Supervisor)

CSIR-National Chemical Laboratory (CSIR-NCL),
Pune 411008
India

July 2019

Abstract

In the last two decades, microfluidic technology has witnessed prolific growth in the areas of chemistry, material science, biology and even point of care diagnostics. Narrow residence time distribution, enhanced transport process, consistent product yield, and inherent safety are considered as the main drivers of microreactor technology. In order to utilize its full potential, it's essential to address a few challenges and handling solids is considered one of the significant barriers.

The objective of this dissertation is to understand the clogging dynamics in multiphase microfluidics and to develop passive particle handling techniques with the special focus on antisolvent precipitation and synthesis of micro particles.

Determination of clogging time is the principal theme of investigation of clogging dynamics in multiphase flow. This includes effects of important multiphase flow parameters such as flow regimes, flow rates, coalescence and vortex formation for an antisolvent precipitation system. Passive techniques for delaying clogging such as inert phase insertion, wall wettability alteration and multipoint injection were proposed and compared quantitatively. Most efficient transport of particles was obtained with the addition of inert phases to the system, especially with inert liquid phases. Solid forming chemical reactions are also demonstrated utilizing the proposed techniques. To overcome the challenges in precipitation impinging jets reactors are explored in detail for continuous manufacturing in such systems in a scaled-up fashion.

CERTIFICATE

This is to certify that the work incorporated in this Ph.D. thesis entitled "***Understanding flow of solids in continuous flow reactors***" submitted by ***Mr. Sayan Pal*** to Academy of Scientific and Innovative Research (AcSIR) in fulfilment of the requirements for the award of the Degree of ***Doctor of Philosophy***, embodies original research work under my guidance. I further certify that this work has not been submitted to any other University or Institution in part or full for the award of any degree or diploma. Research material obtained from other sources has been duly acknowledged in the thesis. Any text, illustration, table etc., used in the thesis from other sources, have been duly cited and acknowledged.

It is also certified that this work done by the student, under my supervision, is plagiarism free.

(Student)
Mr. Sayan Pal
CEPD Division,
CSIR-NCL, Pune

Date : 29.07.2019

Place : Pune

(Supervisor)
Dr. Amol Kulkarni
Principal Scientist,
CEPD Division,
CSIR-NCL, Pune

Declaration by the Candidate

I hereby declare that the thesis entitled **"*Understanding flow of solids in continuous flow reactors*"** submitted by me for the Degree of Doctor of Philosophy to Academy of Scientific & Innovative Research (AcSIR) is the record of work carried out by me at Chemical Engineering and Process Development Division, CSIR-National Chemical Laboratory, Pune – 411008, India, under the supervision of **Dr. Amol Kulkarni**. The work is original and has not formed the basis for the award of any degree, diploma, associateship and fellowship titles in this or any other university or other institute of higher learning. I further declare that the material obtained from other resources has been duly acknowledged in the thesis.

Mr. Sayan Pal
Senior Research Fellow
Chemical Engineering and Process Development Division,
CSIR-National Chemical Laboratory,
Dr. Homi Bhabha Road, Pashan, Pune-411008, Maharashtra, India

Date: 29.07.2019
Place: Pune

Table of Contents

Chapter 5	

Chapter 6	

Acknowledgements

It gives me the deepest of pleasures to extend my warm and humble appreciation to all those who supported, guided and encouraged me in the testing time that is one's PhD tenure. Let it be known that the efforts of these individuals are no less than my own in the successful completion of this thesis.

First and foremost, I would like to take this opportunity to express my deepest sense of appreciation and reverence towards my research supervisor **Dr. Amol Kulkarni** for effortlessly guiding me throughout the course of my PhD, for always motivating and encouraging me and most of all for standing tall as an example to try and emulate throughout my time in NCL. While it is true that the bar he sets is high and I am truly aware of how short I fall when it comes to his expectations, I sincerely thank him for taking an interest in me, encouraging me to pursue the GATE-JRF Fellowship.

I would like to acknowledge the members of my Doctoral Advisory Committee (DAC) members, **Dr. Ashish Orpe**, **Dr. Sanjay Kamble** and **Dr. Kumar Vanka** for their sincere comments, suggestions and constant support. A special thanks to my teachers in NCL Dr. Rajnish Kumar, Dr. Chetan Gadgil, Dr. Mugdha Gadgil, Dr. Ashish Orpe, Dr. Vivek Ranade, Dr. Pankaj Doshi, Dr. Leelavati Narlikar and Dr. V. Ravikumar who once again exposed me to the wonderful subjects of Chemical Engineering.

I am grateful to **Dr. Sourav Pal, Dr. K. Vijayamohanan Pillai** and **Dr. Ashwini Kumar Nangia**, Directors, CSIR-NCL, Pune for allowing me to carry out my research work in India's most prestigious, well-equipped and biggest chemical laboratory. I am grateful for the GATE-JRF Research Fellowship provided by **CSIR-HRDG**. I am also thankful to the AcSIR coordination office, Student Academic office, PP-I workshop, and the various sections of NCL establishment for their continued support.

I find this an exceptional opportunity to acknowledge my parents, **Arun Kumar Paul** and **Sima Paul**. Thank you for your support and encouragement throughout the years, and for providing the basic foundations which have enabled my success. I am truly indebted.

I am indebted to many present and past colleagues at NCL : Mrityunjay, Dr. Gunwant, Dr. Yachita, Chinmay, Dr. Arun, Jaydeep, Shital, Chaitanya, Kristi, Ketan, Prachi, Roopashree, Rajashri, Dr. Atul, Ranjit, Mahesh, Dr. Brijesh, Joy, Suneha, Sheetal, Prabhav and Arshad for providing a stimulating and fun environment in which to learn and grow. I am grateful to my dear

friends Gaurav, Sayantan, Muzammil, Akshay, Deepanjan, Sanjay, Kundan, Sagar, Rajarshi and Eva for their constant encouragement and for always being there with me in my difficult times.

Sayan Pal

Chapter 1

Introduction

1. Introduction

1.1 Microreactors

1.1.1 Advantages and applications of microreactors

Microreactors are made of single or network of confined miniature channels with typical dimensions below 1 mm in which small volumes of fluids are precisely handled [1, 2]. Microreactor research in academia as well industrial environment over the past two decades have markedly changed synthesis approach in chemical industry over a wide range of reactions with increasingly sophisticated designs, and expanding integration levels [3, 4]. A sizable number of reactions was performed in microreactors, witnessing the benefits of controlled residence time, enhanced transport efficiency and mixing, precise reaction control, rapid chemical reactions, allowing for the high product yield, and inherent safety as well [2].

Continuous production of fine and speciality chemicals and active pharmaceutical ingredients (APIs) using microreactors has been investigated extensively for the past two decades [5, 6]. Such reactors are reported to be more beneficial for high value low volume chemicals involving exothermic reactions. Mass-transfer limited reactions are typically benefitted from the small characteristic dimensions of microreactors, because in such systems diffusive effects are significant with respect to the overall rate[4]. Small channel size (hydraulic diameter d_h) offers very high mixing, mass transfer and heat transfer area per unit volume ($a = 4/d_h$), which further helps in efficient heat transfer. A comparison of conventional reactors and microchannels presented in the following table shows the efficiency of the later in terms of mass transfer coefficient and available interfacial area.

Table 1.1. Comparison of mass transfer coefficients and interfacial area in microchannels and conventional reactors [7-11].

Reactor	K_La (s^{-1})	Interfacial Area ($m^2 m^{-3}$)
Packed Bed	0.0034 – 0.005	80-450
Bubble Column Reactor	0.005 – 0.1	5-120
Agitated liquid-liquid Contactor	0.048 – 0.083	32 - 311
Stirred Slurry Reactors	0.02-0.8	25-2000
Two – Impinging Jet Reactor	0.28	1000-3400
Couette–Taylor–Poiseuille flow (CTPF) reactor	0.03-0.45	700-1200
Capillary Microreactor (1 mm)	0.88 - 1.29	830 - 2480
Capillary Microreactor (0.5 mm)	0.90-1.67	1600-3200
Square Microchannel (0.21 mm)	1.61- 8.44	6090-13400

Despite the characteristic high interfacial area in the microchannels, they operate in low Reynolds number regimes (0.1-10), implying the lack of turbulent mixing. Hence the mixing is mainly dependent on molecular interdiffusion which is an inherently slow process. The requirement to enhance the mixing efficiency driven the research on microfluidic mixing schemes [12]. The advantages in terms of mixing efficiency of static mixers over the stirred tank for continuous flow processes have been studied and reviewed by Bayer et al.[13] and Thakur et al.[14] in the early 2000s. Micromixers are developed following the same principle of the static mixers which is to redistribute the fluid in the directions transverse to the main flow, but for enhancing mixing in channels of 10^{-1} to 10^{-3} times smaller length scales. During the last two decades, several review papers [12, 15-19] were published on microfluidic mixing, and close to a hundred new active and passive micromixers were demonstrated for wide varieties of applications. The passive micromixers rely solely on pumping energy and

manipulation of the flow to intertwine the reactants efficiently such as Y-type, T-type, flow focusing, meander-like or serpentine geometries, flow obstacles within micro channels, multi-laminating, split and recombine, chaotic, colliding jet, recirculation flow-mixers. The active micromixers use some form of external energy to achieve mixing. Such examples are periodic variation of flowrate, electrokinetic time pulsed and instability, dielectrophoretic techniques, acoustic fluid shaking, ultrasound, electrowetting-based droplet shaking, electrohydrodynamic force, magneto hydrodynamic flow based techniques, microstirring particles etc. [12, 15].

The excellent heat and mass transfer performance achieved in microreactors allows reactions to be carried out under more aggressive conditions in comparison to conventional batch reactors. From the safety point of view, while performing a potentially hazardous reaction or handling hazardous chemicals, the lesser quantity of accidental chemical release could be easily contained in case of a reactor failure [3, 5]. In microfluidic reactors, the degree of control over local conditions is such that it is often possible to select one product over another with high precision which results in enhanced selectivity [4].

Due to the several aforementioned advantages, microreactors has developed great appeal among synthetic chemists and from the convergence between the organic chemistry, and chemical engineering communities gave birth to "Flow Chemistry" community. Roberge et al. presented how the shift from batch to continuous microreactors can be economically beneficial by means of CAPEX and OPEX analysis [20]. Recently, Jensen et al. [21] have reviewed the environmental and green chemistry benefits accrued by implementation of microreactor based intensified continuous manufacturing devices.

A significant number of important chemical transformations entail varieties of multiphase systems inherently such as gas−liquid, gas−liquid−liquid, liquid−liquid, or solid−liquid−gas etc. Efficient phase mixing by means of more intimate surface contact

between the different phases is necessary for optimum functioning of the microreactor. The usage of microreactors for multiphase processes offers a lucid superiority over conventional methods (such as batch reactors, sparged reactors or stirred vessels) ascribed to the monumental increase in specific interfacial area. Moreover, this also contributes to superior mass as well as heat transfer achieved in the system. Different geometric distribution of the phases inside the microchannels based on the channel, flow properties and flow ratio of the phases resulted in a number of multiphase flow regimes such as bubble, droplet, slug, parallel and annular flow regimes (See fig. 1.1) [22] [4]. Typical channel diameters (0.88− 1.90 mm I.D.) featured in this thesis manifest slug flow regime in particular.

Flow Regimes	Schematic
Slug Flow	
Droplet Flow	
Annular Flow	
Parallel Flow	

Fig. 1.1. Schematic of various flow regimes observed in capillaries

Aside from advancements in intensified single-phase flow chemistry, the sheer appeal of the small sized lab on a chip diagnostic devices, and perfectly spaced uniform sized droplets/ slugs in microchannels was undoubtedly a driving factor in the development of microfluidics. The polydispersity of the droplet size defined as the standard deviation of the size distribution divided by the mean size of the droplet is reported to be as little as 1–3% in high throughputs (up to 100 KHz). The droplets or fluid segments in a microfluidics system can be seen as an

isolated reactor, with low consumption of samples and reagents, minimal dispersion and flexible control [23]. Different hydrodynamic and external force driven droplet manipulation techniques were developed to control the local flow field and the detachment dynamics of individual droplets [24, 25]. The control over microchannel flows enhanced the handling of liquids for the applications-oriented at in materials science as well as biology in addition to chemistry [26, 27].

Certain properties of microfluidic technologies, such as precise manipulation of fluids in a microreactor, rapid sample processing could be applied to biological research for streamlining complex assay protocols, substantial reduction of sample volumes resulting in a reduction of reagent costs and maximized data obtained from precious samples. In recent years microfluidics has gradually become an attractive candidate to replace traditional experimental approaches. Sackman et al. [28] extensively reviewed the use of microfluidic innovations in conventional biomedical research to assess their impact beyond the engineering community in the last decade. Though its been roughly two decades since the inception of microfluidics, and the vast majority of microfluidics research publications still published in engineering journals (85%), a 50 % increase was observed in the share of published microfluidics research in biology and medicine journals [28]. Increasing collaboration between the communities of microfluidics, life sciences, analytics, and bioprocess engineering have seen significant implementation of microfluidics in enzymatic microreactors, manipulation of blood samples for biology research (Haematology and Immunology), cell biology, protein crystallization, applied biocatalysis, bioprocess intensification and integration within microflow systems, diagnostics and assay applications in μ - Total analysis system (μTAS) or Lab on Chip (LoC) devices [28-31].

Despite considerable advancement in synthesis techniques in conventional batch reactors in the past two decades, enhanced control over the nucleation and growth of micro and nanoparticles still remains an immense challenge in the field of materials science [32] . In response to this challenge, microfluidics-based flow synthesis enables the particles to form in a controllable, sustainable, and cost-saving manner with the assistance of selected solvents, ligands, and surfactants which is appealing to industry [33, 34]. In addition to the general benefits of microreactors discussed previously, multiphase flow (droplet or segmented flow) in microreactors provides some unique aspects in particle synthesis. The dispersed liquid compartments (slugs/droplets) are isolated by the continuous phase; they can act as symmetric and individual reactors of size comparable to the reactor length-scale. This feature of droplet microfluidics helps in significantly reducing the unwanted effect of axial dispersion and providing narrow residence time distribution resulting in increased the mono-dispersity of the micro/nano particles [35] . The basic aspects for controlled nucleation and homogeneous particle growth under microflow conditions are mainly compartmentation of a liquid, decoupling between reaction solution and channel wall, and enhanced radial mass and heat transfer by flow-induced internal convection [36]. Based in different systems and flow manipulation, particles can be synthesized in one of three locations - inside dispersed phase droplets/slugs, in continuous-phase or at the interface between the phases [35]. Recent progress in flow synthesis of varieties of organic, inorganic micro/ nano particles was comprehensively reviewed by several authors with specific properties and their practical applications [32-34, 37].

In the early stages of microreactors, glass, ceramic or stainless steel were usually used as the material of construction, but they suffered from high production cost and incapable of fabricating complex geometries with flexibility. With time, inexpensive tube reactors based on perfluorinated polymers like PTFE, PFA etc. became more popular with the flow chemistry

community [38]. With the evolution of the field, the different technologies were invented to fabricate complex microreactor geometries. Various microreactor designs were fabricated using soft lithography as introduced by Whitesides in 1998 [39]. The lithographic methods required complex steps and skilful hands and based on photoresists and polydimethylsiloxane (PDMS) [40]. Moreover, the lithographic methods are usually performed in a clean-room environment, which needs a lot of capital and maintenance costs [41]. A wide range of techniques for fabricating submillimeter size channels aside from soft lithography has been developed for various reasons, including decreased cost, faster turnaround time as well as increased functionality. These developments have allowed microfluidic devices to be fabricated using cheaper and robust materials of construction and geometries, enabling new and advantageous physical behaviours and qualities in microfluidic devices. Gale et al. [42] and Ko et al. [40] have reviewed the recent developments in key microreactor fabrication techniques like hot embossing, molding approaches, polymer laminates and 3D printing. Finally, the chemical compatibility of the material of construction (MOC) with the substrate and reproducibility of the fabrication techniques are the two most important aspects of microreactor fabrication.

1.1.2 Solids in microreactors

Although these features are exciting and every year the number of new examples of flow syntheses are increasing exponentially, the micro and mini fluidic reactors are notably not well suited to handle the processes where the product or byproduct or an intermediate is solid. Primary reasons for considering flow of suspension in small channels are: small channel sizes, large area per unit volume available for deposition of solids and the laminar flow of liquid that may not impose sufficient convective force on (lighter or heavier) particles, are among the most important reasons that limit handling of suspension in small channels. Such a situation usually results in partial or complete clogging of channels by the particles generated during reactions

or due to varying solubility of the reaction mixture from the inlet of the reactor to its outlet. Regions close to back pressure regulators, and sharp turnings in microchannels are heavily susceptible to solid build-up and clogging [43]. In the field of organic synthesis, an abundance of pharmaceutically and industrially relevant chemical reactions entail inorganic crystalline salt formation in stoichiometric amounts [44]. A few such examples include Pd-catalyzed amination, Grignard reactions, Heck reactions, acylations, arylations, and alkylations using acyl, aryl, and alkyl halides, aromatic nitrations, catalytic hydrogenation, diazotization, benzoylation, Nef oxidation, polymerization reactions etc. [45, 46]. In addition to these, clogging issues are also encountered in continuous precipitation and crystallization processes which is a core technology for purification, separation, and control of APIs and other specialty chemicals while performed in microreactors [47, 48]. Many of these processes involve more than one phase, and in several cases the reactions are instantaneous, and they generate solids at the interface. The need to avoid solids is perhaps the most significant weakness of microreactor technology and a big obstacle in its widespread adoption. Roberge et al. [20] studied 86 different reactions at Lonza, a leading chemical manufacturing company in 2005 and concluded that 50% of them would be economically advantageous if performed in a continuous manner in microreactors instead of conventional batch process. However, it was also found that 63% of the reactions which were considered to be advantageous in flow incorporates solids in some form. The inability of microreactors to handle solids left only 18.7% (See Fig. 1.2) of the total considered reactions in the study to be practically performed in flow chemistry. In the early stages of the field, this study demonstrated the need for the importance of research to develop solid handling techniques to utilize the full potential of microreactor technology in a quantitative manner.
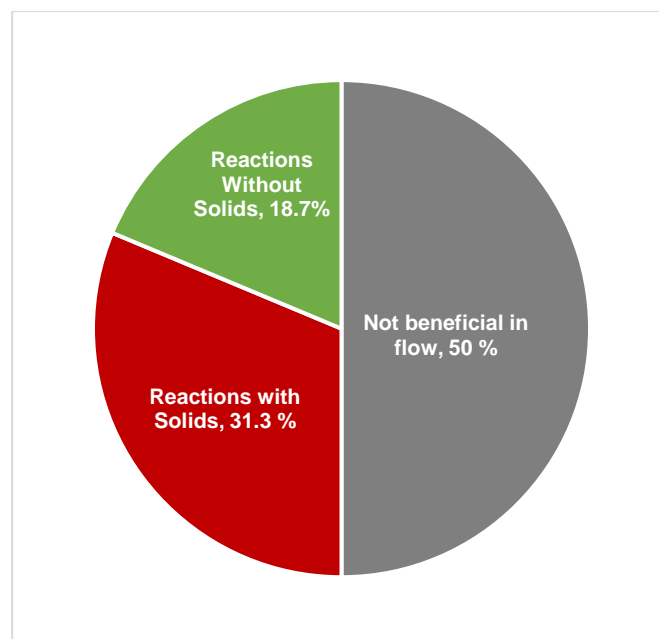
Fig. 1.2. Outline of 86 different reactions surveyed in 2005 in the view of flow chemistry and occurrence of solids [2, 45, 49].

In the decade next to that study several efforts were made to understand clogging which is an incredibly complex, random, and dynamic phenomenon but there are still many gaps in the understanding of clogging in small channels [45, 50-52]. The fundamental understanding of complex particle interactions in the channels has helped in the development of clogging mitigation techniques which are discussed in detail later in the chapter (section 1.3). Majority reviews on microfluidic reaction technology till date state that microreactors are not favoured for solid processing and this perception is generally accepted in the community. Despite the number of efforts to handle solids in flow chemistry and the advancements in micro and nanoparticle formation in flow has exhibited that perception not to be entirely accurate [4].

1.2. Clogging Dynamics

The clogging process is extremely complicated and probably random due to various complex inter-dependent phenomena involved in it, and it is dynamic in nature. A few excellent reports on clogging of small channels acknowledge the complexity involved in this phenomena

[50, 51, 53]. In addition to clogging, generation of solids also adds a new phase to the reaction mixture resulting in a change of flow regimes spatially. Due to the complexity involving relative rates of various parallel and sequential phenomena and stochastic nature of the clogging process no unified mechanism can predict the clogging time. Constriction, bridging and the random detachment of deposits are the three main hydrodynamic mechanisms were reported to cause clogging in single-phase laminar flow in microchannels [54]. Wyss et al. (2006) have reported that the average number of particles that can pass through a pore before it clogs plays a decisive role independent of both flow rate and particle volume fraction. It is a well accepted norm that the mechanism of clogging involves the random occurrence of local particle aggregation leading to large agglomerates, which are large enough to result in physical blocking of channels [55]. Arch formation within a capillary/microchannel, where the particles also have a noticeable adhesive effect on the channel wall [50] is also observed. For very large *Pe*, shear plays a role in bringing particles close to each rather faster than Brownian motion, which enhances the aggregation rate and hence results in clogging of microfluidic devices. Formation of agglomerates or clusters close to the channel wall plays an important role in initializing clogging [56]. It has been observed that once a particle adheres to the wall, it sticks to the wall surface and allows other moving particles get attached. The rate of particle adhesion is found to increase with higher Reynolds number of the system due to the increased frequency of particle/ wall collisions. In contrasting observation, the cluster growth rate is found be faster in lower Re and less dense dendritic structures were formed [57]. Sauret et al. [58, 59] developed a stochastic modelling approach following poisson distribution for clogging time in a membrane like device made of parallel and identical microchannels. In another modelling study, the aggregation dynamics, wall deposition and clogging of rigid microparticles at varying Reynolds number in a straight microchannel by means of Discrete Element Method (DEM) and CFD–DEM coupling approach [60]. While the literature helps to know the possible

mechanisms for clogging in a channel, it does not help in developing a quantitative analysis of when to expect clogging in small channels and the associated time scales for different flow regimes.

In addition to the aforementioned reports, majority of experimental studies so far have focused on clogging in single phase flow in micro-structured porous media in membranes or microchips [19, 51, 57, 59, 61-65], while clogging in tubular microfluidics for a multiphase system, which is more relevant to practising chemical synthesis in a scalable manner, has not been studied substantially. We lack even fundamental investigations on the interaction and transport of solids forming at the liquid-liquid interface, which makes the clogging process in multiphase flow to be considerably contrasting from single phase solid forming systems. The complexity of the particle response to fluid streamlines, forces acting on particles and clusters, and interactions between particles does not allow identification of a single approach to avoid clogging in small channels [59].

1.3. Anticlogging methods

The applicability of certain microfluidic devices (viz. lab-on-a-chip kind of diagnostic systems, flow synthesis of particles, etc.) depends on their capability to maintain flow without clogging: hence it is necessary to evolve methods to prevent clogging. One of the significant bottlenecks of microreactor usage in the chemical industry sector is shortening the reactor lifetime due to clogging and resulting in further breakage of the reactor [4]. Different innovative strategies were developed and reported in the literature in the last decade to manage solids in small channels which can be largely classified into four types – chemical, alternative, passive and active flow manipulation strategies. The chemical strategies change the process chemistry to remove the solid formation issue [44, 46] while the alternative strategies use miniature CSTRs of comparable length scale instead of microreactors. The active and passive

strategies manipulate the flow of different phases with and without an external energy sources [45, 54].

1.3.1. Chemical Strategies

The chemical approach was taken by a few researchers where the homogeneity of the reactive flow system was maintained by preventing solids to form by various methods. Such as changing the chemical synthesis route, performing reactions at lower concentrations or at higher temperatures. Choosing a different solvent to perform reactions or periodic addition of a suitable solvent at the desired reactor zone to dissolve formed solids are also reported to address the clogging problem [46, 66]. Though these solutions are successfully demonstrated to minimize or eliminate solid formation in microreactors, they are typically uneconomical and geared towards a specific synthesis problem and cannot be considered to be a generalized solution across different hydrodynamics and chemistries.

1.3.2. Passive Strategies

Some researchers used a monodispersed droplet flow process to isolate the solid particles from the walls of the microchannel [67, 68]. Perry et al. had identified pH adjustment to effectively diminish the clogging by regulating the electrostatic forces of repulsion between particle-particle interactions [69]. Gera et al. [44] used crystal engineering to add seed crystals of the inorganic salt byproduct to induce controlled heterogeneous growth instead of uncontrolled nucleation. Their modelling approach helped to extend the operating time without fouling of the reactor by means of balanced reaction rate and deposition of the salt onto seed crystals in a compact manner instead of fractal-like agglomerates. However, such methods will not be applicable for non-crystalline materials like polymers or multiple crystalline solids are produced simultaneously.

1.3.3. Active Strategies

Most of the active techniques in literature supply auxiliary acoustic energy in the form of ultrasound to prohibit bridging and accumulation [45, 49, 70, 71]. Ultrasound approach was studied extensively due to the fact that acoustic radiation force is typically higher than the interactions among the fluids, particles, and the capillary wall surface. Acoustic irradiation in the ultrasonic range can be transmitted to the system by different techniques. Freitas et al. had reported a novel ultrasonic flow cell made of a glass capillary surrounded by a steel jacket filled with pressurised water [72]. An ultrasonic horn attached to the jacket was used for transmitting the waves to the system. Usage of an ultrasonic bath had also been shown to inhibit the adhesion and sedimentation of precipitate in the reactor tube [53, 73, 74]. An integrated piezoelectric actuator in the PTFE/ silicon microreactor has been used to directly transmit the acoustic waveform to the reactor, resulting in less particle agglomeration and deposition at the walls [75-77]. This method also provides precise control of the operating frequency compared to ultrasonic baths. In addition to immersion in an ultrasound bath, Horie et al. [78] had introduced inert N_2 gas in a single liquid phase reactive system to enhance the transport of solids. A recent work by Delacour et al. [79] have used a less invasive pulsed ultrasound technique and observed that reducing the effective ultrasound treatment time to 12.5% of residence time in the reactor is adequate to eliminate clogging issues. Ultrasound/piezoelectric actuator (acoustic) based methods were not found to be suitable in practice for scaled-up systems in industrial operations due to various reasons. The main issue in scaling up such systems is the energy implications of using ultrasound compared to traditional methods. Ultrasound waves create cavitation in liquid systems, and the collapse of cavitation bubbles results in very high local temperatures and pressures [80, 81]. Using ultrasound can affect the inherent system, changing the yield and kinetics of the process, or entirely change the process pathways [44, 82]. Nucleation and growth rates are also affected by the use of ultrasonic irradiation [81]. However, such approaches have limited applicability since the rapid decrease

in the intensity of ultrasound with increasing distance from the sonotrode is the primary reason for its unsuitability in larger systems. Apart from this, issues like noise, mechanical constraints, contamination of products by cavitational erosion in the reactor, are areas of concern, as is economic viability because ultrasound based systems consume an enormous amount of energy per unit volume [49, 72, 82]. Magnetic systems had also been reported in the literature to reduce clogging in microchannels. A few microreactor prototypes coupled with magnetic field leverage the advantage of external regulation of solids in the system. External magnetic fields had been used for enhancing the transport of ferromagnetic catalyst particles [83] and magnetic nanocomposites [84] in a microreactor system. Koos et al. [85] had used dual solenoid system analogous to magnetic stirrers for batch systems to agitate solids in suspension which prevents fouling with the help of magnetic stirrer bars. Complications in generation and control of the magnetic field, the necessity of magnetic particles or magnetic stirrer bars in the system, inability to deal with reactive and highly exothermic systems, and severe energy consumption are the bottlenecks in scaling up such a process for industrial operations.

1.3.4. Alternate Strategies

Some researchers have moved towards CSTRs from typical microreactor approach as an alternate proof of concept route to handle solids in the flow. Agitated cell reactor with transverse mixing motion and magnetically stirred miniature CSTR cascade reactor are two such examples reported in the literature [43, 86].

While process specific approaches exist for reduction and preventing clogging, they usually require additional processing equipment and a higher degree of engineering, increasing complexity of the system. Despite significant developments in scale up/ numbering up studies of microreactors, processes involving solids are not explored at this stage. It can be concluded

that while strides have been made in solving the clogging issues in small channels, there is a necessity for further investigation in this area and scope for further improvement.

1.4. Precipitation in microreactors

1.4.1. Microparticles

Microparticles are particles sized between 0.1 and 100 μm. Use of micro-particles is widely reported as a promising way for the improvement of drug bioavailability. Reduction in the particle size enhances its rate of dissolution or reaction, through the enlarged surface area per unit volume [87]. Mainly, size reduction of active pharmaceutical ingredients (APIs) is practiced to increase the bioavailability[88]. Micronization of APIs with desired properties is considered to be an emerging field in the pharmaceutical industry. Beyond these aspects, synthesis of micro particles has made a mark in particle technology owing to some of their unusual properties laying between the bulk material and molecules such as electronic, magnetic and optical properties [89-93]. Microparticles are becoming gradually popular in emerging fields like biosensors, medicines, electronics and alternative energy [94] [33, 95]. In such fields, size, shape, and surface chemistry of the particles are meticulously utilized to optimize their efficacy in terms of dispersity, stability, reactivity, electronic, magnetic, optical behaviour [33].

1.4.2. Micronization

Several techniques for size reduction of different compounds are reported in the literature. However, their applicability is found to be limited due to of poor control over mean particle size, PSD, morphology, and scalability [96]. Traditionally, most chemicals are micronized by different top-down milling processes, which are highly energy intensive and often induce a degree of amorphousness, polydispersity and impurity, affecting product quality

and stability [88, 97]. Moreover, grinding is not suitable for temperature sensitive materials and contamination by the grinding media can never be entirely eliminated. For the case of toxic materials, it results in the production of toxic dust which might result in health hazards. The desired particle size and uniform shape by the grinding route become hard to achieve. Besides, grinding is a relatively expensive and time-consuming procedure. In recent years, because of these foregoing disadvantages of top-down approaches like grinding, a few bottom-up approaches are widely used for the production of micro and nano particles. Different bottom up approaches used for micronization include; evaporative precipitation [98, 99], liquid antisolvent precipitation [100-102], spray drying [103-105], cooling crystallization [106], supercritical precipitation [107-109] and high-pressure homogenization [110-113]. Such methods provide improved control over particle size, morphology and crystallinity in comparison to the top-down methods. Among these methods, the antisolvent precipitation process is widely popular and provides a more convenient procedure and involves atmospheric pressure and no requirement of expensive and sophisticated instrumentation [114]. Scalability of antisolvent precipitation (ASP) is also easily achieved proving a similar mixing intensity to the system. In this process, precipitation of solute is accomplished by adding a non-solvent for solute called as antisolvent [115]. The antisolvent precipitates the solute molecules by replacing the dissolved solute molecule in the solvent with itself thereby reducing the dissolving power of the solvent for the solute. In addition to these, making a continuous ASP system results in consistent product quality including the particle size and the morphology. Moreover, the method is applicable to a wide range of materials such as active pharmaceutical ingredients (APIs), polymers and proteins, various types of inorganic and organic particles such as magnetic materials, hollow capsules, metal-organic materials [88, 89, 116-119].

ASP is extensively used for the production of small-sized API particles such as ibuprofen, glyburide, artemisinin, [120] silibinin, [121] β-carotene, [122] griseofulvin, [123]

and curcumin [124]. Though, significant efforts have been taken into the direction towards the lab scale synthesis of API microparticles in recent years, high throughput synthesis for industrial applications are still in development [125].

1.4.3. Continuous Antisolvent precipitation and relevance to clogging

As ASP is a solvent exchange method, mixing of solvents plays a vital role to produce smaller size particles [126]. The solvent exchange is a diffusion limited phenomenon [127], where fast and efficient mixing can result in small size monodisperse particles [114, 128]. Slow and inefficient mixing results in locally non-uniform nucleation and growth rates leading to poly-dispersed particles. Typically, ASP has been carried out in a classical batch reactor. This batch synthesis is limited to low production rate, poor reproducibility and wider particles size distribution owing to poor mixing and dead time. In the classical batch method, processing large volume and controlled the addition of reagent to achieve homogeneous mixing becomes very difficult. Large size continuous stirred tank reactor or homogenizers have been used for high throughput production of microparticles, but the mixing timescales are not smaller than the precipitation time scales. Moreover, achieving spatial homogeneity in large reactors is challenging [129]. When organic and aqueous phases enter into a microchannel, the large interfacial area as well as very small diffusion path length help to enhance the interfacial mass transfer [130-132]. Use of an organic phase having some solubility in the aqueous phase helps rapid precipitation of the solute dissolved in the aqueous phase. As discussed in the early sections of this chapter, apart from several organic synthesis, precipitation using an antisolvent is one of the most important examples of solids forming in a microchannel [100, 133-135]. Although these examples provide important insights into interfacial precipitation the effect of the flow regimes on the possibility of their agglomeration and subsequent blockage dynamics in a capillary have not been investigated. Along with understanding and mitigation of clogging,

the thesis is also focused on production and clogging free scaleup aspects of microparticles via the antisolvent route.

1.5. Research Objectives

The current thesis focuses on the following major aspects:

- Understand the clogging dynamics in multiphase flow in straight microchannels

- Identification of suitable anticlogging methods and their quantitative comparison

- Optimization of antisolvent precipitation for size controlled microparticles

- Development of clogging free scaled up continuous precipitation methods

1.6. Organization of the Thesis

The thesis entitled **"Understanding flow of solids in continuous flow reactors"** is organized into seven chapters.

A basic introduction to microreactors and their various applications have been given in **Chapter 1**. This chapter also clearly states the occurrence of solids in different forms in continuous flow microreactors and the necessity to handle them. Different methods which are reported in the literature for solid handling in microchannels and their pros and cons have been discussed subsequently. The importance of microparticles and the development of clogging free continuous micronization methods (ASP) were also discussed.

Chapter 2 provides an insight into the microchannel clogging mechanism in liquid liquid multiphase flow which has been hardly explored in the literature. The clogging time for different flow rates, regimes and capillary diameters were explored in a quantitative framework for a specific case of interfacial precipitation. The influence the associated dynamics viz. coalescence of dispersed phase during the flow and the nature of interface on clogging time was also studied.

In **Chapter 3** four different flow manipulation methods that can help reduce clogging by means of efficient particle transport have been experimentally investigated, and their relative performance has been analysed. The performance of these four particle handling methods was evaluated in a quantitative manner to understand the efficacy of the implemented strategies and to identify the timescales for clogging. Some of the strategies were demonstrated for performing chemical reaction involving solids in continuous flow.

Chapter 4 illustrates batch to continuous flow precipitation protocol for antisolvent precipitation of Ammonium Perchlorate (AP). Antisolvent selection and further optimization in batch and continuous framework were performed by studying the effect of process parameters.

In **Chapter 5,** presents a novel design of the confined liquid impinging jet reactor, for handling solids in continuous flow. Mixing performance and jet impingement dynamics in the proposed impinging jet reactor were investigated using CFD followed by the observations on particle size and PSD of the AP particles obtained from the impinging jet reactor. Particle size and PSD obtained in various experimental strategies were compared before summarizing the major findings from the study.

In **Chapter 6,** a systematic study was performed for optimization of the batch precipitation conditions of metformin hydrochloride (MHC) microparticles and the batch process was translated to high throughput continuous process by means of inverted jet reactor. Ultrasound was used to provide superior micromixing in precipitaion process, diminishing induction times for nucleation and providing uniform supersaturation ratio.

Finally, **Chapter 7** is a brief conclusion of this thesis, summarizing overall outcomes and potential future scopes of the research area. A list of publications made out during the research is also attached in the thesis.

1.7. References

1.   Opalski, A.S., Kaminski, T.S., and Garstecki, P., *Droplet Microfluidics as a Tool for the Generation of Granular Matters and Functional Emulsions.* KONA Powder and Particle Journal, **2019**: p. 2019004.

2.   Zhang, J., Wang, K., Teixeira, A.R., Jensen, K.F., and Luo, G., *Design and scaling up of microchemical systems: a review.* Annual review of chemical and biomolecular engineering, **2017**. 8: p. 285-305.

3.   Jensen, K.F., *Microchemical systems: status, challenges, and opportunities.* AIChE Journal, **1999**. 45(10): p. 2051-2054.

4.   Elvira, K.S., i Solvas, X.C., Wootton, R.C., and Demello, A.J., *The past, present and potential for microfluidic reactor technology in chemical synthesis.* Nature chemistry, **2013**. 5(11): p. 905.

5.   Bogdan, A.R. and Dombrowski, A.W., *Emerging Trends in Flow Chemistry and Applications to the Pharmaceutical Industry.* Journal of medicinal chemistry, **2019**.

6.   May, S.A., *Flow chemistry, continuous processing, and continuous manufacturing: A pharmaceutical perspective.* Journal of Flow Chemistry, **2017**. 7(3-4): p. 137-145.

7.   Fernandes, J. and Sharma, M., *Effective interfacial area in agitated liquid—liquid contactors.* Chemical Engineering Science, **1967**. 22(10): p. 1267-1282.

8.   Dłuska, E., Wroński, S., and Ryszczuk, T., *Interfacial area in gas–liquid Couette–Taylor flow reactor.* Experimental Thermal Fluid Science, **2004**. 28(5): p. 467-472.

9.   Schmitz, M., Steiff, A., Weinspach, P.M.J.C.e., and technology, *Gas/liquid interfacial area per unit volume and volumetric mass transfer coefficient in stirred slurry reactors.* **1987**. 10(1): p. 204-215.

10. Bouaifi, M., Hebrard, G., Bastoul, D., Roustan, M.J.C.e., and processing, *A comparative study of gas hold-up, bubble size, interfacial area and mass transfer coefficients in stirred gas–liquid reactors and bubble columns.* Process intensification, **2001**. 40(2): p. 97-111.

11. Ghaini, A., Kashid, M.N., and Agar, D.W., *Effective interfacial area for mass transfer in the liquid–liquid slug flow capillary microreactors.* Chemical Engineering and Processing: Process Intensification, **2010**. 49(4): p. 358-366.

12. Hessel, V., Löwe, H., and Schönfeld, F., *Micromixers—a review on passive and active mixing principles.* Chemical Engineering Science, **2005**. 60(8-9): p. 2479-2501.

13. Bayer, T., Himmler, K., and Hessel, V., *Don't be baffled by static mixers: how to select and size the correct static mixer.(Feature Report).* Chemical Engineering, **2003**. 110(5): p. 50-58.

14. Thakur, R., Vial, C., Nigam, K., Nauman, E., and Djelveh, G., *Static mixers in the process industries—a review.* Chemical Engineering Research and Design, **2003**. 81(7): p. 787-826.

15. Lee, C.Y., Chang, C.L., Wang, Y.N., and Fu, L.M., *Microfluidic mixing: a review.* International journal of molecular sciences, **2011**. 12(5): p. 3263-3287.

16. Mansur, E.A., Mingxing, Y., Yundong, W., and Youyuan, D., *A state-of-the-art review of mixing in microfluidic mixers.* Chinese Journal of Chemical Engineering, **2008**. 16(4): p. 503-516.

17. Suh, Y.K. and Kang, S., *A review on mixing in microfluidics.* Micromachines, **2010**. 1(3): p. 82-111.

18. Lee, C.Y., Wang, W.T., Liu, C.C., and Fu, L.M., *Passive mixers in microfluidic systems: A review.* Chemical Engineering Journal, **2016**. 288: p. 146-160.

19. Kim, Y., Ahn, K.H., and Lee, S.J., *Clogging mechanism of poly (styrene) particles in the flow through a single micro-pore.* Journal of Membrane Science, **2017**.

20. Roberge, D.M., Ducry, L., Bieler, N., Cretton, P., and Zimmermann, B., *Microreactor technology: a revolution for the fine chemical and pharmaceutical industries?* Chemical Engineering & Technology: Industrial Chemistry-Plant Equipment-Process Engineering-Biotechnology, **2005**. 28(3): p. 318-323.

21. Jensen, K.F. and Rogers, L., *Continuous manufacturing-the Green Chemistry promise?* Green Chemistry, **2019**.

22. Plutschack, M.B., Pieber, B.u., Gilmore, K., and Seeberger, P.H., *The hitchhiker's guide to flow chemistry∥.* Chemical reviews, **2017**. 117(18): p. 11796-11893.

23. Yang, C.G., Xu, Z.R., and Wang, J.H., *Manipulation of droplets in microfluidic systems.* TrAC Trends in Analytical Chemistry, **2010**. 29(2): p. 141-157.

24. Christopher, G.F. and Anna, S.L., *Microfluidic methods for generating continuous droplet streams.* Journal of Physics D: Applied Physics, **2007**. 40(19): p. R319.

25. Zhu, Y. and Fang, Q., *Analytical detection techniques for droplet microfluidics—A review.* Analytica Chimica Acta, **2013**. 787: p. 24-35.

26. Garstecki, P. and Hołyst, R., *Ten years of Nature Physics: Go with the flow.* Nature Physics, **2015**. 11(4): p. 305.

27. Mashaghi, S., Abbaspourrad, A., Weitz, D.A., and van Oijen, A.M., *Droplet microfluidics: A tool for biology, chemistry and nanotechnology.* TrAC Trends in Analytical Chemistry, **2016**. 82: p. 118-125.

28. Sackmann, E.K., Fulton, A.L., and Beebe, D.J., *The present and future role of microfluidics in biomedical research.* Nature, **2014**. 507(7491): p. 181.

29. Churski, K., Ruszczak, A., Jakiela, S., and Garstecki, P., *Droplet microfluidic technique for the study of fermentation.* Micromachines, **2015**. 6(10): p. 1514-1525.

30.   Žnidaršič-Plazl, P., *Biotransformations in microflow systems: Bridging the gap between academia and industry.* Journal of Flow Chemistry, **2017**. 7(3-4): p. 111-117.

31.   Scheler, O., Postek, W., and Garstecki, P., *Recent developments of microfluidics as a tool for biotechnology and microbiology.* Current opinion in biotechnology, **2019**. 55: p. 60-67.

32.   Pan, L.J., Tu, J.-W., Ma, H.-T., Yang, Y.-J., Tian, Z.-Q., Pang, D.-W., and Zhang, Z.-L., *Controllable synthesis of nanocrystals in droplet reactors.* Lab on a Chip, **2018**. 18(1): p. 41-56.

33.   Hao, N., Nie, Y., and Zhang, J.X., *Microfluidic synthesis of functional inorganic micro-/nanoparticles and applications in biomedical engineering.* International Materials Reviews, **2018**. 63(8): p. 461-487.

34.   Sebastian, V., Khan, S.A., and Kulkarni, A.A., *Flow synthesis of functional materials.* Journal of Flow Chemistry, **2017**. 7(3-4): p. 96-105.

35.   Park, J.I., Saffari, A., Kumar, S., Günther, A., and Kumacheva, E., *Microfluidic synthesis of polymer and inorganic particulate materials.* Annual Review of Materials Research, **2010**. 40: p. 415-443.

36.   Köhler, J.M., Li, S., and Knauer, A., *Why is micro segmented flow particularly promising for the synthesis of nanomaterials?* Chemical Engineering & Technology, **2013**. 36(6): p. 887-899.

37.   Wang, J., Li, Y., Wang, X., Wang, J., Tian, H., Zhao, P., Tian, Y., Gu, Y., Wang, L., and Wang, C., *Droplet microfluidics for the production of microparticles and nanoparticles.* Micromachines, **2017**. 8(1): p. 22.

38.   Jensen, K.F., *Flow chemistry : microreaction technology comes of age.* AIChE Journal, **2017**. 63(3): p. 858-869.

39. Xia, Y. and Whitesides, G.M., *Soft Lithography.* Annual Review of Materials Science, **1998**. 28(1): p. 153-184.

40. Ko, D., Gyak, K., and Kim, D.P., *Emerging microreaction systems based on 3D printing techniques and separation technologies.* Journal of Flow Chemistry, **2017**. 7(3-4): p. 72-81.

41. Nguyen, H.T., Thach, H., Roy, E., Huynh, K., and Perrault, C., *Low-Cost, Accessible Fabrication Methods for Microfluidics Research in Low-Resource Settings.* Micromachines, **2018**. 9(9): p. 461.

42. Gale, B., Jafek, A., Lambert, C., Goenner, B., Moghimifam, H., Nze, U., and Kamarapu, S., *A review of current methods in microfluidic device fabrication and future commercialization prospects.* Inventions, **2018**. 3(3): p. 60.

43. Browne, D.L., Deadman, B.J., Ashe, R., Baxendale, I.R., and Ley, S.V., *Continuous flow processing of slurries: evaluation of an agitated cell reactor.* Organic Process Research & Development, **2011**. 15(3): p. 693-697.

44. Giri, G., Yang, L., Mo, Y., and Jensen, K.F., *Adding Crystals To Minimize Clogging in Continuous Flow Synthesis.* Crystal Growth & Design, **2018**. 19(1): p. 98-105.

45. Hartman, R.L., *Managing Solids in Microreactors for the Upstream Continuous Processing of Fine Chemicals.* Organic Process Research & Development, **2012**. 16(5): p. 870-887.

46. Kashani, S.K., Sullivan, R.J., Andersen, M., and Newman, S.G., *Overcoming solid handling issues in continuous flow substitution reactions through ionic liquid formation.* Green Chemistry, **2018**. 20(8): p. 1748-1753.

47. Lapkin, A.A., Loponov, K., Tomaiuolo, G., and Guido, S., *Solids in Continuous Flow Reactors for Specialty and Pharmaceutical Syntheses.* Sustainable Flow Chemistry: Methods and Applications, **2017**.

48. Teychené, S. and Biscans, B., *Microfluidic device for the crystallization of organic molecules in organic solvents.* Crystal Growth & Design, **2011**. 11(11): p. 4810-4818.

49. Wu, K. and Kuhn, S., *Strategies for solids handling in microreactors.* Chim. Oggi, **2014**. 32(3): p. 62.

50. Sharp, K.V. and Adrian, R.J., *On flow-blocking particle structures in microtubes.* Microfluidics and Nanofluidics, **2005**. 1(4): p. 376-380.

51. Wyss, H., Blair, D., Morris, J., Stone, H., and Weitz, D., *Mechanism for clogging of microchannels.* Physical Review E, **2006**. 74(6).

52. Pal, S. and Kulkarni, A.A., *Interfacial precipitation and clogging in straight capillaries.* Chemical Engineering Science, **2016**. 153: p. 344-353.

53. Hartman, R.L., Naber, J.R., Zaborenko, N., Buchwald, S.L., and Jensen, K.F., *Overcoming the challenges of solid bridging and constriction during Pd-Catalyzed C−N bond formation in microreactors.* Organic Process Research & Development, **2010**. 14(6): p. 1347-1357.

54. Flowers, B.S. and Hartman, R.L., *Particle Handling Techniques in Microchemical Processes.* Challenges, **2012**. 3(2): p. 194-211.

55. Goldsztein, G.H. and Santamarina, J.C., *Suspension extraction through an opening before clogging.* Applied Physics Letters, **2004**. 85(19): p. 4535.

56. Gudipaty, T., Stamm, M.T., Cheung, L.S.L., Jiang, L., and Zohar, Y., *Cluster formation and growth in microchannel flow of dilute particle suspensions.* Microfluidics and Nanofluidics, **2010**. 10(3): p. 661-669.

57. Sicignano, L., Tomaiuolo, G., Perazzo, A., Nolan, S.P., Maffettone, P.L., and Guido, S., *The effect of shear flow on microreactor clogging.* Chemical Engineering Journal, **2018**.

58. Sauret, A., Somszor, K., Villermaux, E., and Dressaire, E., *Growth of clogs in parallel microchannels.* Physical Review Fluids, **2018**. 3(10): p. 104301.

59. Dressaire, E. and Sauret, A., *Clogging of microfluidic systems.* Soft Matter, **2017**. 13(1): p. 37-48.

60. Shahzad, K., Van Aeken, W., Mottaghi, M., Kamyab, V.K., and Kuhn, S., *Aggregation and clogging phenomena of rigid microparticles in microfluidics.* Microfluidics and nanofluidics, **2018**. 22(9): p. 104.

61. Dersoir, B., de Saint Vincent, M.R., Abkarian, M., and Tabuteau, H., *Clogging of a single pore by colloidal particles.* Microfluidics and Nanofluidics, **2015**. 19(4): p. 953-961.

62. Sendekie, Z.B. and Bacchin, P., *Colloidal jamming dynamics in microchannel bottlenecks.* Langmuir, **2016**. 32(6): p. 1478-1488.

63. Mays, D.C. and Hunt, J.R., *Hydrodynamic aspects of particle clogging in porous media.* Environmental science & technology, **2005**. 39(2): p. 577-584.

64. Massenburg, S.S., Amstad, E., and Weitz, D.A., *Clogging in parallelized tapered microfluidic channels.* Microfluidics and Nanofluidics, **2016**. 20(6): p. 94.

65. Marin, A., Lhuissier, H., Rossi, M., and Kähler, C.J., *Clogging in constricted suspension flows.* Physical Review E, **2018**. 97(2): p. 021102.

66. Kelly, C.B., Lee, C.X., and Leadbeater, N.E., *An approach for continuous-flow processing of reactions that involve the in situ formation of organic products.* Tetrahedron letters, **2011**. 52(2): p. 263-265.

67. Poe, S.L., Cummings, M.A., Haaf, M.P., and McQuade, D.T., *Solving the clogging problem: precipitate-forming reactions in flow.* Angew Chem Int Ed Engl, **2006**. 45(10): p. 1544-8.

68.   Yeap, E.W., Ng, D.Z., Lai, D., Ertl, D.J., Sharpe, S., and Khan, S.A., *Continuous Flow Droplet-Based Crystallization Platform for Producing Spherical Drug Microparticles.* Organic Process Research & Development, **2018**. 23(1): p. 93-101.

69.   Perry, J.L. and Kandlikar, S.G., *Fouling and its mitigation in silicon microchannels used for IC chip cooling.* Microfluidics and Nanofluidics, **2008**. 5(3): p. 357-371.

70.   Hartman, R.L., Naber, J.R., Zaborenko, N., McMullen, J.P., and Jensen, K.F., *Methods for handling solids in microfluidic systems*. **2014**, Google Patents.

71.   Dong, Z., Rivas, D.F., and Kuhn, S., *Acoustophoretic focusing effects on particle synthesis and clogging in microreactors.* Lab on a Chip, **2019**. 19(2): p. 316-327.

72.   Freitas, S., Hielscher, G., Merkle, H.P., and Gander, B., *Continuous contact-and contamination-free ultrasonic emulsification—a useful tool for pharmaceutical development and production.* Ultrasonics sonochemistry, **2006**. 13(1): p. 76-85.

73.   Sedelmeier, J., Ley, S.V., Baxendale, I.R., and Baumann, M., *KMnO4-mediated oxidation as a continuous flow process.* Organic letters, **2010**. 12(16): p. 3618-3621.

74.   Noël, T., Naber, J.R., Hartman, R.L., McMullen, J.P., Jensen, K.F., and Buchwald, S.L., *Palladium-catalyzed amination reactions in flow: overcoming the challenges of clogging via acoustic irradiation.* Chem. Sci., **2011**. 2(2): p. 287-290.

75.   Kuhn, S., Noel, T., Gu, L., Heider, P.L., and Jensen, K.F., *A Teflon microreactor with integrated piezoelectric actuator to handle solid forming reactions.* Lab Chip, **2011**. 11(15): p. 2488-92.

76.   Castro, F., Kuhn, S., Jensen, K., Ferreira, A., Rocha, F., Vicente, A., and Teixeira, J.A., *Continuous-flow precipitation of hydroxyapatite in ultrasonic microsystems.* Chemical engineering journal, **2013**. 215: p. 979-987.

77.   Nilsson, A., Petersson, F., Jönsson, H., and Laurell, T., *Acoustic control of suspended particles in micro fluidic chips.* Lab on a Chip, **2004**. 4(2): p. 131-135.

78. Horie, T., Sumino, M., Tanaka, T., Matsushita, Y., Ichimura, T., and Yoshida, J.-i., *Photodimerization of maleic anhydride in a microreactor without clogging.* Organic Process Research & Development, **2010**. 14(2): p. 405-410.

79. Delacour, C., Lutz, C., and Kuhn, S., *Pulsed ultrasound for temperature control and clogging prevention in micro-reactors.* Ultrasonics Sonochemistry, **2019**.

80. Sander, J.R., Zeiger, B.W., and Suslick, K.S., *Sonocrystallization and sonofragmentation.* Ultrasonics sonochemistry, **2014**. 21(6): p. 1908-1915.

81. Nalajala, V.S. and Moholkar, V.S., *Investigations in the physical mechanism of sonocrystallization.* Ultrasonics sonochemistry, **2011**. 18(1): p. 345-355.

82. Berlan, J. and Mason, T.J., *Sonochemistry: from research laboratories to industrial plants.* Ultrasonics, **1992**. 30(4): p. 203-212.

83. Yahya, N., Puspitasari, P., Koziol, K., Zabidi, N.A.M., and Othman, M.F., *Novel Electromagnetic Microreactor Design for Ammonia Synthesis.* International Journal of Basic and Applied Sciences, **2010**. 10(1): p. 95-100.

84. Asmatulu, R., Zalich, M.A., Claus, R.O., and Riffle, J.S., *Synthesis, characterization and targeting of biodegradable magnetic nanocomposite particles by external magnetic fields.* Journal of Magnetism and Magnetic Materials, **2005**. 292: p. 108-119.

85. Koos, P., Browne, D.L., and Ley, S.V., *Continuous stream processing: a prototype magnetic field induced flow mixer.* Green Processing and Synthesis, **2012**. 1(1): p. 11-18.

86. Mo, Y. and Jensen, K.F., *A miniature CSTR cascade for continuous flow of reactions containing solids.* Reaction Chemistry & Engineering, **2016**. 1(5): p. 501-507.

87. Lince, F., Marchisio, D.L., and Barresi, A.A., *Strategies to control the particle size distribution of poly-ε-caprolactone nanoparticles for pharmaceutical applications.* Journal of colloid and interface science, **2008**. 322(2): p. 505-515.

88.   Thorat, A.A. and Dalvi, S.V., *Liquid antisolvent precipitation and stabilization of nanoparticles of poorly water soluble drugs in aqueous suspensions: Recent developments and future perspective.* Chemical Engineering Journal, **2012**. 181: p. 1-34.

89.   Horn, D. and Rieger, J., *Organic nanoparticles in the aqueous phase—theory, experiment, and use.* Angewandte Chemie International Edition, **2001**. 40(23): p. 4330-4361.

90.   Kolhatkar, A., Jamison, A., Litvinov, D., Willson, R., and Lee, T., *Tuning the magnetic properties of nanoparticles.* International journal of molecular sciences, **2013**. 14(8): p. 15977-16009.

91.   Liang, J., Liu, J., Xie, Q., Bai, S., Yu, W., and Qian, Y., *Hydrothermal growth and optical properties of doughnut-shaped ZnO microparticles.* The Journal of Physical Chemistry B, **2005**. 109(19): p. 9463-9467.

92.   Dick, K., Dhanasekaran, T., Zhang, Z., and Meisel, D., *Size-dependent melting of silica-encapsulated gold nanoparticles.* Journal of the American Chemical Society, **2002**. 124(10): p. 2312-2317.

93.   Ghosh Chaudhuri, R. and Paria, S., *Core/shell nanoparticles: classes, properties, synthesis mechanisms, characterization, and applications.* Chem. Rev., **2011**. 112: p. 2373-2433.

94.   Silva, A.S., Tavares, M.T., and Aguiar-Ricardo, A., *Sustainable strategies for nano-in-micro particle engineering for pulmonary delivery.* J. Nanopart. Res., **2014**. 16: p. 2602.

95.   Sanguansri, P. and Augustin, M.A., *Nanoscale materials development–a food industry perspective.* Trends Food Sci. Technol., **2006**. 17: p. 547-556.

96. Dalvi, S.V. and Dave, R.N., *Controlling particle size of a poorly water-soluble drug using ultrasound and stabilizers in antisolvent precipitation.* Industrial & Engineering Chemistry Research, **2009**. 48(16): p. 7581-7593.

97. Chiou, H., Chan, H.-K., Prud'homme, R.K., and Raper, J.A., *Evaluation on the use of confined liquid impinging jets for the synthesis of nanodrug particles.* Drug development and industrial pharmacy, **2008**. 34(1): p. 59-64.

98. Chen, X., Young, T.J., Sarkari, M., Williams III, R.O., and Johnston, K.P., *Preparation of cyclosporine A nanoparticles by evaporative precipitation into aqueous solution.* International Journal of Pharmaceutics, **2002**. 242(1-2): p. 3-14.

99. Kakran, M., Sahoo, N., Li, L., Judeh, Z., Wang, Y., Chong, K., and Loh, L., *Fabrication of drug nanoparticles by evaporative precipitation of nanosuspension.* International journal of pharmaceutics, **2010**. 383(1-2): p. 285-292.

100. Zhao, H., Wang, J.-X., Wang, Q.-A., Chen, J.-F., and Yun, J., *Controlled liquid antisolvent precipitation of hydrophobic pharmaceutical nanoparticles in a microchannel reactor.* Industrial & Engineering Chemistry Research, **2007**. 46(24): p. 8229-8235.

101. Zu, Y., Wu, W., Zhao, X., Li, Y., Wang, W., Zhong, C., Zhang, Y., and Zhao, X., *Enhancement of solubility, antioxidant ability and bioavailability of taxifolin nanoparticles by liquid antisolvent precipitation technique.* International journal of pharmaceutics, **2014**. 471(1-2): p. 366-376.

102. Beck, C., Dalvi, S.V., and Dave, R.N., *Controlled liquid antisolvent precipitation using a rapid mixing device.* Chemical Engineering Science, **2010**. 65(21): p. 5669-5675.

103. Vehring, R., *Pharmaceutical particle engineering via spray drying.* Pharmaceutical research, **2008**. 25(5): p. 999-1022.

104.   Sansone, F., Picerno, P., Mencherini, T., Villecco, F., D'ursi, A., Aquino, R., and Lauro, M., *Flavonoid microparticles by spray-drying: Influence of enhancers of the dissolution rate on properties and stability.* Journal of Food Engineering, **2011**. 103(2): p. 188-196.

105.   Rattes, A.L.R. and Oliveira, W.P.J.P.T., *Spray drying conditions and encapsulating composition effects on formation and properties of sodium diclofenac microparticles.* **2007**. 171(1): p. 7-14.

106.   Abbas, A., Nobbs, D., and Romagnoli, J.A., *Investigation of on-line optical particle characterization in reaction and cooling crystallization systems. Current state of the art.* Measurement Science and Technology, **2002**. 13(3): p. 349.

107.   Reverchon, E., Adami, R., Caputo, G., and De Marco, I., *Spherical microparticles production by supercritical antisolvent precipitation: interpretation of results.* The Journal of supercritical fluids, **2008**. 47(1): p. 70-84.

108.   Kawashima, Y. and York, P., *Drug delivery applications of supercritical fluid technology.* **2008**, Elsevier.

109.   Mukhopadhyay, M. and Dalvi, S.V., *Mass and heat transfer analysis of SAS: effects of thermodynamic states and flow rates on droplet size.* The Journal of supercritical fluids, **2004**. 30(3): p. 333-348.

110.   Freitas, C. and Müller, R.H., *Spray-drying of solid lipid nanoparticles (SLN TM).* Eur. J. Pharm. Biopharm., **1998**. 46: p. 145-151.

111.   Komai, Y., Kasai, H., Hirakoso, H., Hakuta, Y., Katagi, H., Okada, S., Oikawa, H., Adschiri, T., Inomata, H., and Arai, K., *Preparation of organic microcrystals using supercritical fluid crystallization method.* Jpn. J. Appl. Phys., **1999**. 38: p. L81.

112.   Silva, A., González-Mira, E., García, M., Egea, M., Fonseca, J., Silva, R., Santos, D., Souto, E., and Ferreira, D., *Preparation, characterization and biocompatibility studies*

on risperidone-loaded solid lipid nanoparticles (SLN): high pressure homogenization versus ultrasound. Colloids Surf. B, **2011**. 86: p. 158-165.

113. Calvör, A., McIller, B.W.J.P.d., and technology, *Production of microparticles by high-pressure homogenization.* **1998**. 3(3): p. 297-305.

114. Zhao, H., Wang, J.-X., Wang, Q.-A., Chen, J.-F., and Yun, J., *Controlled liquid antisolvent precipitation of hydrophobic pharmaceutical nanoparticles in a microchannel reactor.* Ind. Eng. Chem. Res., **2007**. 46: p. 8229-8235.

115. Acton, Q.A., *Advances in Nanotechnology Research and Application: 2012 Edition.* Scholarly Editions, **2012**.

116. Zhang, S., Ferté, N., Candoni, N., and Veesler, S., *Versatile Microfluidic Approach to Crystallization.* Organic Process Research & Development, **2015**. 19(12): p. 1837-1841.

117. Lee, S.H.S., Dawood, M., Choi, W., Hatton, T.A., and Khan, S.A., *Hierarchical materials synthesis at soft all-aqueous interfaces.* Soft Matter, **2012**. 8(14): p. 3924-3928.

118. Liu, J., Liu, F., Gao, K., Wu, J., and Xue, D., *Recent developments in the chemical synthesis of inorganic porous capsules.* Journal of Materials Chemistry, **2009**. 19(34): p. 6073-6084.

119. Ameloot, R., Vermoortele, F., Vanhove, W., Roeffaers, M.B., Sels, B.F., and De Vos, D.E., *Interfacial synthesis of hollow metal-organic framework capsules demonstrating selective permeability.* Nat Chem, **2011**. 3(5): p. 382-7.

120. Khan, S., Matas, M.d., Zhang, J., and Anwar, J., *Nanocrystal preparation: low-energy precipitation method revisited.* Crys. Growth Des., **2013**. 13: p. 2766-2777.

121. Wu, W., Zu, Y., Wang, L., Wang, L., Li, Y., Liu, Y., Wu, M., Zhao, X., and Zhang, X., *Preparation, characterization and antitumor activity evaluation of silibinin*

nanoparticles for oral delivery through liquid antisolvent precipitation. RSC Adv., **2017**. 7: p. 54379-54390.

122.   Horn, D., *Preparation and characterization of microdisperse bioavailable carotenoid hydrosols.* Macromol. Mate. Eng., **1989**. 166: p. 139-153.

123.   Beck, C., Sievens-Figueroa, L., Gärtner, K., Jerez-Rozo, J.I., Romañach, R.J., Bilgili, E., and Davé, R.N., *Effects of stabilizers on particle redispersion and dissolution from polymer strip films containing liquid antisolvent precipitated griseofulvin particles.* Powder Tech., **2013**. 236: p. 37-51.

124.   Thorat, A.A. and Dalvi, S.V., *Liquid antisolvent precipitation and stabilization of nanoparticles of poorly water soluble drugs in aqueous suspensions: recent developments and future perspective.* Chem. Eng. J., **2012**. 181: p. 1-34.

125.   Dendukuri, D. and Doyle, P.S., *The synthesis and assembly of polymeric microparticles using microfluidics.* Advanced Materials, **2009**. 21(41): p. 4071-4086.

126.   Matteucci, M.E., Hotze, M.A., Johnston, K.P., and Williams, R.O., *Drug nanoparticles by antisolvent precipitation: mixing energy versus surfactant stabilization.* Langmuir, **2006**. 22: p. 8951-8959.

127.   Heyer, H., *Kinetics of Precipitation. Von AE Nielsen. International Series of Monographs on Analytical Chemistry. Haupt-Herausg. R. Belcher und L. Gordon. Vol. 18. Pergamon Press, Oxford-London-Edinburgh-New York-Paris-Frankfurt 1964. 1. Aufl., X, 153 S., zahlr. Abb., mehrere Tab., geb.£ 2.0. 0.* Angew. Chem. Int. Ed., **1965**. 77: p. 745-745.

128.   Horn, D. and Rieger, J., *Organic nanoparticles in the aqueous phase—theory, experiment, and use.* Angew. Chem. Int. Ed., **2001**. 40: p. 4330-4361.

129. Hartman, R.L., McMullen, J.P., and Jensen, K.F., *Deciding whether to go with the flow: evaluating the merits of flow reactors for synthesis.* Angew. Chem. Int. Ed., **2011**. 50: p. 7502-7519.

130. Zhao, C.X. and Middelberg, A.P., *Two-phase microfluidic flows.* Chemical Engineering Science, **2011**. 66(7): p. 1394-1411.

131. Wang, H., Nakamura, H., Uehara, M., Miyazaki, M., and Maeda, H., *Preparation of titania particles utilizing the insoluble phase interface in a microchannel reactor.* Chemical Communications, **2002**(14): p. 1462-1463.

132. Hisamoto, H., Saito, T., Tokeshi, M., Hibara, A., and Kitamori, T., *Fast and high conversion phase-transfer synthesis exploiting the liquid–liquid interface formed in a microchannel chip.* Chemical Communications, **2001**(24): p. 2662-2663.

133. Ali, H.S., Blagden, N., York, P., Amani, A., and Brook, T., *Artificial neural networks modelling the prednisolone nanoprecipitation in microfluidic reactors.* Eur J Pharm Sci, **2009**. 37(3-4): p. 514-22.

134. Zhu, W.Z., Wang, J.-X., Shao, L., Zhang, H.-x., Zhang, Q.-x., and Chen, J.-F., *Liquid antisolvent preparation of amorphous cefuroxime axetil nanoparticles in a tube-in-tube microchannel reactor.* International journal of pharmaceutics, **2010**. 395(1): p. 260-265.

135. Su, Y.F., Kim, H., Kovenklioglu, S., and Lee, W.Y., *Continuous nanoparticle production by microfluidic-based emulsion, mixing and crystallization.* Journal of Solid State Chemistry, **2007**. 180(9): p. 2625-2629.

Chapter 2

Understanding clogging dynamics in multiphase flow
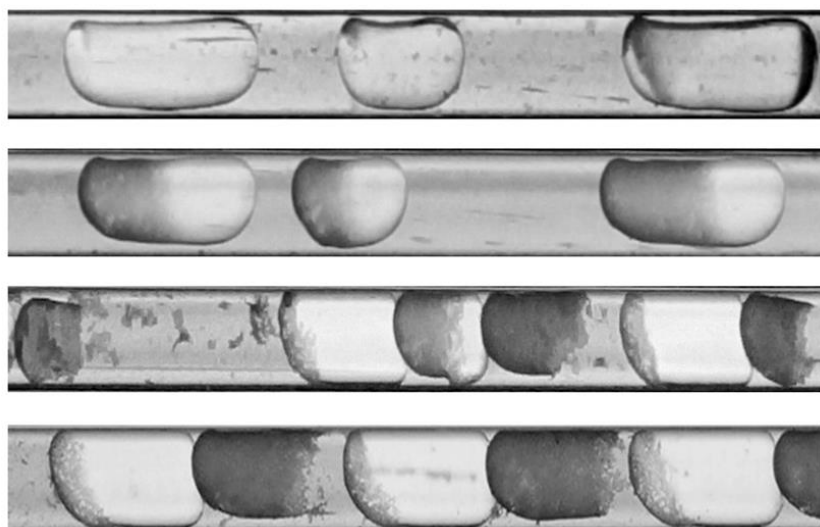
2. Understanding clogging dynamics in multiphase flow[1]

In the previous chapter, a comprehensive review of clogging of microreactors in solid forming processes and studies to handle them were presented. This chapter deals with the understanding of clogging in multiphase system with specific focus on clogging time in different flow regimes and channel diameters. The study reported in this chapter uses an antisolvent precipitation method to generate solids in microchannels. A thorough work was carried out to understand the clogging phenomena arising from interfacial precipitation a multiphase flow system. Clogging of the capillaries was studied for a range of conditions that result in different flow regimes. The particle formation and clogging were explored using the visually tracking a moving slug in real time. Effect of different parameters such as flow regimes, channel diameters, flow rates were studied in detail.

2.1 Introduction

Different engineering and chemistry oriented benefits of using microreactors have driven exciting innovations, and the number of new examples of flow syntheses is increasing exponentially every year. Despite this, the microfluidic approach poses severe challenges for the reactions where the product or byproduct or an intermediate is solid. In the previous chapter, the inability of typical microreactors to handle processes involving solids in different capacities were discussed. In addition to that, the sheer importance of handling such processes in microreactors to fulfil the true potential of the flow chemistry was also discussed in detail. Apart from popular

examples in organic synthesis, many important processes such reactive and antisolvent precipitation involve more than one phase, and in several cases the reactions are instantaneous, and they generate solids at the interface. A study conducted by Roberge et al.[1] in the last decade illustrated the understand and handle the flow of solids in microchannels.

The clogging process is extremely complicated and stochastic as it entails various complex inter-dependent phenomena. A few excellent reports on clogging of small channels acknowledge the complexity involved in this phenomena [2-4]. In addition to clogging, generation of solids also adds a new phase to the reaction mixture resulting in a change of flow regimes spatially. The three main hydrodynamic mechanisms causing clogging single-phase laminar flow were constriction, bridging and the random detachment of deposits [5]. In the previous chapter, further details on the formation of agglomerates or clusters were discussed. The rate of particle adhesion to the channel wall and growth was found to be dependent on Reynolds Number of the system. In addition to several experimental studies to understand clogging in microchannels, a few modelling studies involving stochastic and CFD-DEM modelling were also performed [6, 7]. While the literature discussed in the previous chapter helps to know possible mechanisms for clogging in microchannel, the majority are performed in micro-structured porous media and focused on single phase flow. Moreover, these studies do not help in developing a quantitative analysis of when to expect clogging in microchannels and the associated time scales for different flow regimes of multiphase flow. We lack even fundamental investigations on the interaction and transport of solids forming at the liquid-liquid interface, which makes the clogging process in multiphase flow to be considerably contrasting from single phase solid forming systems. In order to explore these features in a quantitative framework, the present work aims at exploring the clogging time for different flow regimes for a specific case of interfacial precipitation.

In the present work, solid particles were generated in the microchannels by means of antisolvent precipitation [8-11]. Use of an organic phase having solubility in the aqueous phase helps rapid precipitation of the solute (typically a water-soluble salt dissolved in the aqueous phase).

This chapter provides an insight into the microchannel clogging mechanism in liquid-liquid multiphase flow which has been hardly explored in the literature. The effect of flow rates of the fluids and capillary diameters on clogging time during interfacial precipitation was explored. This chapter also aimed at determining the influence of (i) various flow regimes and (ii) the associated dynamics viz. coalescence of slugs during the flow and the nature of interface on clogging time. In view of this, the present chapter is organized as follows: after Introduction, we have given the details of the experiments and the experimental set-up. Subsequently, effects of various parameters viz. flow regimes, shell formation interfacial area, coalescence and capillary number on clogging time is presented. A model is presented that helps to estimate the extent of mass transfer of anti-solvent into the solvent and predicts the solute equilibration time t_0, which can be correlated with the experimentally measured clogging time. The predictions of equilibrium time obtained from simulations were compared with the clogging time. Finally, we conclude by giving quantitative information that will help to select the right set of conditions that can help avoid clogging in such systems.

2.2. Experimental Section

The experiments aimed at observation of clogging and measurement of clogging time in straight glass capillaries. Saturated salt (NaCl) solution of water and acetone were pumped in the

capillary. Acetone acts as an antisolvent, and it resulted in salting out of NaCl particles along the capillary length. The process of precipitation goes through nucleation and growth stages. Beyond a certain particle size depending upon the flow rates, once the gravitational force/settling velocity becomes higher than the convective flow, the particles can settle in the capillary. Straight glass capillaries with a specific inlet arrangement (see Fig. 2.1) were used for these experiments. Among the three inlets, two were connected to syringe pumps (HO-SPLF 1, Holmarc Opto-Mechatronics) and the third inlet was connected to a digital manometer (HTC PM-6205, range 0.01-34 kPa) to monitor the transient pressure buildup as the capillary undergoes clogging. The saturated salt solution was introduced from the first inlet, and the antisolvent was introduced through the second inlet, which forms the continuous and dispersed phase, respectively. Fig. 2.1 shows the arrangement of the inlet section for both the phases, where the dispersed phase slugs/drops are sheared off by the cross-flowing continuous phase. Both, acetone and saturated salt solution were introduced in the capillary at equal flow rates (0.2 ml/min to 5 ml/min). With the above range of flow rates, it was possible to change the residence time in the capillary by 25 times. Capillaries of four different diameters ranging from 0.88 to 3.62 mm were used for these experiments and were positioned in a perfectly horizontal manner. The time when the fluids start flowing in to the channel to the time when the pressure build-up reached the tolerance criteria (30kPa), is considered as clogging time. A digital microscope with a high speed camera (Zeiss - Stereo Discovery v2.0) was used to get the images of precipitating interface and the nature of salt agglomeration. A high resolution camera (Sony SLT-A37K) was used for monitoring the liquid-liquid flow regimes and the time scales of precipitation resulting in clogging inside the capillaries. In order to monitor the interfacial precipitation happening over a specific slug as it moves in the capillary a double rail traversing system was used for mounting a camera (Sony) and it was moved along the length of

the capillary to track the slug continuously till it leaves the capillary. This arrangement helped to monitor the interfacial precipitation in real time along the capillary length. A backlight with a suitable antiglare diffuser was used for facilitating imaging.
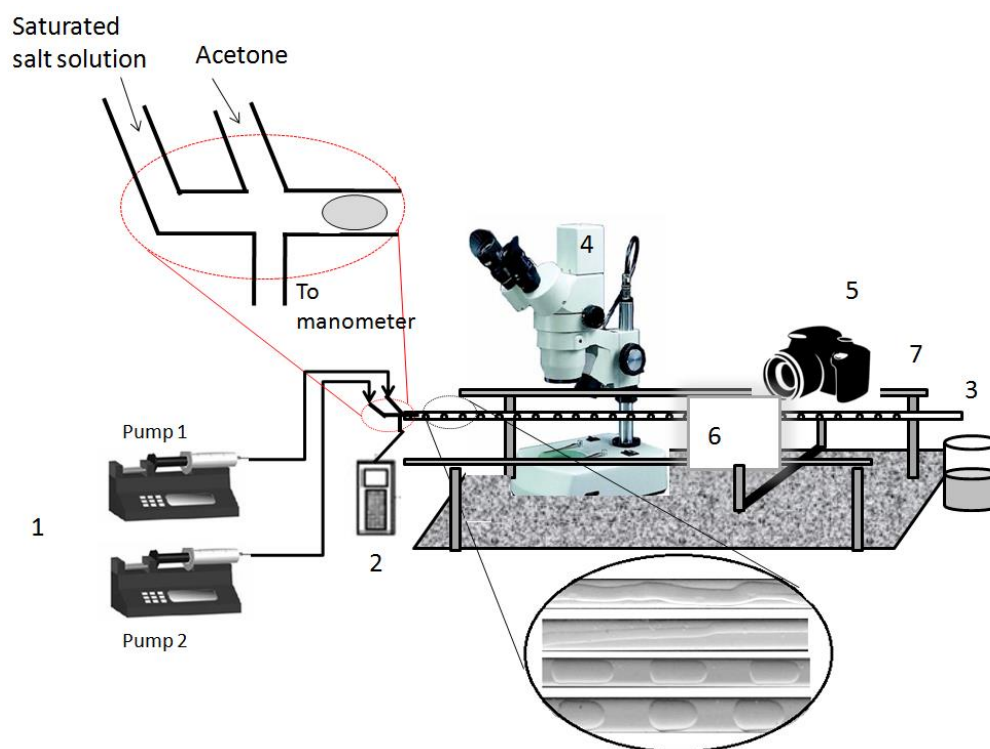
Fig.2.1. Schematic representation of the experimental setup for clogging visualization. (1) Syringe Pumps: Pump 1 for continuous phase (Sat. NaCl Solution), Pump 2 for Syringe Pump for dispersed phase (Acetone), (2) Manometer, (3) Glass capillary, (4) Digital microscope with high speed camera, (5) High resolution DSLR camera, (6) Back light source and diffuser and (7) Traversing system for lateral movement of the camera

All the images were analyzed using ImageJ (v1.47) and Virtual Dub (v1.10.4) software. The data was used to obtain the information on flow regimes, slug lengths, size of the precipitated crystals and the crystal shells. Experiments were performed several times, and the data was averaged over many slugs. Specific interfacial area of the slugs were calculated by image analysis

of the captured images. Slugs were assumed to be made of two hemispherical caps and a middle cylindrical section.

2.3. Results and Discussions

2.3.1. Flow regimes and clogging time

2.3.1.1. Flow Regimes

Extensive experiments were carried out to understand clogging inside the small straight capillaries in terms of clogging time (θ_{clog}). In the aqueous solution saturated with common salt, addition of acetone initially creates two immiscible phases. As explained in the previous chapter, different flow regimes were observed when the two solutions enter into the capillary depending upon the flow rates and the capillary diameter. The images of flow regimes captured at the inlet section (at 15 cm from the inlet of the 1 m long capillary) are shown in Fig. 2.2 and the flow regime map of the present system is shown in Fig. 2.3.

The experimental observations corresponding to the two-phase system undergoing spatiotemporal salting out effect in different capillary sizes are discussed subsequently. It was observed that the 0.88mm diameter capillary produced small droplets behind the slugs, which coalesce downstream at $Q_W = Q_{Ac} = 0.2$ mL/min. For the flow rates $1.0 < Q_T < 2.0$ mL/min, an unsteady parallel flow developed at the inlet contacting point and transitioned to slug flow downstream into the capillary channel. The regime transition point was observed to oscillate to some extent along the length of the capillary at fixed flow rates. At $Q_T = 2.8$ mL/min, slugs of non-uniform lengths were observed, while at higher flow rates viz. 4-10 mL/min, mostly annular flow was observed (See Fig. 2.3). In this kind of small diameter capillary, the effect of gravity was not

significant as film thickness at top and bottom of the continuous phase slugs was observed to be similar.

For the 1.43mm diameter capillary, stable and uniform slug flow was observed at 0.4 mL/min without any slug deformation, beyond which the slug detachment dynamics and the mass transfer near the inlet Y-joint together induced deformation in the slugs. This resulted in the generation of non-uniform size slugs. At higher flow rates, enhancement in mixing and interfacial mass transfer induced the precipitation rapidly thereby making the solution turbid. At the initial stage of nucleation, very small particles were seen to follow the flow path inside the water slug, which eventually grew. At $Q_T = 10$ ml/min, it resulted in parallel flow with wavy interface resulting in rapid precipitation of salt giving slurry, which eventually agglomerated and clogged the channel.

In 1.90mm diameter capillary, stable and uniform slug flow was observed at low flow rates (~ 0.5 mL/min) but due to coalescence slug sizes changed downstream. For $Q_T = 1.4$ to 2.8 mL/min, parallel flow with wavy interface (PFWT) was observed at the orifice for acetone, which eventually got transitioned into the slug flow over a distance of 0.2 to 0.3 m. This slug flow remained stable for almost equal distance and then once again for transitioned into PFWT. In such a situation, the precipitated particles formed solid shells/hemispherical caps at the rear of the acetone slugs. The length of these caps was smaller than those formed in smaller diameter capillaries. Interestingly, at $Q_T = 2.8$ mL/min, the shells detached very easily from the interface and came off into the continuous phase. At higher flow rates beyond 4 ml/min, parallel flow was observed and salting out was almost instantaneous with several small particles throughout the capillary. With rapid nucleation and growth of particles and decreasing overall density of the liquid (due to the dissolution of acetone in water), particles tend to settler rather rapidly thereby resulting in faster clogging of the channels.

For the largest capillary under consideration, i.e. 3.62 mm diameter capillary, at all the flow rates under consideration, stable parallel flow was observed with a relatively smoother interface (PFST). A layer of precipitated NaCl was found to be formed at the interface while some of the particles were sedimented at the bottom capillary surface. Since the capillary was larger in size, clogging was not observed for a sufficiently longer span.

To summarize, slug flow is observed in smaller capillary diameters for a total flow rate of 2.8 ml/min. The relative variation between the interfacial tension, gravity and convection led to different regimes. These flow regimes would vary eventually along the capillary length of the capillary as the inward mass transfer of acetone would increase the length of continuous aqueous phase while the salting out will decrease the viscosity of the aqueous phase. These effects will change the interface tension from the inlet to outlet thereby showing different flow regimes. These observations vary for individual capillary diameter and the flow rate ranges. It is desirable to compare them in terms of dimensionless numbers (viz. Bond number $Bo = [gL^2 \Delta \rho]/\sigma$, which signifies the ratio of gravitational force to surface tension force) that will facilitate to draw some design and operational guidelines [12]. L is the characteristic length, which is the capillary diameter d in the present system. For a fixed density difference and interfacial tension, the value of numerator will increase in proportion to d^2, which implies that with an increase in the capillary diameter gravitational force becomes stronger and leads to layer separation, i.e. parallel flow. For example, Fig. 2.4 shows that for the 0.88 mm diameter capillary, gravitational force is relatively negligible (5% of surface tension force) when compared with the 3.62 mm capillary, where it is quite comparable with surface tension force (85%). Thus, two-phase flow in smaller diameter capillaries will preferably result into slug flow and larger capillaries would always result in parallel flow.

d (mm)→ Q$_T$(mL/ min)↓	0.88mm	1.43mm	1.90mm	3.62mm
0.4				
0.8				
1.0				
1.4				
2.0				
2.8				
4				
10				

Fig. 2.2: Flow regimes at a distance of 15cm from the inlet of the capillary.
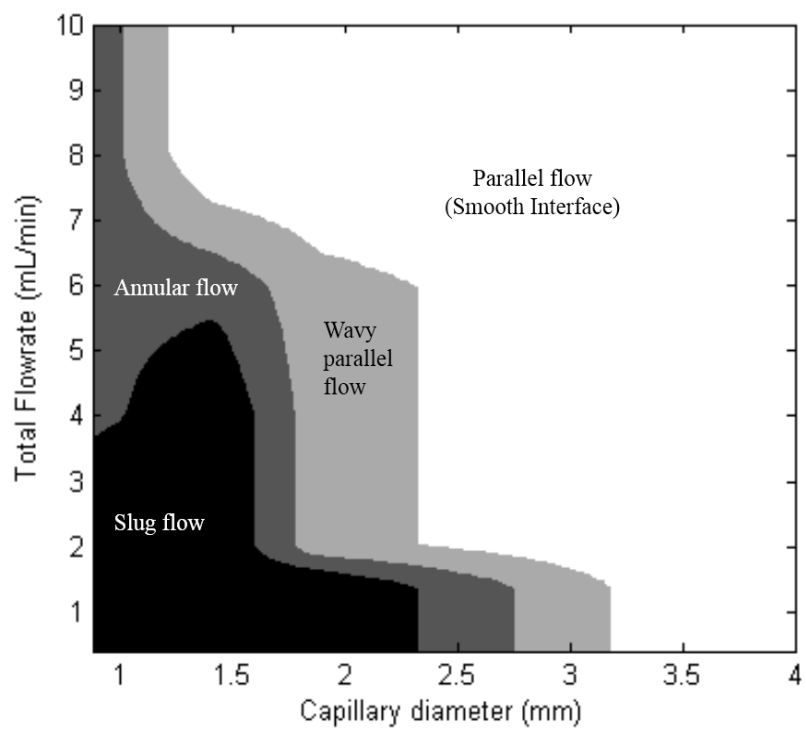
Fig. 2.3: Flow regime map at the inlet section of the capillary
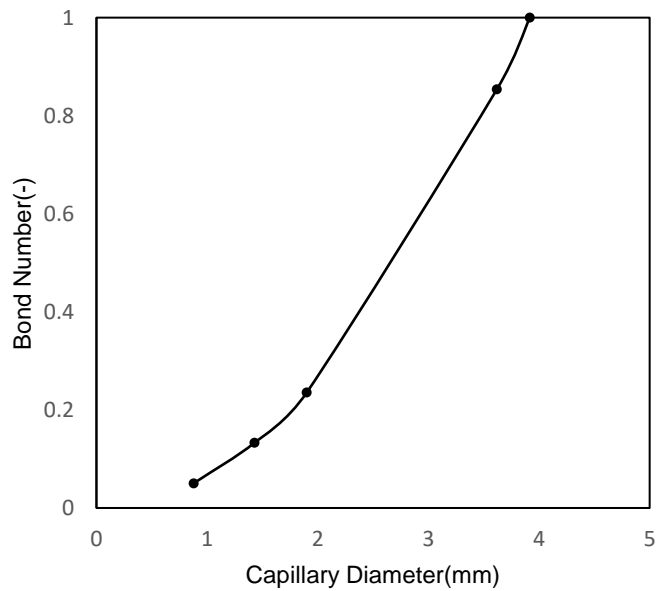
Fig. 2.4: Bond number for different capillary diameters

2.3.1.2. Solid formation in different flow regimes

At lower flow rates (0.4 - 0.6 ml/min of each phase) rectangular crystals of sizes between 40-280 μm are formed at the tail of the acetone slugs (see Fig 2.7a). It was observed that during the course of interfacial precipitation in the slug flow regime, the salt crystals are accumulated at the rear end of the slug and the local hydrodynamics induce them to form hemispherical shells, which grow towards the front as the slugs approach towards the outlet. Understanding the hydrodynamics of liquid-liquid slug flow is important in understanding the particle precipitation and clogging phenomena. Internal circulation in the dispersed phase slugs plays a deciding role in solid particle deposition and aggregation. Presence of multiple co-rotating asymmetric vortices located at the front and rear of the plug is reported in the literature [13]. The spatial disparities in Laplace pressure between the front and rear end of the hemispherical caps and the centre of the slug play a significant role in plug deformation, the spatial variation of film thickness, establishing the flow patterns within the plug.

Fig. 2.5a demonstrates the bulging of the acetone slugs near the hemispherical caps reduce the film thickness of the wetting phase i.e. saturated aqueous NaCl solution. A small decrease in the film thickness causes a local increase in the tangential shear force resulting in circulating flow in the cap regions that confirms the observations from the literature (Fig. 2.5b) resulting from the asymmetric Laplace vortices. Due to reverse alignment of the internal vortices and high shear rate near the film the precipitated particles of sodium chloride travels to the stagnation zone at the back, starts aggregating and forms a shell subsequently. As the slug moves through the capillary a comparatively thin and small shell starts forming at the front of the slugs due to the front cap vortices. However, in most cases, the residence time of the slugs inside the capillary is less than the time required to form a front shell. As the slugs advance along the capillary, the film thickness reduces resulting in higher shear in the film, which subsequently releases the solid shells formed at the back of the slugs.
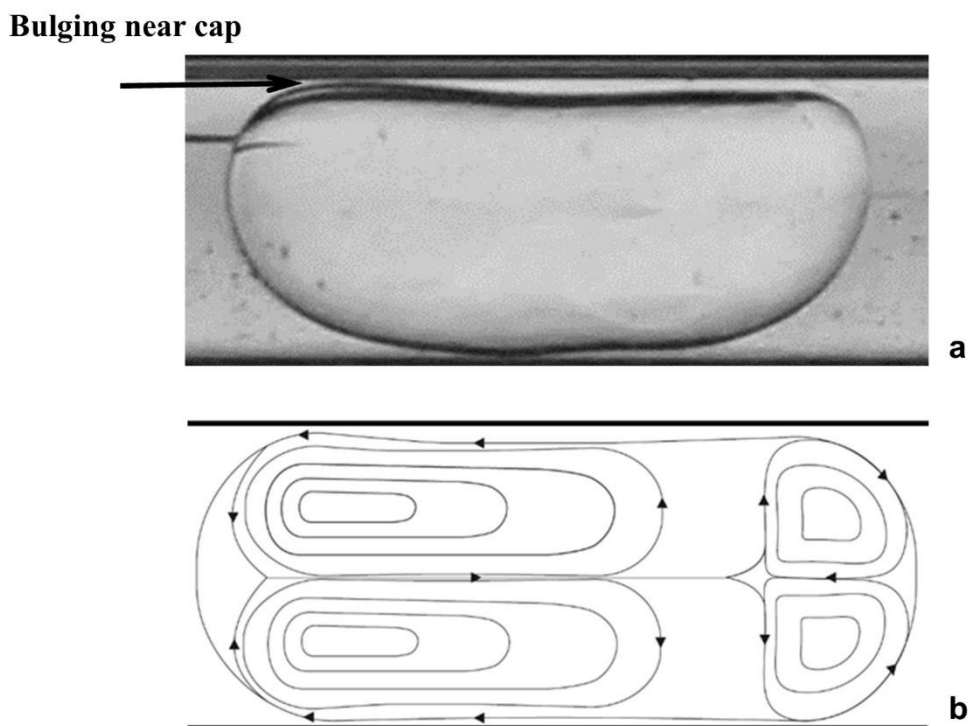
Bulging near cap

Fig. 2.5. (a) Bulging of the acetone slugs near the front and rear caps (1.43mm capillary diameter and 0.5ml/min flow rate of water and acetone); (b) Schematic of Laplace vortices which develop in a plug as it moves through the channel [14]. Flow is from left to right.

Fig. 2.6 shows that as the slugs move along the capillary, the shells expand to the front side of the slugs and eventually gets detached from it. Usually, lower superficial velocity (in higher diameter capillaries) results in thinner films, which imply poor internal circulation and hence poor interfacial mass transfer. This results in slow salting out, and hence no visible shell formation is evident. Moreover, the fragility of shells or their non-cohesiveness increases with increasing capillary channel diameter.

When the length of these shells was 30 to 40% of the slug length, they detached very easily from the interface and came off into the continuous phase. Internal circulation in the dispersed phase pushes all the particles in the rear section of a slug. Since the low-pressure
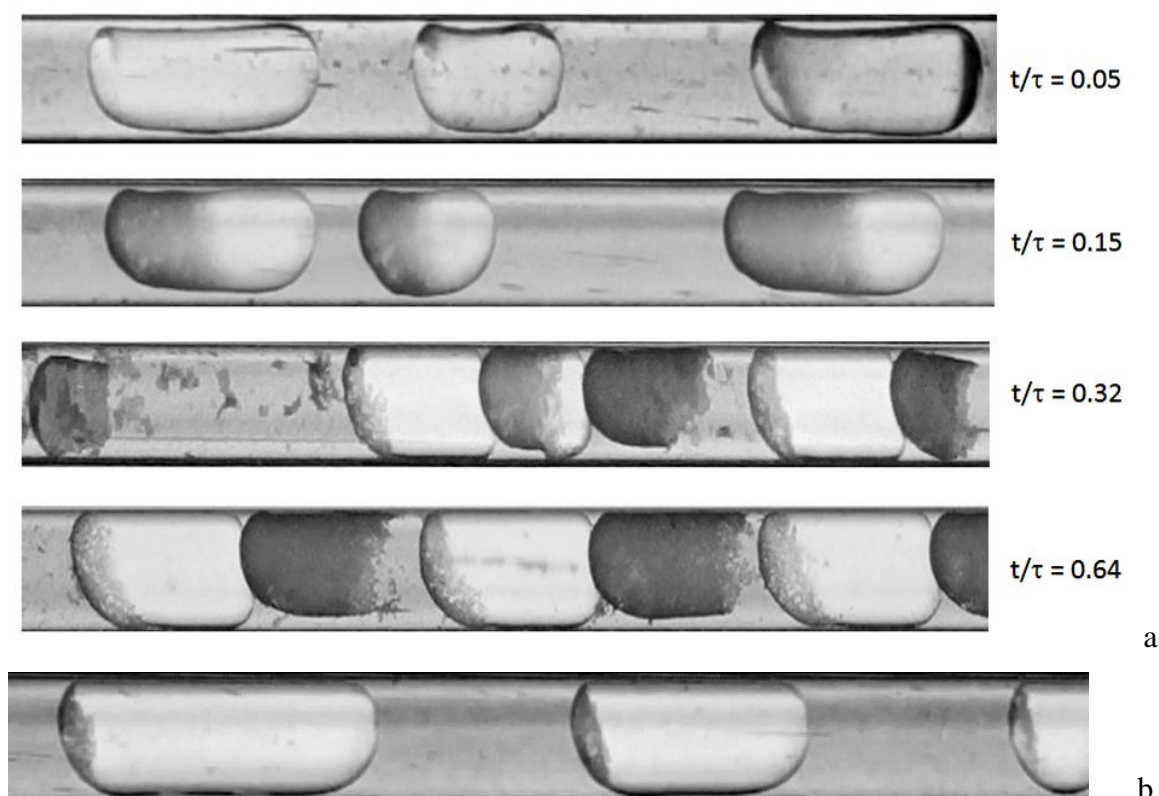
Fig. 2.6: (a) Different stages of formation, detachment and re-precipitation of shells at the rear cap of the slugs for 1.43mm capillary diameter and 0.5ml/min flow rate of continuous and dispersed phase, (b) Shell formation at the rear of the dispersed phase slugs at 500 mm from the inlet in 1.9 mm diameter capillary at 0.5 ml/min flow rates of continuous and dispersed phase. Flow is from left to right.

zones act as cusps [14] [15] and it is difficult for the individual particles to escape from there and they continue to grow in size and also form a network. Eventually, as the slugs travel, they grow sufficiently (in the form of a half capsule) and being heavier (ρ_{NaCl} = 2170 kg/m^3) than both the phases, they would try to settle and overcome the interface forces. Thus the relative dominance of individual forces acting on particles follows a sequence of phenomena viz. (i) inertial forces when they are tiny (nucleated and visible) make them follow the streamline in the continuous phase, (ii) pressure forces when they grow and enter in the low-pressure zone of the continuous phase, (iii) interfacial forces when further grown particles get entrained in the interface, (iv) adhesion forces between the nucleating and growing particles making them

form a network of particles while staying at the interface, (v) inertial force that allows these shells to get detached from the dispersed phase and finally (vi) the gravitational force that overcomes the interfacial and pressure forces and allows the shell to settle in the capillary. In the slug flow regime, pressure gradient over the surface of a slug increases with increasing flow rates [16]. The detached shells further undergo associative growth and form clusters in the continuous aqueous phase. As more and more acetone gets dissolved in water, the acetone phase disappears, and the overall density of the liquid phase decreases significantly. These two effects are happening simultaneously in the capillary result in rapid settling of salt shells. Though the precipitation inception time varied over a wide range of flow rates and flow regimes, the aggregation of shells inevitably generates closed packed clusters, which subsequently result in clogging of the capillary.

At higher flow rates (>4 ml/min) parallel flow was observed, and higher superficial velocity enhances the shear at the interface between the two phases, which further induces rapid mass transfer, faster nucleation and growth. With rapid nucleation and growth of particles and decreasing overall density of the liquid (due to the dissolution of acetone in water), several small particles tend to settle down rapidly throughout the capillary, thereby resulting in faster clogging of the channels. Fig. 2.7 shows different solid formation pattern in different flow regimes.
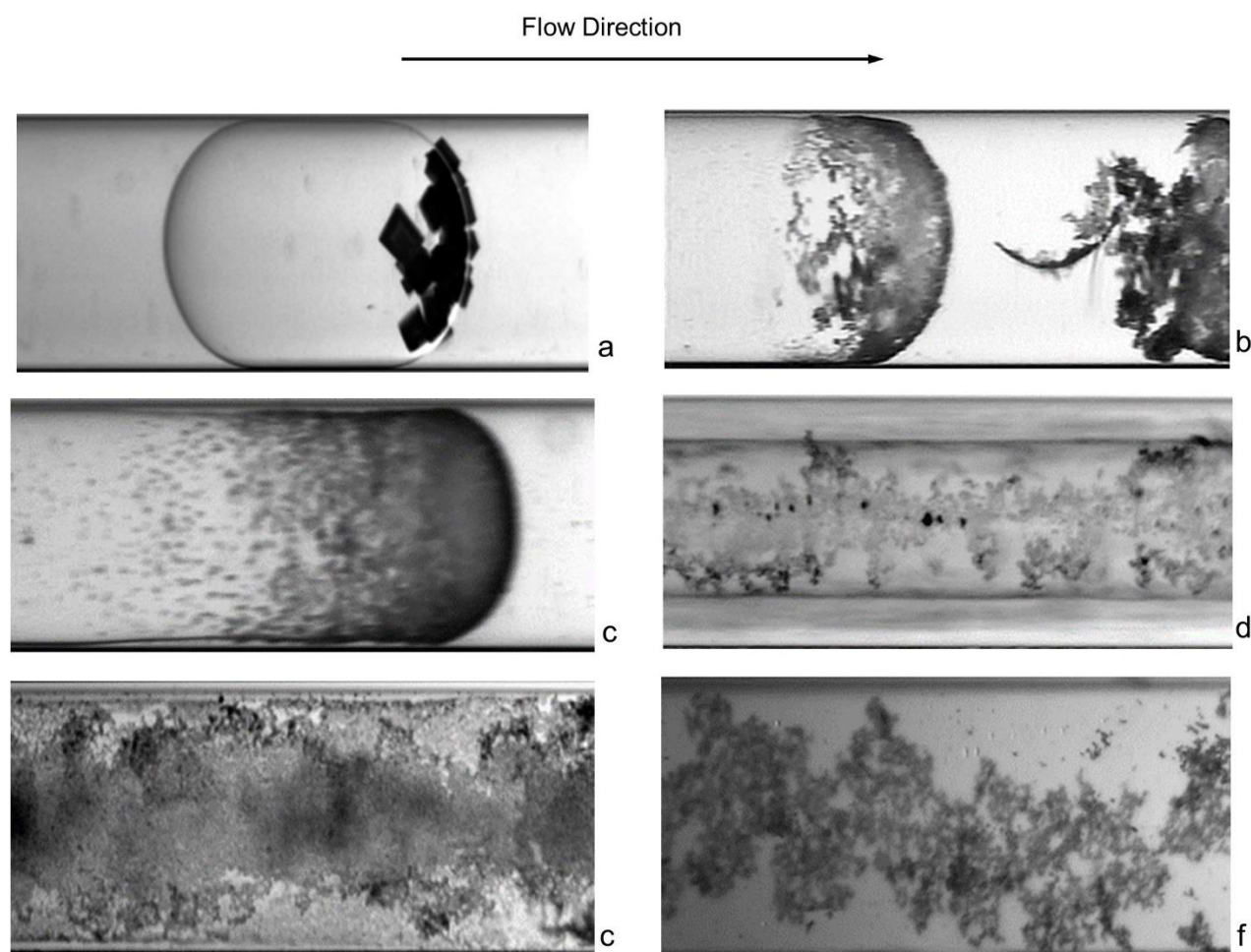
Fig. 2.7: Micrographs of sodium chloride crystals and shells formed in various flow regimes : (a) Particle formation in slug flow, (b) and (c) Shell formation at rear end of slugs in slug flow, (d) Particle formation at annular interface, (e) and (f) Sheet formation in along the interface in parallel flow

2.3.1.3. Clogging Time

In order to find the relationship between the clogging time and the flow regimes at the inlet section of the capillary, experiments were carried out over a wide range of flow rates and capillary diameters until the capillary is clogged. Fig. 2.8 shows the variation in θ_{clog} for different capillary diameters and total flow rate (of pure acetone and saturated aqueous NaCl solution). The data plotted over the regime map helps to identify the boundaries between the

three main flow regimes viz. slug flow, parallel flow and annular flow. The analysis showed that both, θ_{clog} as well as the rate of reduction in θ_{clog} decreased with increasing flow rate. This implies that higher flow rates lead to faster clogging. Also, the enhancement in the flow rates results in a nonlinear variation in the reduction in θ_{clog}.

In general, in slug flow and parallel flow regimes, the clogging time showed power law behaviour with flow rate. The nature of variation was similar for all the capillaries used in this work, and the slope was independent of flow regime. Typical behaviour followed the below correlations:

$$\log(\theta_{clog}) = 4.3 - (0.02d\text{-}0.83)\log(Re) \tag{2.1}$$
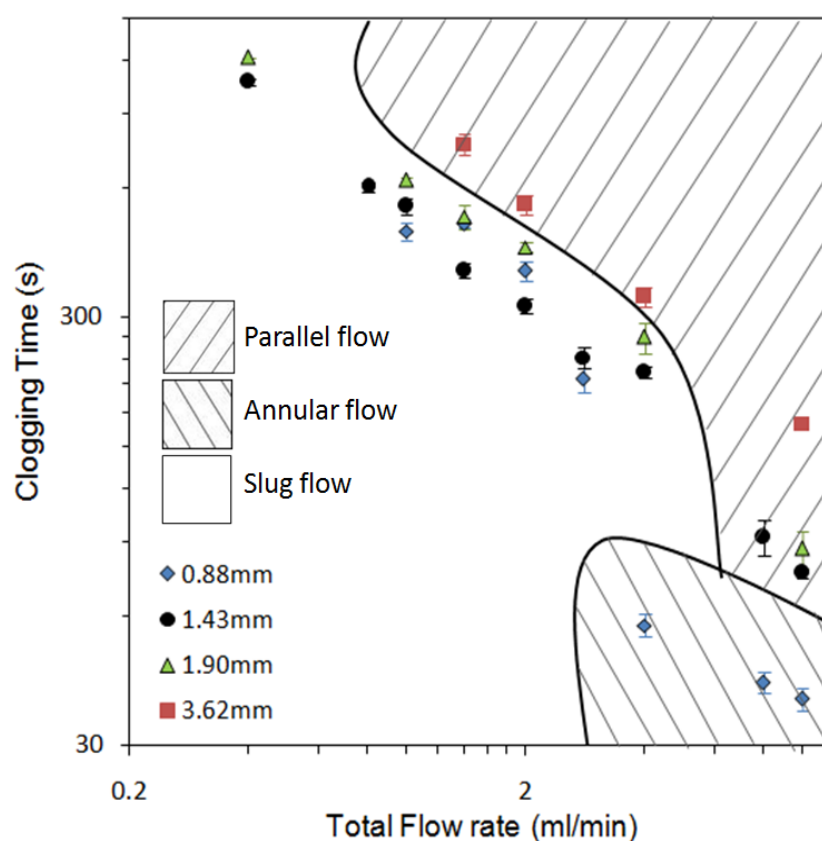
Fig. 2.8. Change of clogging time with total flow rate for capillaries of different diameter (The legends show the capillary diameters). At a fixed flow rate we get different flow regimes in capillaries of different diameter as the importance of surface tension forces compared to body forces/gravity forces increases with decreasing capillary diameter

Here Re is the mixture Re estimated using capillary diameter (d) and total flow rate of the two phases. At identical flow rate, the smallest diameter capillary had the shortest θ_{clog}. In other words, at a constant flow rate, the smallest diameter capillary would have the highest velocity and hence the highest shear rate, which would result in extremely rapid mass transfer between the two phases. For the range of flow rates under consideration, shear rates were calculated using Equation 2 [17]:

$$\gamma = \frac{8u}{d} = \frac{32Q_T}{\pi d^3} \qquad (2.2)$$

For 0.88 mm and 3.62 mm capillaries the shear rate was seen to vary from 99.7 to 2492.4 s^{-1} and 1.43 to 35.8 s^{-1}, respectively. This variation in the shear rate supports smaller θ_{clog} for smaller capillary as well as at the higher flow rates. The effect of flow regimes on clogging dynamics is discussed separately.

2.3.2. Effect of interfacial area

For the present example of interfacial precipitation, the specific interfacial area for mass transfer plays a decisive role in determining the clogging time. Interfacial mass transfer of the antisolvent to the aqueous phase leads to nucleation, growth, crystallization, cluster formation, phase separation, settling of solid particles, possible adhesion during growth on the channel surface and eventually clogging of the capillaries. Also due to mass transfer, the effective interfacial area of the dispersed phase (antisolvent) per unit volume of dispersed phase continues to increase from inlet to the outlet. Thus, along the capillary length, the concentration gradient would decrease while the interfacial area increases. This would allow the flux across the interface to go through a maximum, depending upon the flow regime. A variety of flow regimes (viz. slug, parallel, annular etc.) observed during the experiments result in a significant difference in specific interfacial area under various operating conditions. The interfacial area is measured by post-processing of the images captured at a distance of 15 cm from the inlet

and plotted as a function of total flow rate (Fig. 2.9) At identical total flow rates, capillary with smaller diameter resulted in higher interfacial area. Among all the observed flow regimes slug flow is witnessed over a wide range of flow rates. It is known that internal circulation in the slugs enhances the diffusive mass transport between the two phases and the mass transfer rates increases with increasing flow rates [18-20]. Thus, higher interfacial area and higher circulation rates, both help in rapid interfacial mass transfer and precipitation, respectively, which results in faster salting out effects. However, with increased flow rate the residence time also decreases and it gives lesser time for mass transfer. These counteracting effects on mass transfer work simultaneously. Nevertheless, the first effect becomes quite predominant and subsequently increases the rate of precipitation, which results in faster clogging of the capillary with increasing flow rate.
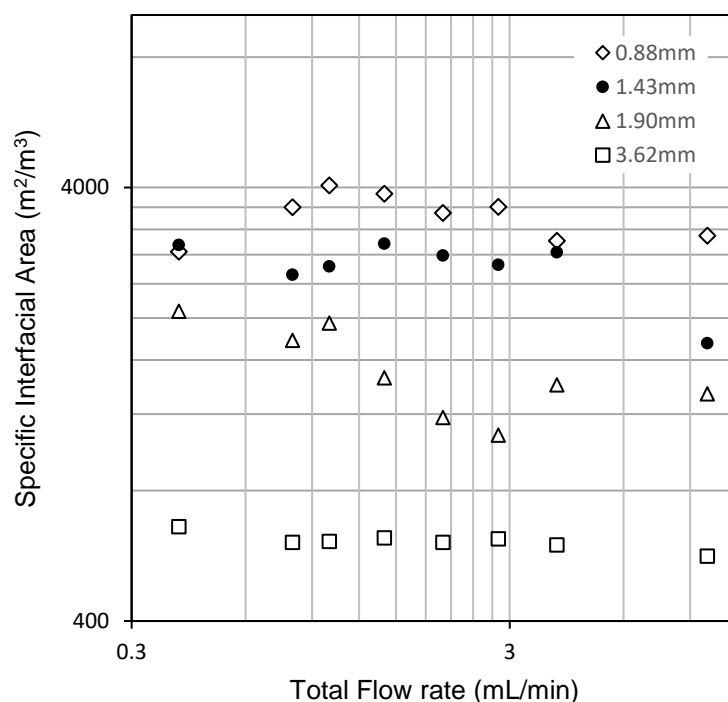
Fig. 2.9. Specific interfacial area in different capillaries and flow rates (in different flow regimes)

In 0.88 mm, 1.43 mm and 1.90 mm diameter capillaries, an unstable parallel flow formed at the inlet, which subsequently formed slugs and drops downstream in the channel for flow rates

beyond 0.5 ml/min. The aforementioned transition/breakage point was observed to move downstream of the capillary with increasing flow rates. Similar observations are reported in the literature for cross-flowing shear induced droplet formation in T-junctions [21]. At higher flow rates (i.e. 3 – 5 ml/min) annular flow is observed instead of slug flow or parallel flow only for the case of the smallest diameter capillary (0.88mm). Annular flow regime provides a higher interfacial area between the two phases ensuring increased precipitation rate and lowers the clogging time. Moreover, in the annular regime, acetone forms the core, which keeps revolving or oscillating and also reduced in size from inlet to the outlet (Fig. 2.10). These effects together result in rapid settling of salt particles precipitated in the annulus and clogs the capillary relatively faster. For 1.43 mm and 1.9 mm diameter capillaries the flow regime was mostly slug flow.

(a)

(b)

(c)

(d)
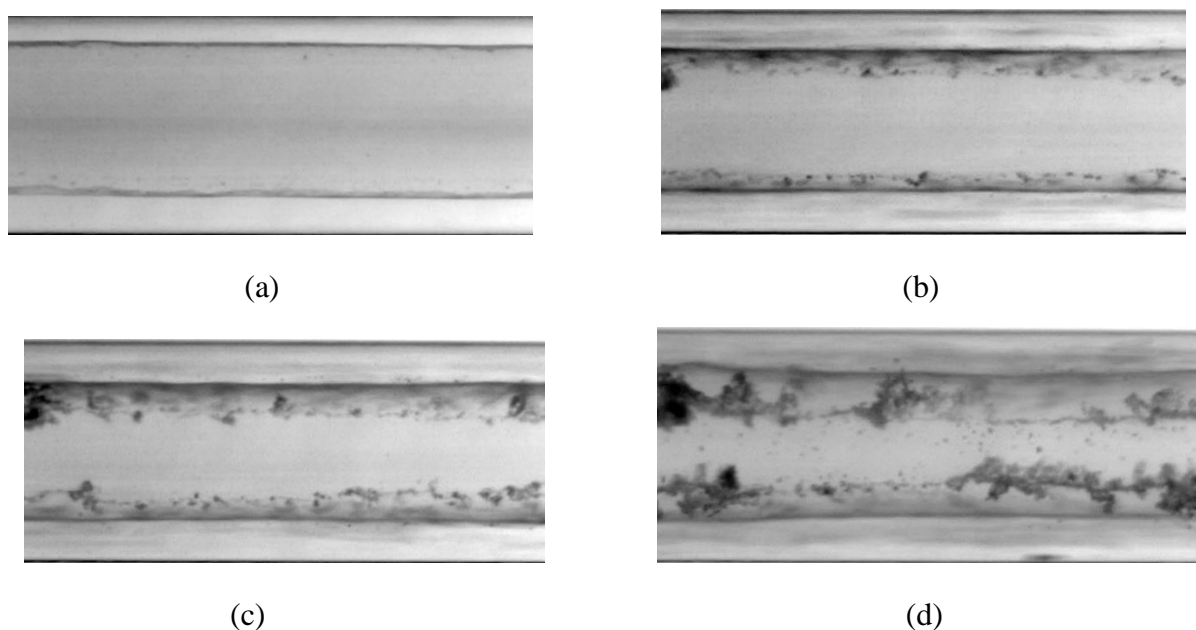
Fig. 2.10. Reduction in core size with time for the case of annular flow (4 ml/min total flow rate in 0.88 mm diameter capillary). (a) → (b) → (c) → (d) with increasing time. (a) 0.601 mm, (b) 0.554 mm, (c) 0.539 mm, (d) 0.528 mm

The clogging times for capillary with larger diameter (viz. 3.62 mm) was observed to be significantly higher than the smaller capillaries. This is due to the regime with the stable

parallel flow with a smooth interface, which provides a lower specific interfacial area, lower shear at the interface and lower mass transfer than slug flow, annular flow and even parallel flow with wavy interface (Fig. 2.11). The motion due to the wavy interface affects the boundary layer and perturbations forming at the interface significantly increases the mass transfer compared to a parallel flow with a smooth interface. These phenomena were highly reproducible in larger capillaries.

(a)

(b)
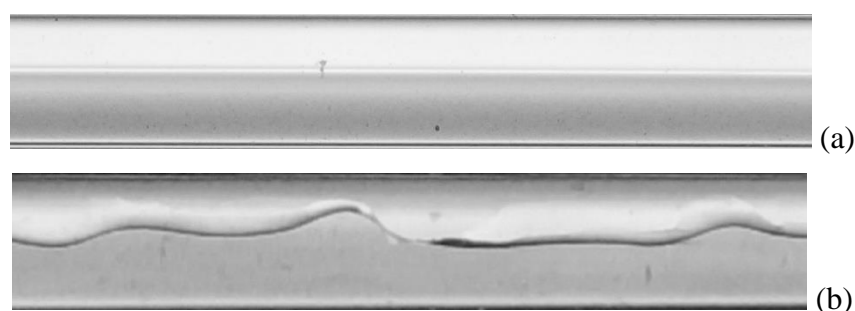
Fig.2.11. (a) Stable parallel flow with smooth interface in 3.62 mm diameter capillary, (b) Unstable parallel flow with wavy interface in 1.90 mm diameter capillary. For both the cases the total inlet flow rate is 1.4 mL/min.

2.3.3. Effect of Coalescence of slugs

Coalescence is the process by which two or more dispersed phase bubbles/ slugs or droplets merge while contacting resulting in formation of a single daughter phase. At the initiation of the flow of the two phases, the detachment and movement of the slugs were uninterrupted, and their coalescence was found to be very rare. The inception of interfacial precipitation actually resulted in momentary interruption of the flow of slugs destabilizing the flow. The solid formation dynamics at the downstream of a capillary showed interesting backward effects on upstream. Transient variation in the physical properties of the continuous phase and enhanced drag of the dispersed phase (due to accumulation of salt at the rear end) slow down the slug with more accumulated salt in its rear, which gets coalesced upon coming in contact with the next slug. In addition to this, pressure waves generated during such

coalescence events happening at the downstream of the capillary disturbs the steady flow of the upstream slugs and induce a cascade of similar events resulting in the destabilization of the entire slug assembly. Moreover, the salt particles in consecutive water slugs accumulate into a single large slug due to coalescence of acetone slugs, which further leads to a densely packed structure that subsequently clogs the capillary. A schematic representation of this has been presented in Fig. 2.12. At higher flow rates, coalescence was seen to be an effect of non-uniform slug lengths. Higher degree of coalescence at higher flow rates causes a reduction in clogging time.

Direction of flow

(a)

(b)

(c)

(d)
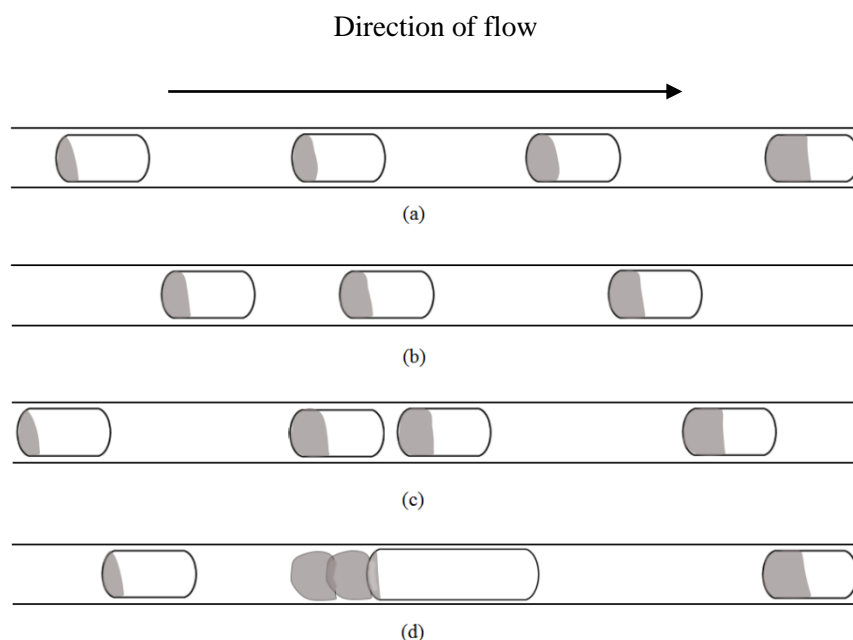
Fig. 2.12. Schematic representing coalescence of slugs favoring clogging. (a) → (b) → (c) → (d) with increasing time

2.3.4. Effect of Capillary Number

The capillary number ($Ca\sim$) represents the relative effect of viscous forces vs. interfacial tension forces acting across an interface between two immiscible liquids. Although water and acetone are miscible, saturated aqueous solution of sodium chloride and pure acetone are only partially miscible (without salting out) and form slug flow in a capillary. Higher Ca

led to faster clogging (Fig. 2.13). The change in the flow regime induced a rapid decrease in clogging time at higher Ca. Kurup et al. have reported that for liquid-liquid slug flow for 0.0001 < Ca <0.01, medium size slugs deform due to the Laplace pressure difference alongside the length of the slugs. Higher Ca corresponds to higher velocity in the capillary where the vortices become smaller in front and wider at the rear of the slug due to the increase in shear forces and deformation of the slugs [14]. This vigorous motion at the rear end of slug leads to a reduction in the tendency of formation of the solid shells. In such a situation instead of shell formation, associative growth followed by cluster formation of precipitated salt particles takes place in the continuous aqueous phase leading to relatively faster clogging. In view of this, smaller Ca would help to avoid induction of rapid clogging in the capillaries, which imply lower velocity or use of smaller capillary length or using continuous fluid of relatively higher viscosity or lower interfacial tension. While the later two parameters are governed by the system under consideration, change of velocity (and even capillary diameter) or capillary length are relatively easy to avoid clogging.
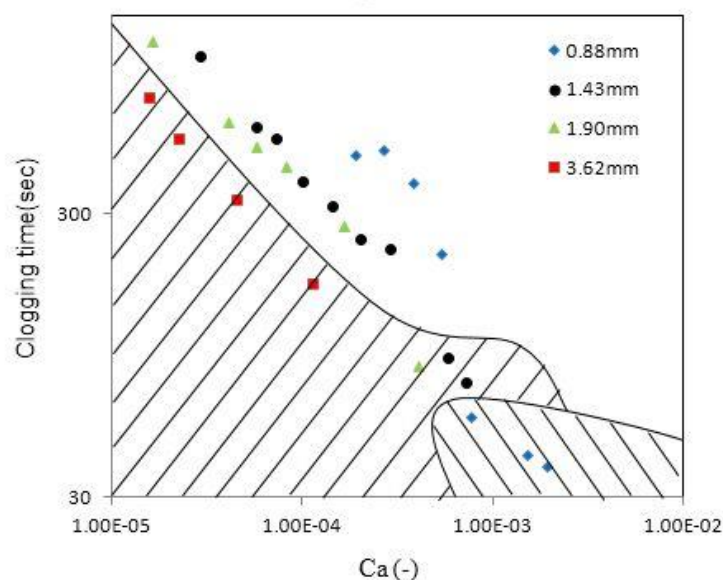
Fig. 2.13. Effect of continuous phase capillary number (Ca_c) on clogging time for capillaries of different diameter. Inset shows capillary diameters. Thin slanted lines correspond to the

region of parallel flow, thick slanted lines correspond to annular flow and open area corresponds to the slug flow.

2.3.5. Prediction of Equilibrium Time

The salting out phenomena due to dissolution of acetone in the saturated solution of salt mainly happens due to mass transfer of acetone. The extent of mass transfer and the rate of mass transfer govern the rate of precipitation and hence the clogging time. In order to predict the clogging time in a capillary in such situations here, we have developed a model that can help to predict the transient precipitation kinetics. The predicted time needed to achieve complete saturation of the continuous phase with acetone was compared with the experimentally measured clogging time. The moles of salt that precipitate for given moles of acetone that dissolve in the initially saturated salt solution in water were precisely calibrated and used to predict the amount of salt that is precipitated for a corresponding amount of acetone mass that has got transferred to the aqueous phase.

The model system comprised of a control volume comprising of two dispersed phase liquid half slugs (acetone) surrounded by the film of the continuous phase and one continuous phase liquid slug (saturated sodium chloride solution). All simulations were performed considering constant ratio of flow rates of aqueous sodium chloride solution and acetone over a flow rate range of 0.2 ml/min to 5 ml/min. Capillaries of diameters (d) ranging from 0.88 mm to 3.62 mm were used. The slug length has been assumed from a correlation in the literature [22]. The solution domain used and boundary conditions are represented in Fig. 2.14.
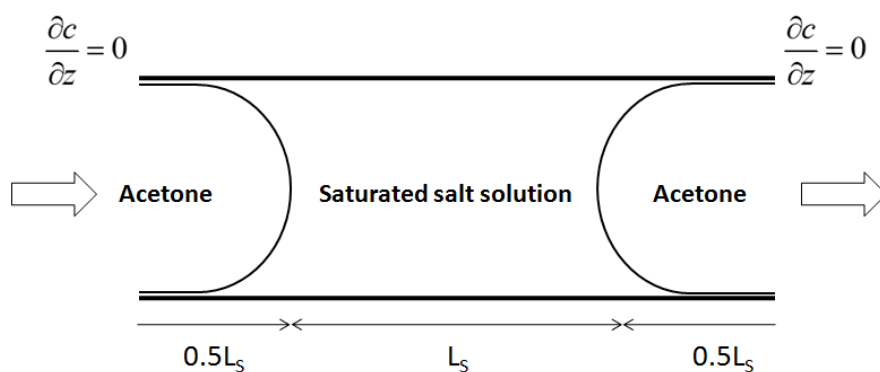
Fig. 2.14. Control volume for model and boundary conditions

The convection-diffusion equation (see equation 2.3) with appropriate diffusion coefficient, mass transfer coefficient and superficial velocity for the estimation of the extent of mass transfer of dispersed phase (acetone) slug into the continuous phase (saturated NaCl solution).

$$\frac{dc}{dt} = D\frac{\partial^2 c}{\partial z^2} - u\frac{\partial c}{\partial z} - K_l a\left(c - c_{eq}\right) \tag{2.3}$$

The initial boundary conditions at $t = 0$ include the $c_{acetone}$ as 13.6 kmol/m^3 in the acetone slug and zero in continuous aqueous NaCl solution. No flux boundary condition was used at both the boundaries of dispersed phase half liquid slugs. Mass transfer coefficient for different flow rates and diameter were obtained using correlation (Equation 3) from the literature and shown in equation 2.4 [23, 24].

$$K_L a = \frac{0.111 U_d^{1.19}}{\left((1-\varepsilon_d)L_{UC}\right)^{0.57}} \tag{2.4}$$

Equation 2.3 was solved in MATLAB$^®$ for the acetone concentration (c) in the continuous phase, using the above stated initial and the boundary conditions. The results are shown in Fig. 2.15. The temporal change in the average concentration of acetone in the

continuous aqueous slug was simulated, and it was found to reach a plateau, which corresponds to the equilibrium time for mass transfer between the two phases. Equilibrium time for all the experiments at different flow rates using different capillary diameter were estimated and compared with the experimentally measured clogging time.
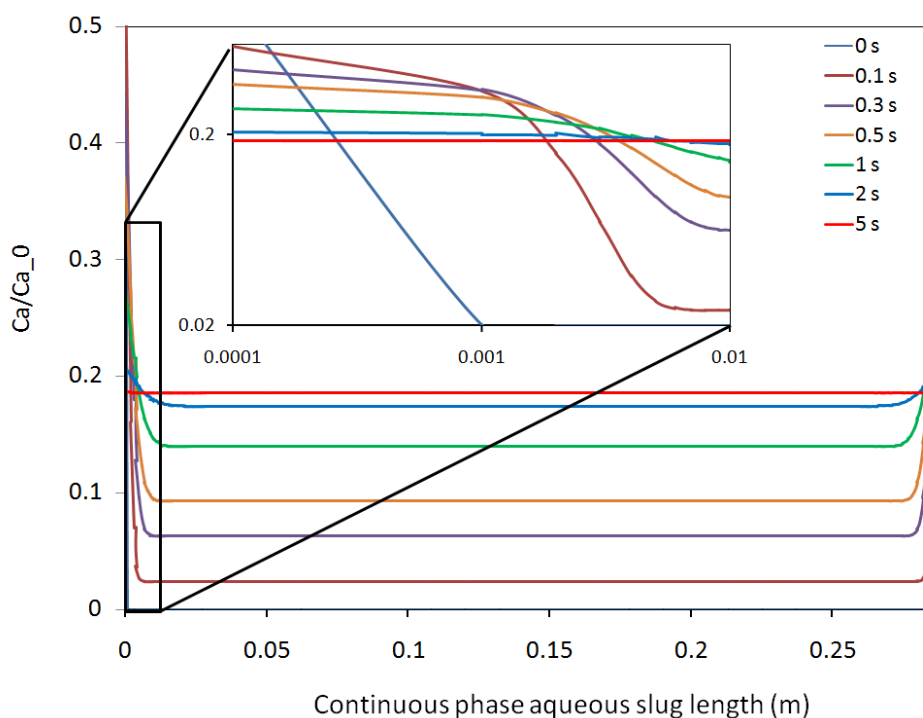
Fig. 2.15. Transient dimensionless acetone concentration profile along the length of the continuous phase NaCl solution slug (d = 1.43 mm and Q_T = 0.5 mL/min).

Fig. 2.16 shows the change of the equilibrium time with the total flow rate for cylindrical capillaries of 0.88mm to 3.62 mm diameter. The trend of equilibrium time achieved from the model is similar to the trend of experimental clogging time as a function of total flow rate shown in Fig. 2.8. We can observe that though the equilibrium time follows the same trend as a function of total volumetric flow rate, the values of equilibrium times are quite smaller than clogging time. This indicates that although the mass transfer of acetone in aqueous phase is very fast, crystal formation, their motion and setting to block the capillary takes significantly longer time as the slugs move along the capillary length.
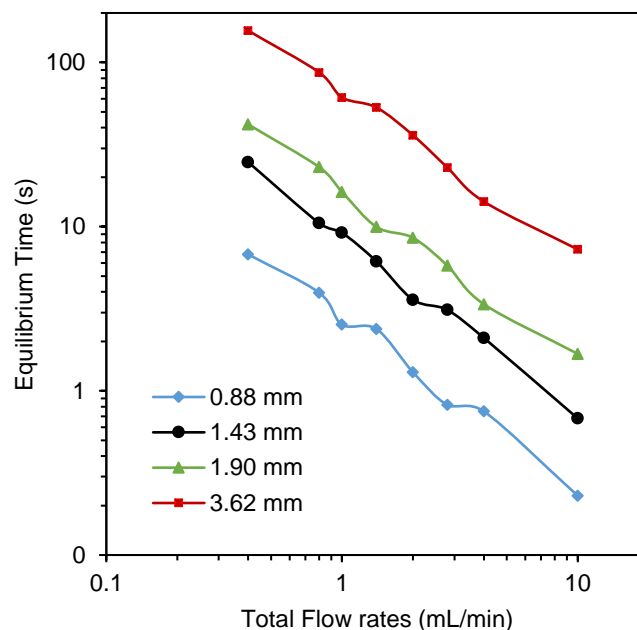
Fig. 2.16. Equilibrium time as a function of total flow rate for different capillary diameters.

2.4. Conclusion

Experiments were carried out to study the clogging time in straight capillaries of different diameters for a model system comprising of saturated salt solution and acetone for a range of conditions. Change in flow rates and capillary dimensions resulted in variation the flow regimes, interfacial area, Capillary number, internal circulation and the nature of the interface. In order to obtain real-time variation in the nature of flow, individual slugs were tracked in real time, and the nature of interfacial precipitation was used for understanding the clogging dynamics. In the slug flow regime, the precipitated particles formed solid shells/hemi spherical caps at the rear of acetone slugs and detached very easily from the interface and settled on the capillary wall surface. Subsequently, the detached shells undergo associative growth to form clusters. It has been clearly observed that the formation of stable shells at the rear of a slug was found to be favourable for delaying clogging in the capillaries.

For the case of parallel flow regime, if the interface is wavy, salting out was almost instantaneous with several small particles setting down throughout the capillary, which led to

faster clogging of the channels but for a smooth interface clogging time is comparatively higher due to slower mass transfer rate. In slug flow and parallel flow regimes, the clogging time showed power law behaviour with total flowrates. At a fixed flow rate, capillary with smaller diameter resulted in the higher interfacial area and got clogged faster. The relative rates of interfacial mass transfer, precipitation and the flow (i.e. residence time) govern the clogging dynamics. The simulations of the average concentration of acetone in the continuous aqueous slug showed that a steady state is reached within a few seconds of contact. This implies, interfacial mass transfer is quite fast and not the most effective factor in clogging, while crystal formation, growth and agglomeration, which subsequently block the capillary takes significantly longer time as the slugs travel. These experimental and modelling findings will be helpful in devising a methodology that will help to select the right set of conditions that can help avoid clogging in such systems. Though the variation in precipitation kinetics in another system will change the time scales of clogging, that change will be effective for all the experiments performed. So, the trends found for clogging time in this work are not bounded by this kinetic limitation. Building upon the present work, further studies were performed by comparing the effect of various clogging prevention methods on clogging time in the next chapter.

2.5. Notations

θ_{clog} Clogging time (s)

Q_T Total flow rate (ml/min)

Re   Reynolds Number (-)

Bo   Bond Number (-)

g   Gravitational acceleration(cm/s^2)

L   Characteristic length (cm)

d   Capillary Diameter (cm)

Δρ   Density difference between wetting and non-wetting phases (g/cc)

σ   Surface Tension (Dyne/cm)

γ   Shear rate (s^{-1})

c   Molar concentration (moles/cc)

D   Diffusivity (cm^2/s)

u   Superficial velocity (cm/s)

k_La   Overall mass transfer coefficient (s^{-1})

Ca   Continuous phase capillary number (-)

2.6. References

1.   Roberge, D.M., Ducry, L., Bieler, N., Cretton, P., and Zimmermann, B., *Microreactor technology: a revolution for the fine chemical and pharmaceutical industries?* Chemical Engineering & Technology: Industrial Chemistry-Plant Equipment-Process Engineering-Biotechnology, **2005**. 28(3): p. 318-323.

2.   Hartman, R.L., Naber, J.R., Zaborenko, N., Buchwald, S.L., and Jensen, K.F., *Overcoming the challenges of solid bridging and constriction during Pd-Catalyzed C−N bond formation in microreactors.* Organic Process Research & Development, **2010**. 14(6): p. 1347-1357.

3.   Sharp, K.V. and Adrian, R.J., *On flow-blocking particle structures in microtubes.* Microfluidics and Nanofluidics, **2005**. 1(4): p. 376-380.

4.   Wyss, H., Blair, D., Morris, J., Stone, H., and Weitz, D., *Mechanism for clogging of microchannels.* Physical Review E, **2006**. 74(6).

5.   Flowers, B.S. and Hartman, R.L., *Particle Handling Techniques in Microchemical Processes.* Challenges, **2012**. 3(2): p. 194-211.

6.   Shahzad, K., Van Aeken, W., Mottaghi, M., Kamyab, V.K., and Kuhn, S., *Aggregation and clogging phenomena of rigid microparticles in microfluidics.* Microfluidics and nanofluidics, **2018**. 22(9): p. 104.

7. Sauret, A., Somszor, K., Villermaux, E., and Dressaire, E., *Growth of clogs in parallel microchannels.* Physical Review Fluids, **2018**. 3(10): p. 104301.

8. Ali, H.S., Blagden, N., York, P., Amani, A., and Brook, T., *Artificial neural networks modelling the prednisolone nanoprecipitation in microfluidic reactors.* Eur J Pharm Sci, **2009**. 37(3-4): p. 514-22.

9. Zhu, W.-Z., Wang, J.-X., Shao, L., Zhang, H.-x., Zhang, Q.-x., and Chen, J.-F., *Liquid antisolvent preparation of amorphous cefuroxime axetil nanoparticles in a tube-in-tube microchannel reactor.* International journal of pharmaceutics, **2010**. 395(1): p. 260-265.

10. Zhao, H., Wang, J.-X., Wang, Q.-A., Chen, J.-F., and Yun, J., *Controlled liquid antisolvent precipitation of hydrophobic pharmaceutical nanoparticles in a microchannel reactor.* Industrial & Engineering Chemistry Research, **2007**. 46(24): p. 8229-8235.

11. Su, Y.F., Kim, H., Kovenklioglu, S., and Lee, W.Y., *Continuous nanoparticle production by microfluidic-based emulsion, mixing and crystallization.* Journal of Solid State Chemistry, **2007**. 180(9): p. 2625-2629.

12. Zhao, Y., Chen, G., and Yuan, Q., *Liquid-liquid two-phase flow patterns in a rectangular microchannel.* AIChE Journal, **2006**. 52(12): p. 4052-4060.

13. Kurup, G.K. and Basu, A.S., *Field-free particle focusing in microfluidic plugs.* Biomicrofluidics, **2012**. 6(2): p. 22008-2200810.

14. Kurup, G.K. and Basu, A.S., *Shape dependent Laplace vortices in deformed liquid-liquid slug flow.* Proceedings of the IEEE Engineering in Medicine and Biology Conference (EMBC), **2011**.

15.   Sarrazin, F., Loubiere, K., Prat, L., Gourdon, C., Bonometti, T., and Magnaudet, J., *Experimental and numerical study of droplets hydrodynamics in microchannels.* AIChE Journal, **2006**. 52(12): p. 4061-4070.

16.   Kreutzer, M.T., Kapteijn, F., Moulijn, J.A., Kleijn, C.R., and Heiszwolf, J.J., *Inertial and interfacial effects on pressure drop of Taylor flow in capillaries.* AIChE Journal, **2005**. 51(9): p. 2428-2440.

17.   Darby, R., *Chemical Engineering Fluid Mechanics, Revised and Expanded.* **2001**: Taylor & Francis.

18.   Kashid, M.N. and Agar, D.W., *Hydrodynamics of liquid–liquid slug flow capillary microreactor: Flow regimes, slug size and pressure drop.* Chemical Engineering Journal, **2007**. 131(1-3): p. 1-13.

19.   Ghaini, A., Kashid, M.N., and Agar, D.W., *Effective interfacial area for mass transfer in the liquid–liquid slug flow capillary microreactors.* Chemical Engineering and Processing: Process Intensification, **2010**. 49(4): p. 358-366.

20.   Kashid, M.N., Gerlach, I., Goetz, S., Franzke, J., Acker, J., Platte, F., Agar, D., and Turek, S., *Internal circulation within the liquid slugs of a liquid-liquid slug-flow capillary microreactor.* Industrial & engineering chemistry research, **2005**. 44(14): p. 5003-5010.

21.   Tice, J.D., Song, H., Lyon, A.D., and Ismagilov, R.F., *Formation of droplets and mixing in multiphase microfluidics at low values of the Reynolds and the capillary numbers.* Langmuir, **2003**. 19(22): p. 9127-9133.

22.   Garstecki, P., Fuerstman, M.J., Stone, H.A., and Whitesides, G.M., *Formation of droplets and bubbles in a microfluidic T-junction—scaling and mechanism of break-up.* Lab on a Chip, **2006**. 6(3): p. 437-446.

23. Berčič, G. and Pintar, A., *The role of gas bubbles and liquid slug lengths on mass transport in the Taylor flow through capillaries.* Chemical Engineering Science, **1997**. 52(21): p. 3709-3719.

24. Raimondi, N.D.M., Prat, L., Gourdon, C., and Tasselli, J., *Experiments of mass transfer with liquid–liquid slug flow in square microchannels.* Chemical Engineering Science, **2014**. 105: p. 169-178.

Chapter 3

Development and Quantitative Comparison of Strategies to Delay Clogging
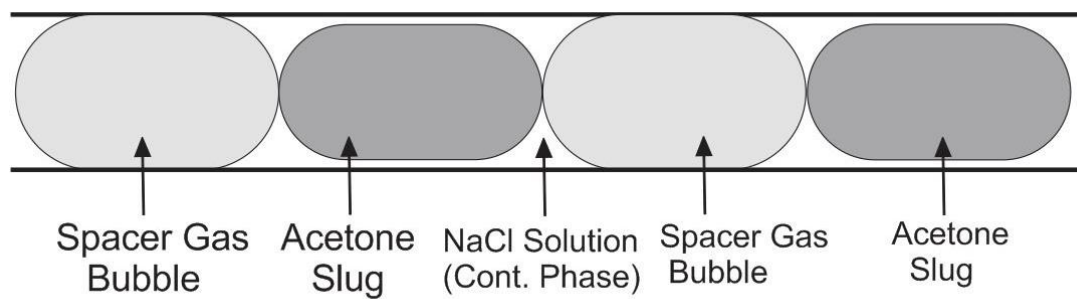
3. Development and Comparison of Strategies to Delay Clogging [2]

It is challenging to achieve non-stop flow of a liquid-solid suspension through small channels as it eventually leads to clogging. Understanding of clogging in multiphase precipitating system with specific focus on clogging time and clogging mechanism was reported in the previous chapter. In the view of that, four different techniques for enhancement of solid handling processes in microchannels were reported in this chapter. These techniques include dosing of the inert gas phase, dosing of the inert and immiscible liquid phase, and changing the wall wettability and multi-point injection, which, in principle, individually follow different mechanisms to delay clogging. An antisolvent based method for precipitation of salt was used to generate solid particles during flow. Clogging time at various flow rates from all the methods was measured and analysed. In addition to that, this chapter presents a quantitative comparison of the reported strategies for two different diameters. Irrespective of the method of delaying clogging, the scaling law of clogging time as a function of residence time was seen to remain unchanged. These observations were found to be true for a different precipitating system as well. Among these methods, dosing of an inert, immiscible liquid has been identified as the most effective and robust method to delay clogging while enhancing transport of particles in segmented flow.

3.1. Introduction

Despite the range of benefits of microreactors described in the first chapter, they are not recommended to be used for process involving solids. Owing to smaller dimensions, micro and milireactors are susceptible to clogging by solids that can get generated in reactions as well as precipitation/crystallization. Clogging is an incredibly complex, random,

and dynamic phenomenon, and there are still many gaps in the understanding of clogging in small channels [1-4]. The clogging mechanism in single and multiphase flow is explained and studied in the previous chapter. The complexity of the particle response to fluid streamlines, forces acting on particles and clusters, and interactions between particles does not allow identification of a single approach to avoid clogging in small channels [5]. The applicability of micro and mili-fluidic devices for flow chemistry applications, lab-on-a-chip kind of diagnostic systems, flow synthesis of micro and nanoparticles is hugely influenced by their ability to retain continuous flow without the occurrence of clogging. Hence it is essential to develop methods to prevent clogging. Significant efforts have been made towards that regard since the mid 2000's by means of a wide variety of strategies. Earlier in this decade, Hartman et al.[1] and Kuhn et al.[6] reviewed the reported methods. In addition, the strategies reported the aforementioned reviews, the recent advancements in the literature to managing solid particles in micro and mini channels could be technically classified into four types - chemical, passive, active flow manipulation and alternative strategies. These four strategies were discussed in detail in chapter 1 (section 1.3). The shortcoming and limited applicability of the wide range methods were reiterated in the both the detail reviews. Apart from cavitation related disadvantages, issues like noise, mechanical constraints, contamination of products by erosion in the reactor, are areas of concern. In addition to that scalability and economic viability are also probable bottlenecks for ultrasound and magnetism based systems, as they consume an enormous amount of energy per unit volume [6-8]. Moreover, the active strategies were developed mostly for single phase flow systems, and their usage in multiphase systems would disrupt the flow regimes significantly. As a result, there is a necessity for further investigation in this area.

In this chapter, four novel methods that can help reduce clogging in small channels in a multiphase system have been proposed. They were focused on manipulating the segmented

flow regime in order to transport the solid particles in an efficient manner by means of passive methods rather than using external forces. The methods were experimentally investigated, and their relative performance has been analysed. In a gas-liquid-liquid (G-L-L) flow system air is used as the gas phase to sweep the solid particle agglomerates in the liquid-liquid system. In a second method, transport of precipitated solids is enhanced by trapping them into the low-pressure zones of the immiscible inert liquid slugs. In addition to that, the inert liquid phase escalated the recirculation of the solids in the continuous phases making them less susceptible to settle. The third strategy used in this work was the mitigation of the wall interactions, indirectly dissuading the solid particles by means of intrinsic flow properties. Changing the wettability of the channel walls (hydrophilic to hydrophobic) results in wetting phase inversion [9, 10]. Solid-particle interactions with the channel walls become restricted as they are formed inside the non-wetting phase under the modified conditions. The fourth method focuses on the gradual formation of solid particles in microchannels. A multipoint injection method [11] was implemented to restrict the interaction of the two reagents using the sequential addition of one of the reagents instead of single point addition. These four methods have been chosen as they do not need any external arrangements to be made viz. magnetic/ultrasonic field or use of the vibrating platform or a piezoelectric oscillator, etc. These four approaches are relatively easy to implement, which is why their behavior was evaluated in a quantitative manner to identify the timescales for clogging.

The present chapter details the four aforesaid strategies; clogging mechanism and quantitative analysis of the associated timescales have been presented. Thereafter, a comparison of different methods is carried out to understand the efficacy of the implemented strategies, in comparison to the reference data without implementing any methods to delay or avoid clogging. Finally, the synthesis of Barium sulphate and Indigo dye was chosen as the case study for solid forming chemical reactions. Barium sulfate has several medical and radio

imaging applications due to its radio-opaque properties and water insolubility. It is used in diagnosing gastrointestinal medical conditions and root canal fillings. It also has applications in pigments & adhesives industry, making pyrotechnic compositions, textiles, rubber and catalyst supports. Indigo and its derivatives are used as blue dye for cotton yarn, wool and silk but mainly for denim cloth for jeans. It is used as food colourant agent as well. The above mentioned inorganic and organic solid forming chemical reactions are performed in micro channels in a clogging free manner, demonstrating the aforementioned techniques.

3.2. Experimental Section

3.2.1. Chemicals

Sodium chloride particles were obtained by mixing a saturated aqueous solution of sodium chloride (Thomas Baker, AR grade) and acetone to undergo antisolvent precipitation. Toluene (Thomas Baker, AR grade) was used as an inert phase. Barium sulphate particles were obtained by mixing an aqueous solution of barium chloride dihydrate (Thomas Baker, 99% purity) with an aqueous solution of sodium sulphate (Loba Chemie, 99% purity). The concentration of both the solutions was varied from 0.05 M to 0.5 M. To clean the capillaries after the reaction; it was washed first with water saturated solution of sodium carbonate (Loba Chemie, 99.5% purity) followed by acetic acid (Thomas Baker, 99.8% purity). Indigo particles were synthesized using Baeyer-Drewson method. 2-nitrobenzaldehyde (Thomas Baker, 99%, 0.33M in acetone) and Sodium hydroxide solution (Thomas Baker, AR Grade, 1M in water) was mixed at room temperature to undergo aldol condensation followed by cyclization and oxidative dimerization to indigo. Dimethyl sulfoxide (Loba Chemie, 99%) was used to wash the capillaries after performing the reaction to remove any indigo particles sticking to the wall surface. Deionized water was used to make all the aqueous solutions.

3.2.2. Methods

Experiments were carried out to measure the clogging time in straight capillaries. In order to generate solids in flow, antisolvent precipitation and two reactions were selected. Antisolvent precipitation of NaCl was used to characterize the clogging reduction methods, which were demonstrated subsequently by performing two chemical reactions. Glass capillaries of two different diameters of 1.43 mm and 1.90 mm were used. Both the capillaries were 100 cm long having two Y-junction inlet geometries and were positioned in an entirely horizontal manner. For the experiments involving the injection of inert gas and immiscible liquid phase, the saturated salt solution was introduced continuously along with the inert phases (air and toluene, respectively) using a Y-joint generating slug flow, while antisolvent acetone was introduced subsequently using a similar Y-joint (see Fig. 3.1a, case 1). Flow rates of the three phases, which ranged from 0.2 ml/min to 5 ml/min, were controlled by three separate syringe pumps (Holmarc Optomechatronics, India). All the experiments were performed, keeping a constant ratio of flow rates of aqueous NaCl solution and acetone. The inert phase flow rates were also kept the same as that of the aqueous NaCl solution and acetone flow rates. The flowrate of a single phase is used for the figures in this chapter.

A digital manometer (AZ Instruments, China) was attached to a third inlet junction to monitor the transient pressure buildup inside the capillary due to clogging. A pressure drop of 30 kPa was considered as the clogging criteria in this chapter, as the flow stops completely when the pressure drop reached that value.

For wettability variation experiments, PTFE and functionalized glass channels were used for precipitation and reaction experiments, respectively. Horizontally placed straight PTFE (Polytetrafluoroethylene from IDEX Health & Science) channels (1.90 mm diameter)

connected to a PTFE T-joint (see Fig. 3.1a, case 2) were used. For hydrophobic functionalization of the glass capillaries, they were treated at 60°C with Octyltrimethoxysilane (Sigma Aldrich, 96%), an eight-carbon long silane that interacts with the silanol groups on the glass capillary surface. This creates a layer of hydrophobic alkyl groups on the surface, reducing its affinity to the aqueous phase. The effect of varying the wettability of the capillary wall surface on the clogging time was studied. Saturated salt solution and acetone flowrate were kept in the same range for the hydrophobic PTFE capillaries as before.

For multipoint injection experiments, a straight glass capillary having multiple inlets was fabricated using both Y and T joints (see Fig. 3.1b). The saturated aqueous solution of NaCl was employed through one of the inlets of the Y-joints located at the start of the capillary while acetone was pumped through four equally spaced inlets to the capillary.

The Barium Chloride solution and inert phase (Toluene or Air) were injected into the capillary by means of a Y junction, and the Sodium sulphate solution was introduced into capillary 3 cm downstream via a second Y junction. Similarly, for the synthesis of indigo, the inert gas phase and the 2-nitrobenzaldehyde solution were inserted into the capillary by means of the first Y junction and the NaOH solution was inserted via the second Y junction (see fig. 3.1) . In both the cases, 1 mL/min flowrate was maintained for all the streams by means of syringe pumps (Holmarc, India) and a filtration assembly was connected to the outlet of the capillary which consisted of a Whatman Grade 1 filter paper, Büchner funnel and a vacuum pump (Buchi, Switzerland). Filtered barium sulphate particles were washed with water deionized water and then dried, while indigo particles were first washed with deionised water followed by ethanol and then dried.
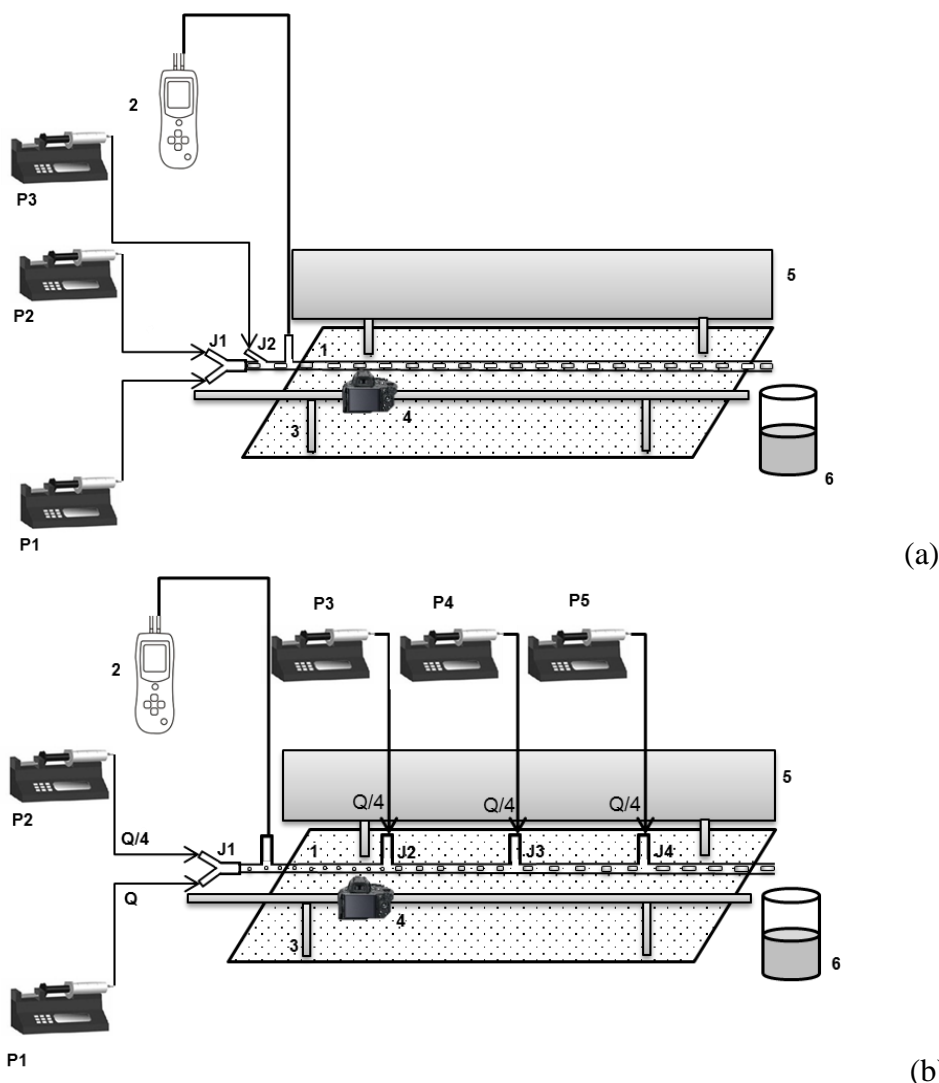
Fig. 3.1. (a) Schematic representation of the experimental setup for inert gas/liquid insertion (case 1) and wall wettability change (case 2) experiments. Only syringe pumps (P1-P5) were used for all experiments. (2) Manometer, (3) Camera Rail, (4) DSLR Camera, (5) Diffused light source, (6) Collection bottle. (**Case 1.** (1) Glass Capillary, (P1) Pump for Sat. NaCl Solution, (P2) Pump for inert gas/liquid phase, (P3) Pump for dispersed phase (Acetone), (J1, J2) 1st and 2nd Y-joint, (**Case 2.** (P1) Pump for continuous phase (Sat. NaCl Solution), (P2) Pump for dispersed phase (Acetone), (J1) Inlet Y joint, (1) Teflon Capillary. P3 and J2 is removed), **(b)** Schematic representation of the experimental setup for multipoint antisolvent insertion experiments using a Glass Capillary. (P1) Syringe Pump for continuous phase (Sat. NaCl Solution), (P2-P5) for Syringe Pump for dispersed phase (Acetone), (J1) Inlet Y joint, (J2-J4) Antisolvent inlets

A high-resolution camera (Sony SLT-A37K) with a recording speed of 25 frames per second and a shutter speed of 0.25 ms – 30 s was used to record the slug breakup process,

liquid-liquid flow patterns, and solid transport. To observe the flow along the length of the capillary, a double rail traversing system (Holmarc Optomechatronics, HC-2) was used to move the camera (Sony SLT-A37K) parallel to the capillary length. A backlight with an antiglare diffuser was used for the visualisation and imaging. The entire set-up was constructed to monitor how the aforementioned methods inhibit clogging of the channel in real time by the solid particles, arising from antisolvent precipitation. All measurements were performed in triplicate. The schematics of the experimental setups used in this chapter are shown in Fig. 3.1.

3.3. Results and Discussion

In a multiphase flow system, different flow fields in different flow regimes affect clogging in capillaries. Our experiments were mostly limited to the slug flow regime, where particles were observed to travel to the rear of the dispersed phase slugs, agglomerate, and form a shell depending upon the residence time. As the dispersed phase slugs move along the channel length, shells detach from the rear section of the slugs, undergo associative growth and form clusters in the continuous phase [4]. This data on clogging time from our previous work has been used as the basis for comparison of results among different methods (dosing of inert gas/liquid phase, changing the wall wettability and multi-point injection) that delay clogging of capillaries.

3.3.1. Effect of dosing of an inert phase on clogging time

3.3.1.1. Effect of dosing inert gas on clogging time (θ_{clog_g})

Experiments were carried out to understand the effect of injecting an inert gas phase in the liquid-liquid precipitating flow. The transient variation in the suspension flow rate inside straight glass capillaries was monitored by measuring the pressure drop at the inlet of the capillary. The total time until which the capillary could support the flow of the suspension or the time when the capillary became clogged was measured as the clogging time (θ_{clog}).

Gas slugs were formed at the first Y-junction under the squeezing effect of the aqueous phase. The generated gas-liquid (saturated salt solution in water) flow then entered through an inlet of the second Y-junction where it encounters the acetone phase (antisolvent) entering from the other inlet of the Y-junction. The dispersed acetone phase slugs were observed to undergo detachment in the presence of the gas slugs or by the continuous aqueous phase. Both the shearing effect of the aqueous continuous phase and the splitting effect of the bubbles controlled the break-up of the dispersed acetone phase at the second Y-junction. Finally, based on the detachment dynamics at the second Y-junction, a combination of liquid-liquid and gas-liquid flow pattern was formed. Over a wide range of flow rates (0.2 - 5.0 ml/min for each phase), squeezing, dripping, and jetting regimes were observed having different breakup mechanisms and breakup points. Similar observations in slug detachment was observed by Wang et al. [12] for non-precipitating gas-liquid-liquid systems. At lower flow rates, a three-phase slug/droplet alternate flow with one dispersed liquid phase slug trailed by one gas bubble was formed in the downstream capillary (Fig. 3.2b). At higher flow rates, G-L-L slug flow regime was observed where two or more acetone slugs are formed with one gas slug.

(a)

(b)
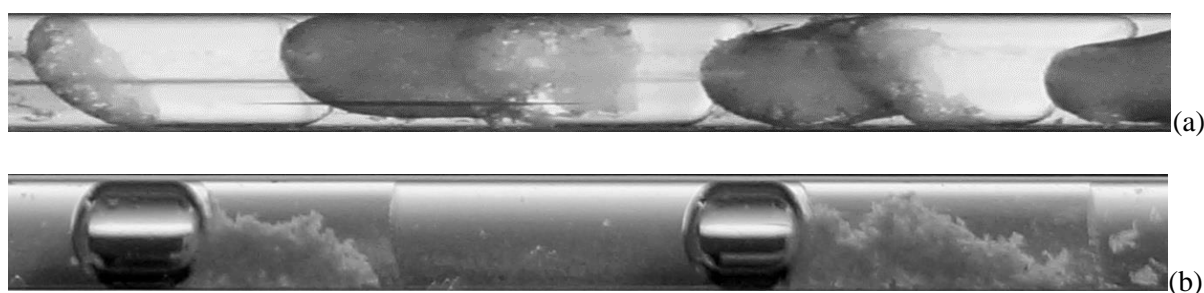
Fig. 3.2. Comparison of solid formation in (a) liquid-liquid and (b) gas-liquid-liquid flow system

The gradual formation of the solid cluster which eventually clogs the capillary is shown in Fig. 3.3. The growth of the cluster took place as a large number of particles joins the cluster in comparison to the number of particles which comes off the cluster. The initial

particle adherence of solids on the wall was random, but in time it formed an arc over the side walls. Due to cluster formation on the wall surface, the channel opening started to reduce with time subsequently resulting in clogging.

| 50 s | 300 s | 500 s |

| 800 s | 900 s | 1100 s |
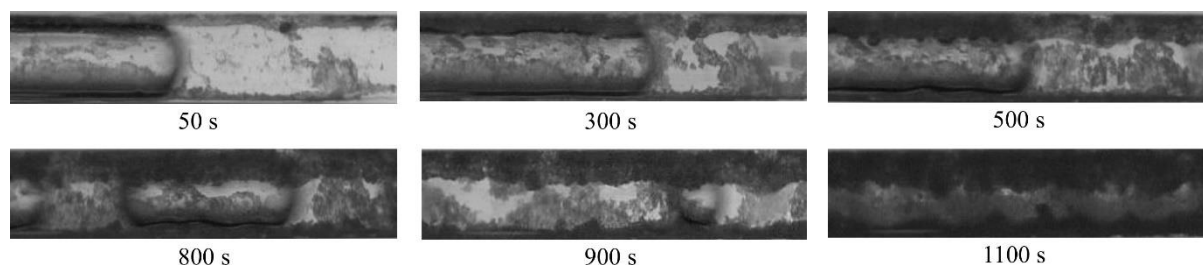
Fig. 3.3. Clog/Cluster formation and growth as a function of time with the use of G-L-L flow (at 200 mm from the antisolvent inlet junction (J2) for 1 ml/min flow rate of each phase)

The clogging time in this system was monitored and plotted as a function of flow rate. The 1.43 mm and 1.90 mm diameter capillaries were chosen for these studies as the slug flow regime was observed in those two diameters over a wide range of flow rates. Fig. 3.4a and 3.4b show how the introduction of the gas phase increased the clogging time compared to the standard liquid-liquid system (salt solution-acetone) in glass capillaries of 1.43 mm and 1.90 mm diameters respectively. It can be observed that the presence of gas phase significantly delays clogging irrespective of flow rate. A rise of 3.7-7.3 times and 3.9-7.8 times in the Y-intercept is shown in Fig. 3.4a and 3.4b respectively which directly represents the delay in clogging. As the film thickness enclosing the gas slugs was negligible, the inert gas segments swept rapidly through the capillary enhancing the transport of precipitated salt in the liquid segments. A change in the viscosity of the system due the gas phase slugs disrupts the stagnant zone at the rear of the acetone slugs which prevents shell formation as observed in the previous chapter. Similar enhancement of solid transport was recorded for a sodium sulphate based antisolvent system under identical conditions (see Fig 3.4c).

The introduction of inert air slugs into the flow of an aqueous solution of NaCl and acetone changed the flow regime from slug/parallel/annular liquid-liquid flow to slug flow of

three phases (gas-liquid-liquid) for a wide range of the flow rates. This resulted in a higher specific interfacial area, and subsequently, higher overall mass transfer rates.

(a)

(b)

(c)
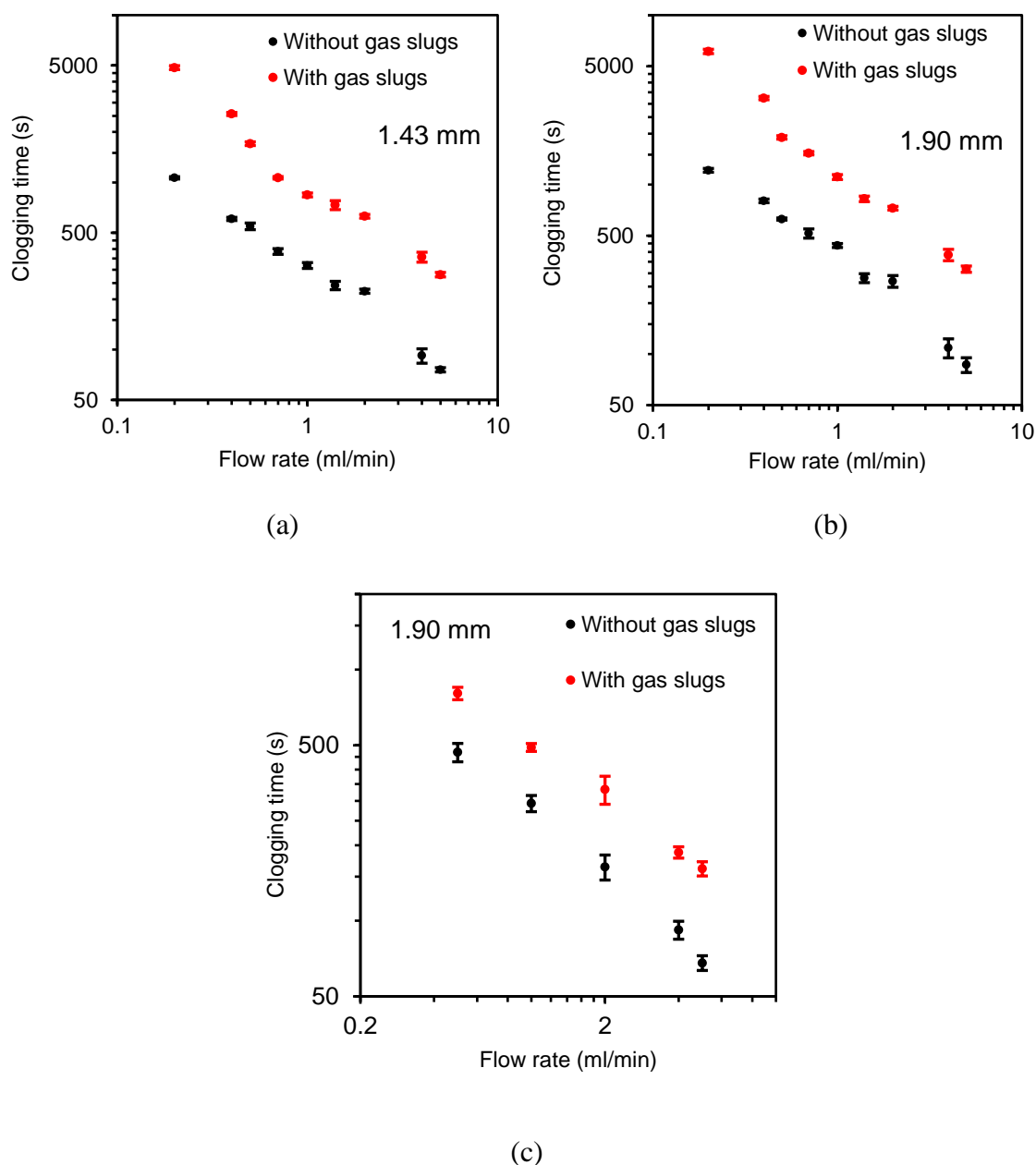
Fig. 3.4. Effect of the inert gas phase dosing on clogging time in straight glass capillaries. (a) 1.43 mm diameter (for sodium chloride), (b) 1.90 mm diameter (for sodium chloride), (c) 1.90 mm diameter (for sodium sulphate)

Su et al. [13] first reported that gas slugs could be used as micro agitators for better mixing and mass transfer characteristics in a two-phase microcapillary system. Later, Assman et al. [14] reported that addition of the gas phase leads to an increase in mass transfer at higher

flow velocities while no significant difference results for lower flow velocities. A higher mass transfer rate will give rise to a greater amount of precipitate formation per unit time which would help in faster clogging of the capillaries. However, enhancement in the mass transfer coefficient in the presence of a gas slug was reported to decrease significantly with a higher gas fraction (Q_{gas}/Q_{total}) as the distance between two consecutive liquid slugs was increased [15]. These counteracting effects on clogging time worked simultaneously, although the first effect became quite predominant and helped in delaying clogging.

It is known that downstream particle deposition with time was found to be the primary reason behind clogging in glass capillaries. However, in the presence of gas bubbles, such effects were severely reduced. On the other hand, as in this case, particle formation and their deposition neighbouring the second Y-junction, where the antisolvent enters the tube, was observed to be the primary reason for clogging.

In addition to these effects, coalescence of the neighbouring slugs was reported to accelerate the solid packing formation inside the capillary in such a multiphase system [4]. Coalescence occurs when two slugs of the same phase get closer and come into contact due to their motion in the flow. The inert gas segments prevented slug coalescence acting as immiscible spacers which resulted in an increase in clogging time (see Fig. 3.5).
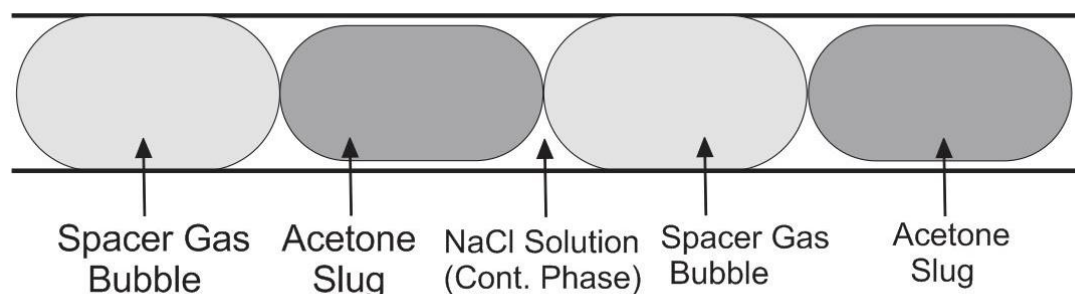
Fig. 3.5. Schematic of gas bubbles working as a spacer to prevent coalescence

3.3.1.2. Effect of dosing of inert liquid phase on clogging time (θ_{clog_1})

Toluene is used as an inert liquid phase with respect to air in the experiments discussed in the previous section. Toluene slugs were formed at the first Y-junction by the squeezing of the aqueous phase, and acetone was inserted in the second Y junction. The acetone phase came in contact with the continuous phase first which was a saturated aqueous solution, and the salt precipitated out due to the antisolvent effect. Acetone went into the dispersed phase slugs partially as it had some solubility in the dispersed toluene phase. A major fraction of the precipitated salt particles started accumulating at the stagnation zone formed due to the asymmetric Laplace vortices at the rear of the dispersed phase slugs. Subsequently, they started aggregating and form a shell at the rear slug end. The rest of the precipitated particles kept recirculating in the dispersed and continuous phase due to the strong Taylor vortices formation in the segmented flow. These two modes of solid particle transport hindered the adhesion and sedimentation of the solid particles in the vicinity of the capillary walls. Fig. 3.6 shows how the introduction of the immiscible liquid phase increased the clogging time compared to a standard liquid-liquid system (salt solution-acetone) in a 1.90 mm diameter glass capillary. In fact, for flow rates less than 1 ml/min (shaded area in the Fig. 3.6), most of the particles are effectively transported by recirculation in the continuous phase or entrapment in the rear stagnant zone of the slugs with time. It was observed that if the inert phase slugs do not get tangled by the flow and surface irregularities, the dispersed phase segments transported precipitated product out of the capillary. With increasing flow rates, clogging cannot be avoided primarily due to intense mass transfer resulting in rapid precipitation: the clogging time was observed to decrease. This is due to the instability of the flow regime. The flow regimes in the capillary tend to form a wavy parallel flow which is ineffective in solid transport and leads to packing formation subsequently. It is essential to note that all types of flow regimes are not desirable for the efficacy of solid

transport and control of the flow regimes is very critical. The lack of stable control of the flow in the desired slug flow regime leads to clogging due to flow instability, particle sedimentation and packing formation, all acting in sequence or simultaneously.
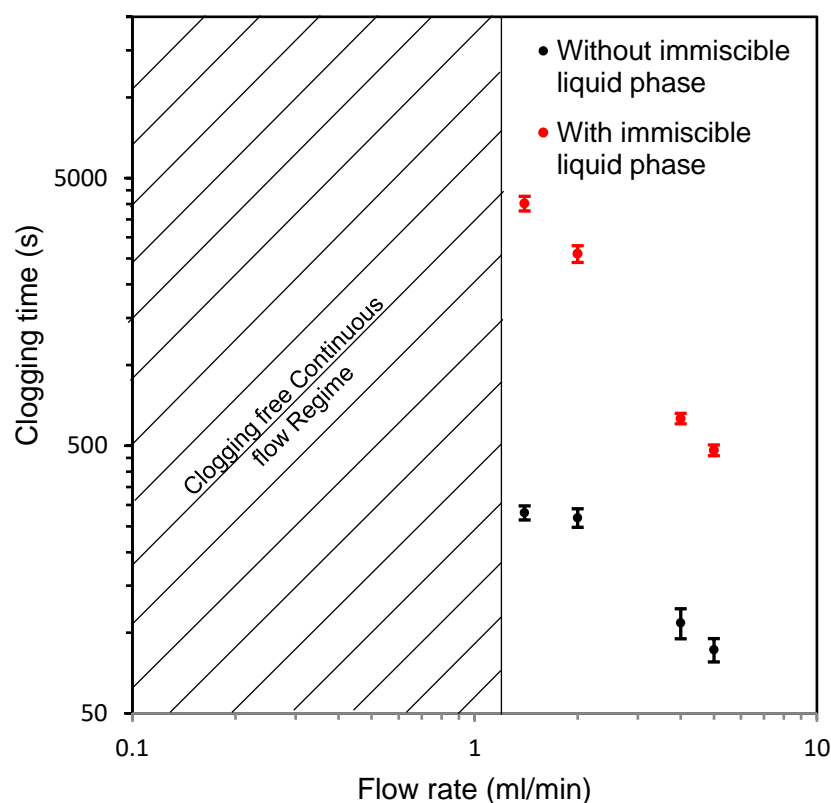
Fig. 3.6. Effect of the inert liquid phase dosing on clogging time in straight glass capillaries

A fraction of the particles tended to form a packing but were continuously obstructed by the inertia of the liquid phase slugs. This resulted in an undulatory nature of the transient pressure drop of the system (see Fig. 12). For flowrates of 1 ml/min or lower of each of the phases, the aforementioned slug flow micro-capillary system allowed us to carry out the salting out process continuously for more than 2-3 hours without clogging despite some periodic rise in pressure drop. It is worthwhile to mention that this surge in pressure drop is still four to six times lower than the pressure drop tolerance maintained for measurement of clogging time. In fact, the long-term operation was not hampered by these undulations in

pressure drop as it was always restored to the original value. Encouraged by these results, we wondered if the aforementioned technique could also handle other inorganic salts. It was observed that the technique could work for precipitated particles of sodium sulphite for flow rates of 1 ml/min.

3.3.2. Effect of wettability inversion of capillary walls on clogging time (θ_{clog_w})

In a glass capillary with salt solution and acetone being fed through a Y- joint, the precipitated salt particles formed solid shells at the rear end interface of the dispersed phase slugs. They detached along the capillary length and subsequently were inclined to settle on the capillary wall surface. To prevent shell formation and settling of solid shells on the wall, their formation can be restricted in the dispersed phase, since in that scenario, they do not come in contact with the wall surface. This can be achieved by changing the wall wettability.

In microfluidic systems, flow regimes are influenced by surface wetting properties of the microchannel wall material [16], [17], [18]. The wetting properties of the fluid-wall interface are highly decisive in the geometric distribution of the components of the flow. Typically, water-in-oil (W/O) slugs/droplets are developed in hydrophobic channels, while oil-in-water (O/W) slugs/droplets are developed in hydrophilic channels [9]. By changing the capillary wall material from glass to PTFE, the surface changes from a hydrophilic to hydrophobic, which results in a wetting behaviour completely opposite to that of the hydrophilic glass capillaries. The saturated salt solution starts to form the dispersed phase and acetone forms the continuous phase. Fig. 3.7(a-b) demonstrates this interchange of continuous and dispersed phases. The solids were found to remain enclosed inside the dispersed phase, and a film of the acetone phase restricted the precipitated salts from coming in contact with the capillary walls. This restricted the accumulation of the precipitating solids at the capillary wall making the microchannels less susceptible to clogging. Fig. 3.7c

represents how the change in the wall wettability leads to an increase in the clogging time while other conditions are kept the same.

(a)

(b)

(c)
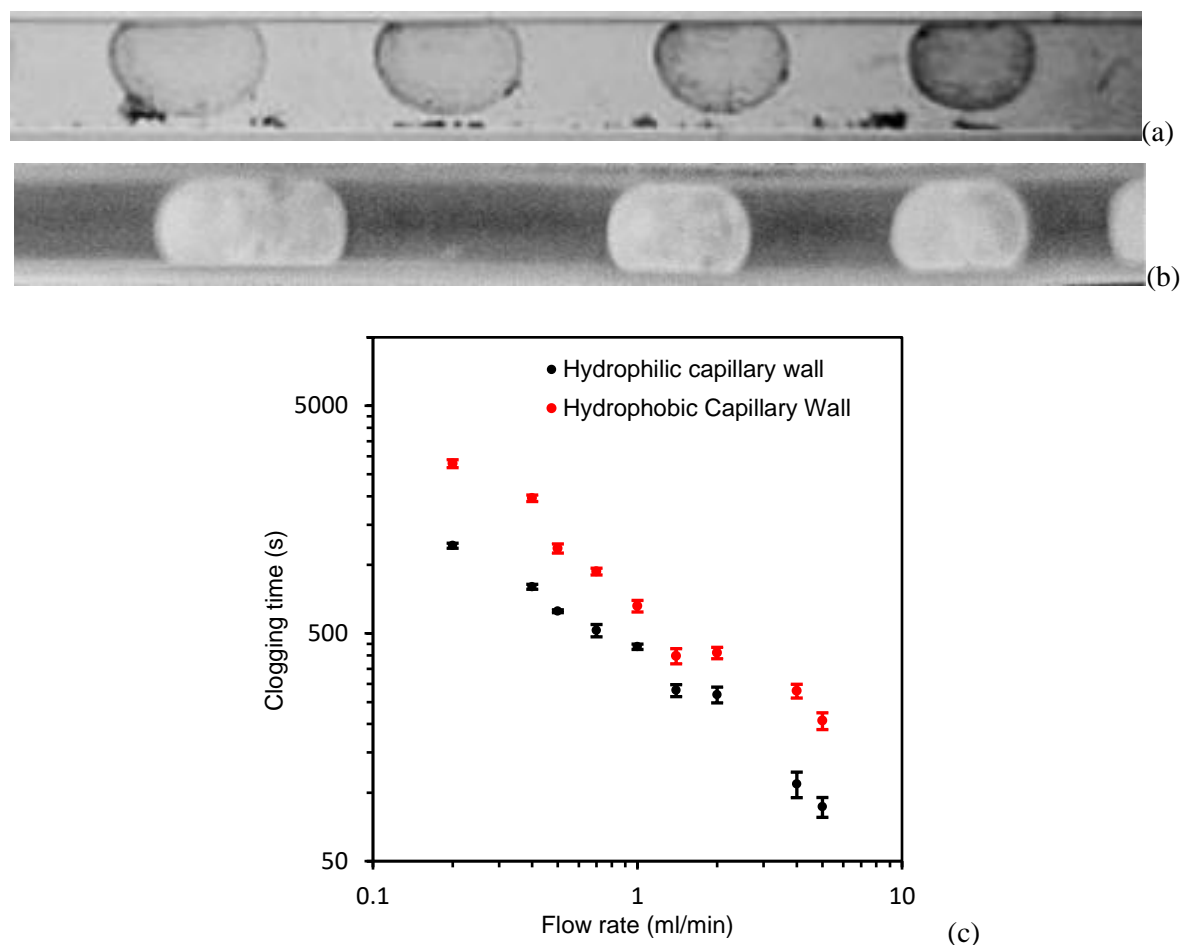
Fig. 3.7. Comparison of transport of the precipitated solids in the microcapillary for (a) hydrophilic and (b) hydrophobic capillary of 1.43 mm diameter at 1 mL/min flow rates of both the phases and (c) The effect of surface wettability on clogging time in a 1.90 mm diameter capillary.

Fig. 3.8 depicts the dimensionless pressure drop profile across the capillaries, ($\Delta P/\Delta P0$, normalized to the initial, without solid only, pressure drop). In hydrophobic capillaries, clogging was observed following the rapid escalation in the pressure drop, while for the case of hydrophilic capillaries, a relatively gradual increase in the pressure drop was observed. However, the dimensionless pressure drop reached the tolerance value ($\Delta P/\Delta P0 = 100$) after 5 reactor volumes in hydrophobic capillaries compared to 1.5 reactor volumes in hydrophilic capillaries. Based on our experimental observations, it is apparent that the change in capillary

wall wettability is capable of handling clogging to a certain tolerance and thus can help to considerably increase residence time compared to the hydrophilic or wetting walls. As higher contact angles relates to higher hydrophobic nature of the wall surface, MOCs of higher contact angle would be preferred for enhanced handling of solids.
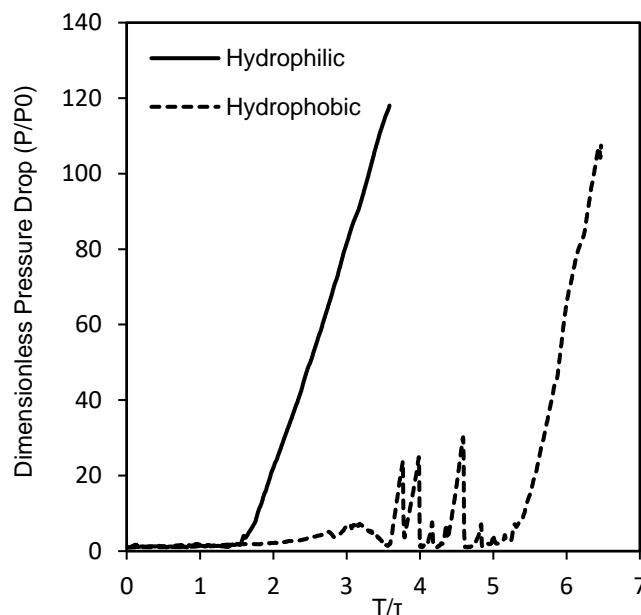
Fig. 3.8. Change in dimensionless pressure drop with (dimensionless) time in hydrophilic and hydrophobic capillaries of 1.90 mm diameter (0.5 ml/min flow rate of each phase)

3.3.3. Effect of multipoint insertion of antisolvent on clogging time (θ_{clog_m})

A multipoint injection technique has been reported to be used for the gradual increase of the concentration of one reactant over the reactor length for highly exothermic systems [19]. This technique distributes the heat generation throughout the reactor resulting in prevention of hotspots. A similar method was used here for the gradual generation of solids in microchannels. Distributing the solids throughout the capillary length reduces the chances of agglomeration and eventual blocking of channels. The antisolvent, which is the dispersed phase, was employed with multipoint dosing results in a sequential increase in flow ratio with the length of the capillary. This changed the flow regimes along the channel length as well.

In the first section of the capillary (J1-J2, see Fig. 3.1b), droplet flow was observed due to a low flow ratio, while from the second dosing point (J2), slug flow was observed. At the fourth dosing point (J4), the flow ratio reached the maximum value, and solid cluster formation started taking place (see Fig. 3.9f and 3.10). As a result, packing formation was
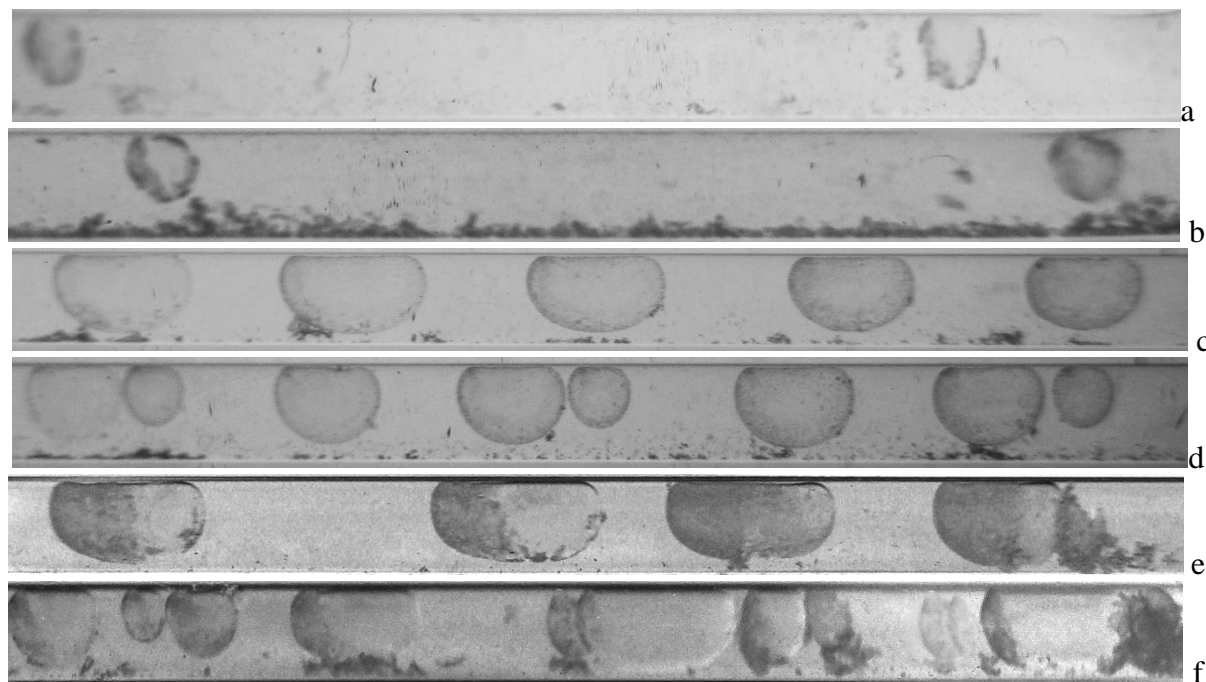
Fig. 3.9. Change flow regimes along the capillary length for the multipoint injection system (Diameter 1.9 mm and total flowrate 2 ml/min). (a-b) J1-J2, (c-d) J2-J3, (e) J3-J4, (f) J4-capillary outlet

mostly encountered only at the forth inlet junction: it is shown as a function of time in Fig. 3.10. Clogging at the onset of the capillaries can be avoided using this technique.

Fig. 3.11 represents how the multipoint injection technique can help in reduction of clogging in small capillaries. The gradual generation of solids throughout the system results in less susceptibility to clogging. In our previous work, we have observed that for the smaller diameter capillaries (< 2 mm), occurrence of parallel and annular flow results in faster clogging. Multipoint injection technique restricts the flow regimes in slug and droplet flow even for the case of the highest flowrates (see Fig. 3.9). This results in a reduction of

clogging, especially in the higher flowrate regime. The number of counteracting effects working simultaneously along the length of the capillary pose several challenges in the understanding of the dynamics of spatially varying mass transfer. The change in mass transfer rates along the length of the capillary is complicated and needs to be well understood to investigate the clogging of the capillary due to interfacial precipitation in such a multipoint system.

(100 s)   (300 s)

(400 s)   (500 s)
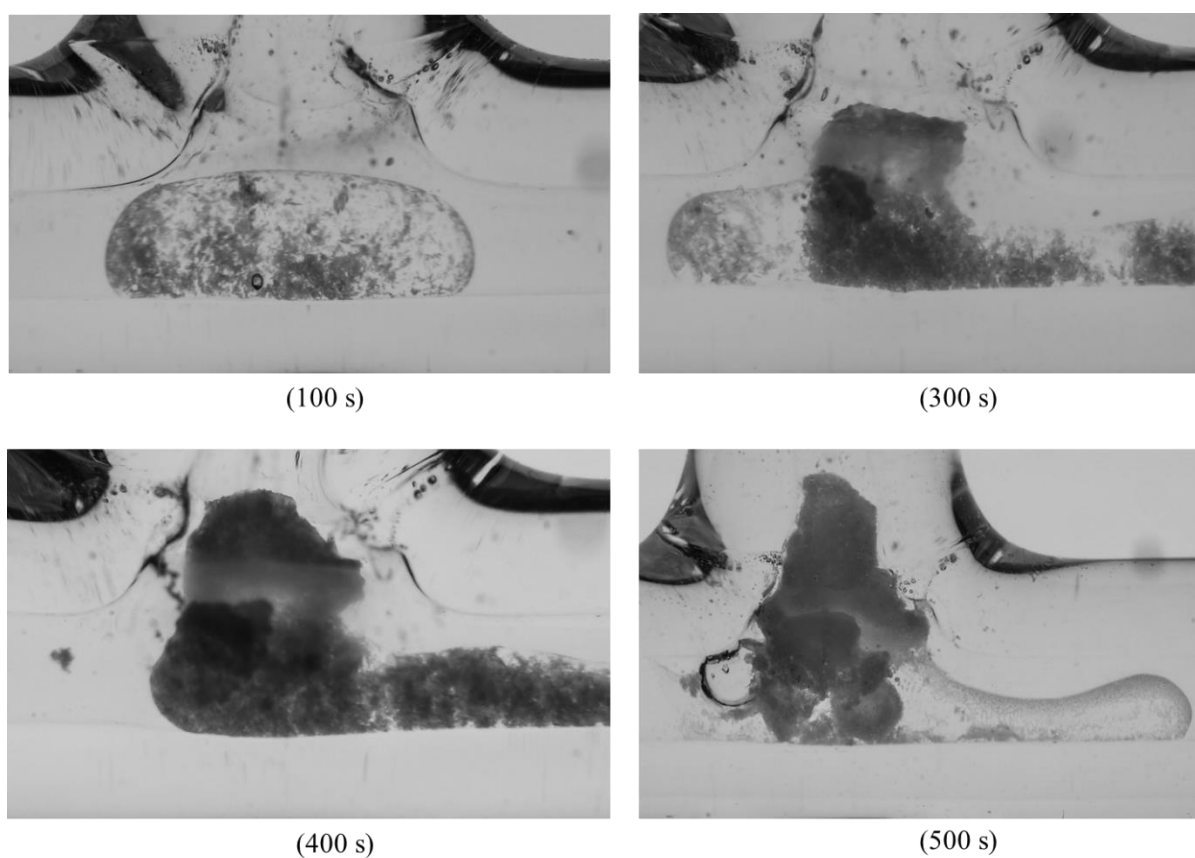
Fig. 3.10. Images representing packing formation and growth at the 4th inlet of antisolvent as a function of time - (a) 100s, (b) 300s, (c) 400s, (d) 500s. (For 1 ml/min total flow rate of both phases in 1.90 mm diameter capillary)

The counteracting effects working simultaneously on the rate of clogging here include: (i) The overall increase in specific interfacial area (increasing mass transfer), (ii) Decrease in internal circulation rate along the capillary length due to slug length increase (decreasing mass transfer), (iii) Increase in internal circulation rate due to velocity/ total flowrate

increase, (increasing mass transfer), and (iv) Increase in flow ratio at the injection points. (increase in mass transfer along the capillary length). Investigation of these would require modelling/ CFD to a greater extent and will be explored separately.
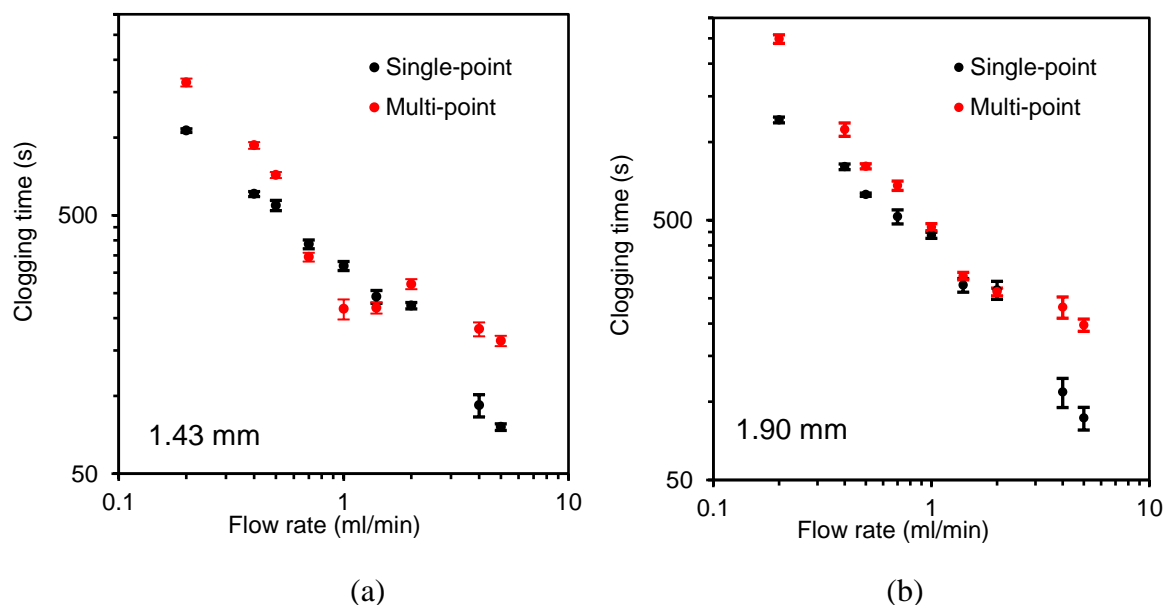
Fig. 3.11. Change of clogging time with multipoint injection of antisolvent for (a) 1.43 mm and (b) 1.90 mm diameter straight glass capillary

3.3.4. Comparison of proposed methods for reduction of clogging time

The aforementioned four methods, viz. the introduction of immiscible and inert gas/liquid phase, wall wettability change and use of multipoint injection system are demonstrated to improve solid handling capabilities of the microfluidic system. In this section, we present our findings on the comparison of the performance of these strategies that work through different principles. We observed that the clogging time or the time when a surge in pressure drop happens, increased in the following order hydrophilic – multipoint – hydrophobic - inert gas insertion - inert immiscible liquid insertion (see Fig. 3.12).
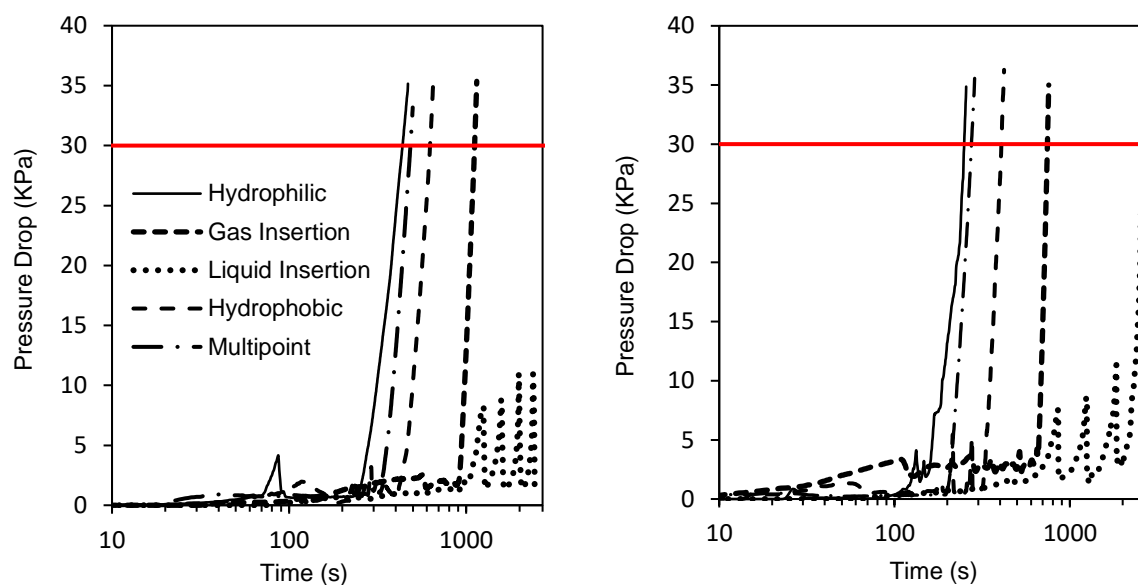
Fig. 3.12. Variation in pressure drop with time for different methods: (a) 1.0 ml/min, (b) 2.0 ml/min of each phase in 1.90 mm diameter capillary. The red line indicates clogging criteria.

The average length of the capillary over which clogging occurs was observed to vary in different methods and is described as clogging length. No specific section of the capillary was seen to induce clogging when the experiments are repeated. For the hydrophilic capillary, packing formation started at the inlet joint prior to the capillary; for gas insertion it moved downstream, and once a rigid packing was formed, pressure drop shot up and reached the tolerance value. For inert liquid insertion, packing often formed a few centimetres from the antisolvent inlet leading to pressure drop increase, but the inert liquid phase disrupted the packing formation repeatedly achieving a continuous flow of solids despite the pressure drop varying continuously. For a hydrophobic capillary, the average packing formation length moved further downstream. For multipoint addition of antisolvent, the flow ratio reached a maximum value at the fourth dosing point, and bridging and packing formation occurred predominantly there. The dimensionless clogging lengths from various methods are compared in Fig. 3.13.
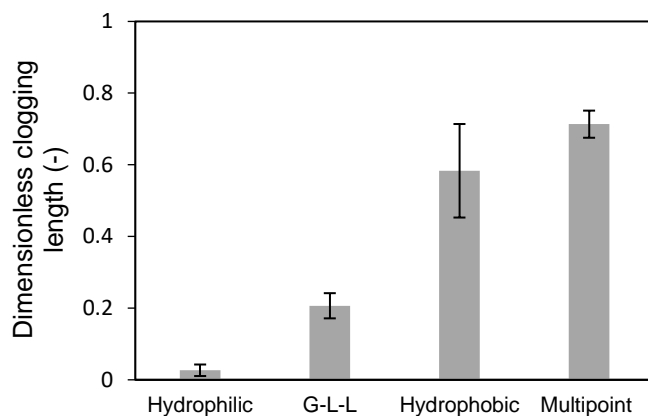
Fig. 3.13. Variation of dimensionless clogging length in different methods (for 1 ml/min flow rate of each of the phases)

(a)
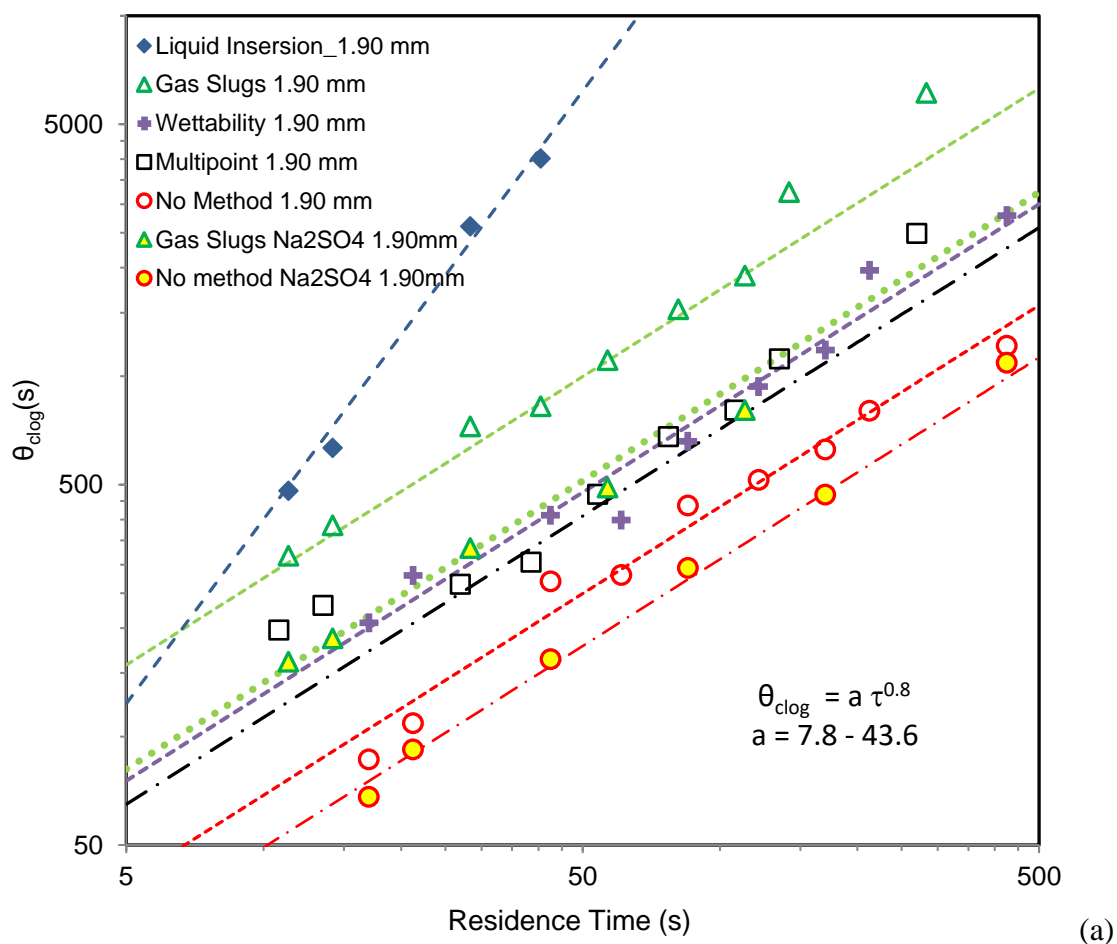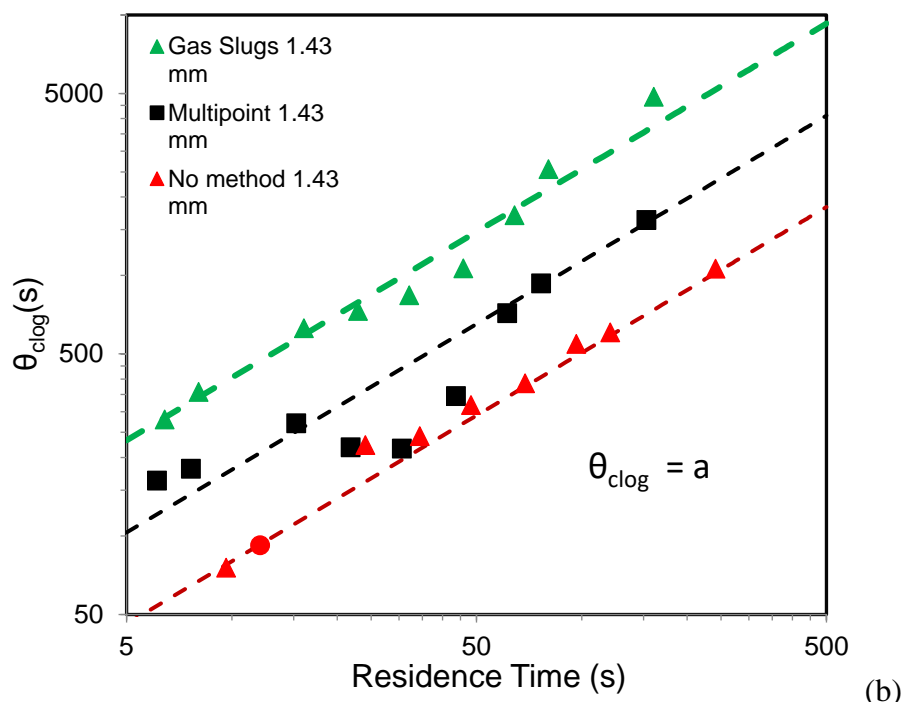
Fig. 3.14. Variation of clogging time as a function of total residence time in (a) 1.90 mm dia. capillary, and (b) 1.43 mm dia. Capillary.
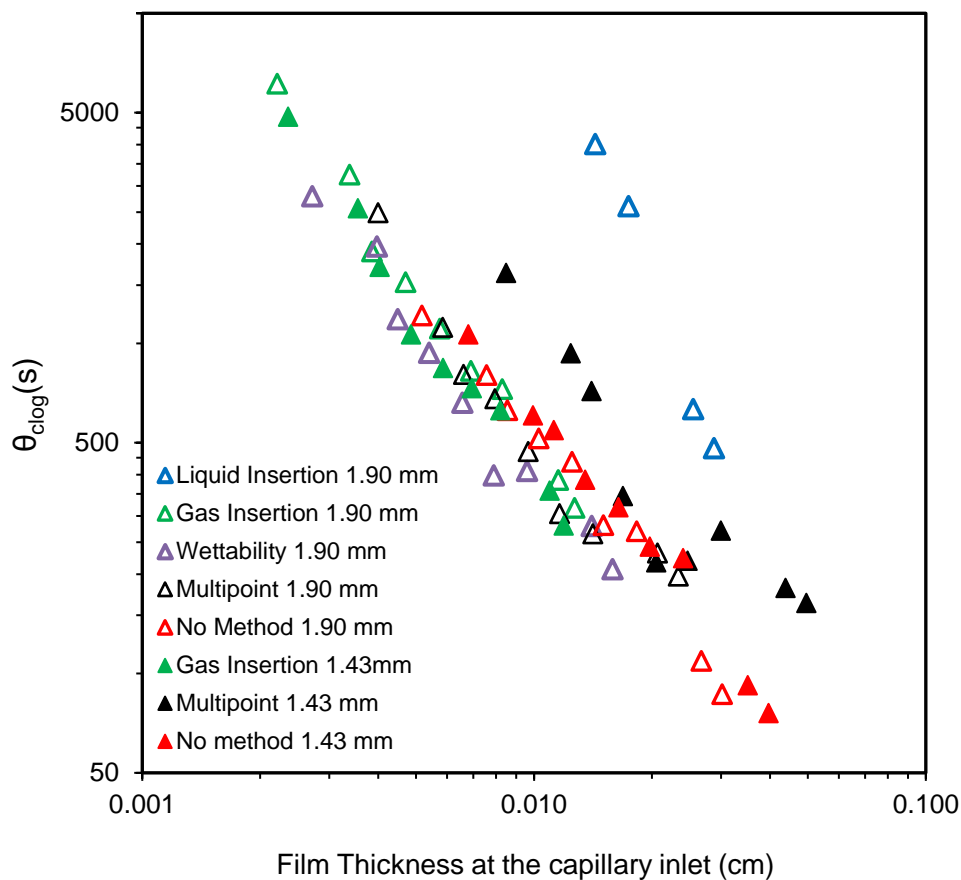
Fig. 3.15. Variation of clogging time as a function of film thickness of the continuous phase

Upon plotting the clogging time as a function of the residence time in the capillary (Fig. 3.14a), it was observed that for both the capillaries, the data approximately shows a power law behaviour which can be represented as $\theta_{clog} = \alpha\ \tau^{0.8}$, where α corresponds to the intercept on the ordinate. Only inert liquid phase insertion which facilitates *clogging-free* flow at flow rates below 1 ml/min corresponds to a different exponent in the power law fit. It is interesting that the slopes of the lines for all the methods are very similar. Thus, only an increase in the intercept accounts for the delay in clogging. For the 1.90 mm diameter capillary, the value of α was seen to increase from 7.8 to 43.6, with the lowest being for the experiments without any method to delay clogging, and the highest values corresponding to the insertion of inert gas slugs in the 'acetone-salt water' segmented flow. Even for a different salt precipitated using the same antisolvent, the same power law behaviour was observed. Capillaries of different diameter were also found to follow this near power law behaviour (see Fig. 3.14b). The reason behind this 'method specific' variation in the clogging time can be explained on the basis of the fluid dynamics in the vicinity of the capillary wall.

For the case of only acetone-salt water system, at the inlet of the capillary, the system would show a segmented liquid-liquid flow and water will be the continuous phase. Along the capillary length, as acetone diffuses in water, the acetone slug length would decrease, and water slug length would increase depending on the thermodynamically governed volume expansion due to solubility. Since the contact angle of the acetone-water mixture on a glass capillary is smaller than water alone, it is expected that the film thickness would increase so far the liquid-liquid segmented flow remains. Beyond this, there would only be acetone-water mixture with suspended salt particles.

On the other hand, in the presence of an inert gas phase, while the abovementioned scenario would remain valid to some extent but due to variation in dispersed phase systems, the liquid-

phase film thickness was different. Film thickness for gas bubbles and liquid slugs at different flow rates and diameters are estimated from correlations reported in the literature which gives reasonable estimations. For gas bubbles equation 3.1 [20] is used and for liquid slugs equation 2 [21] is used. Equation 3.2 is reported to be valid for capillary numbers higher than a critical capillary number Ca^*. This critical capillary number (Ca^*) is based on viscosity (μ_c) and density (ρ_c) of the continuous phase, Capillary radius (r) and interfacial tension (σ) and represented in equation 3.3 [22].

$$\frac{h}{r} = \frac{1.34 Ca^{2/3}}{1 + 1.34 \left(2.79 Ca^{2/3}\right)} \tag{3.1}$$

$$\frac{h}{r} = 0.35 Ca^{0.354} We^{0.097} \tag{3.2}$$

$$Ca^* = \left(\frac{\mu^2}{\rho r \sigma}\right)^{3/4} \tag{3.3}$$

Here, h is the film thickness, r is the capillary diameter, Ca is continuous phase Capillary number, and We are the continuous phase Weber number. The film thickness for gas bubbles and liquid slugs are compared in Fig 3.16.
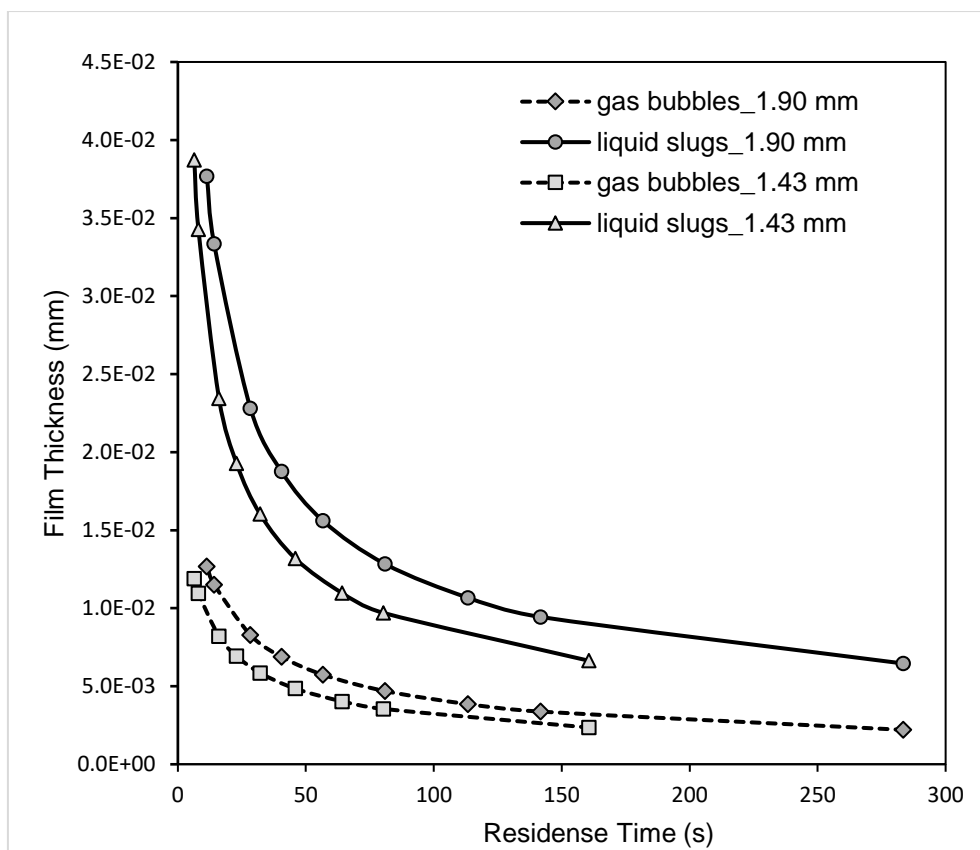
Fig. 3.16. Comparison of estimated film thickness for gas bubbles and liquid slugs

In this case, gas slugs would enforce spatial continuous variation in the film thickness of the continuous phase. This situation would lead to continuous variation in the slip length and hence would delay particle settling. Also, for the gas-liquid interface, viscous dissipation would be much lower than the liquid-liquid interface, which will result in a continuous variation in the flow patterns in the continuous phase. The variation in the estimated liquid film thickness at the entrance of the capillary is shown in Fig. 3.17.
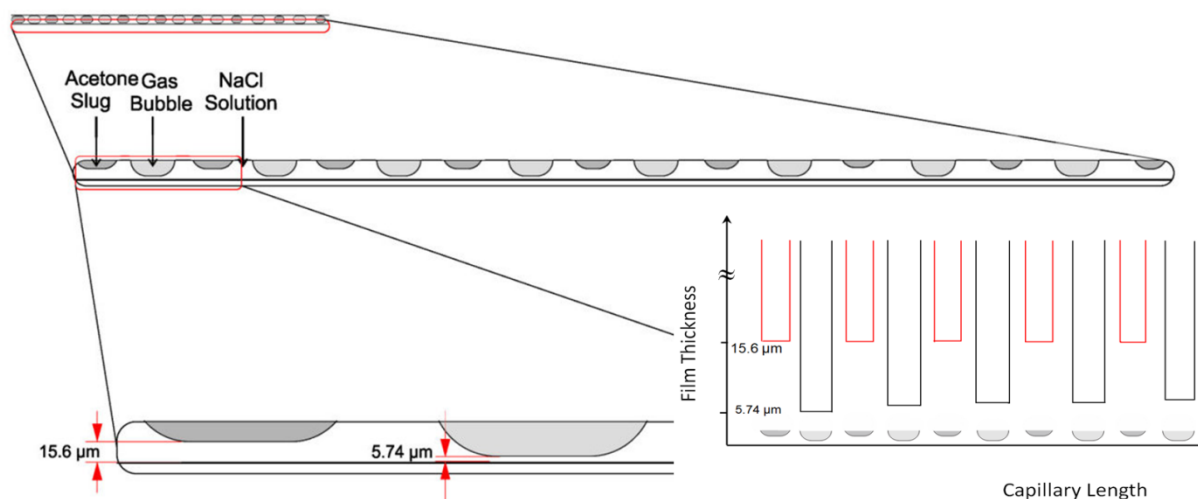
Fig. 3.17. Schematic of the difference in film thickness between gas bubbles and acetone slugs in continuous salt-water and schematic of variation in film thickness along the length of the capillary at the entrance section.

The clogging time was seen to have an inverse dependence on film thickness irrespective of the technique used here, which clearly indicates that lower film thickness leads to continuous sweeping of the capillary surface, which delays the particle settling, and hence, the clogging. Thus, the higher the inert phase flow rate, more can the clogging be significantly delayed, or even eliminated**.**

Along with the sweeping of the capillary surface, the insertion of immiscible inert liquid phase helps in transport of the precipitated particles by trapping them in the low-pressure stagnant zones at the rear of the dispersed phase slugs. With the use of immiscible liquid phase instead of gas induces more intense circulation vortex in the continuous phase which should help in the transport of the precipitated solid particles. On the other hand, inertial effects are stronger in the presence of a second liquid when compared to a gas phase. For the case of the non-wetting capillary wall, the solid formation and deposition procedure at the wall is different. In this case, the solids remain enclosed inside the dispersed phase, and a film of the continuous acetone phase restricts the precipitated salts from coming in contact with the capillary walls. Here, although acetone will be the continuous phase in the entrance

section, as the slugs move along the capillary, it eventually becomes a homogeneous liquid with a relatively lower contact angle than water alone. In such a case, it will have close-to-zero velocities at the wall throughout the capillary length and would not significantly help in delaying clogging. In conclusion, utilizing inert liquid phase slugs is the most effective way of delaying clogging in small channels and straight capillaries. More work on evaluating the efficacy of this approach for helical coils and other flow reactor designs and at handling different types of solids is in progress. Since every method of delaying clogging follows a different mechanism, development of a suitable mathematical model that helps predict the clogging time for segmented flow for other capillary sizes and flow rates is being developed separately.

3.3.5. Synthesis of Barium Sulphate and Indigo in continuous flow microchannels

The previous section of the chapter was focused on methods of particle handling and antisolvent precipitation of sodium chloride was used to characterize clogging. The efficient techniques found in that study was used here for solid forming chemical reactions. An inorganic substitution reaction was chosen as a case study, forming Barium Sulphate particles which are insoluble in water. In addition to that an organic synthesis of insoluble indigo dye was performed in an aforementioned technique.

Initially, synthesis of Barium Sulphate particles were performed without using any of the aforementioned methods keeping the flowrates at 1 ml/min. Due to higher density (4.5 g/cc), particles were found to settle and form deposits in the form of constrictions on the capillary wall surface which eventually leads to clogging.

A number of research papers have employed droplets as separate reactors enclosed in carrier phases in microfluidic systems which minimizes the possibility of clogging but adopting such systems involve a huge percentage of dead volume in carrier phases[23]. For example, Poe et

al. [23] reported a 70% dead volume in droplet flow particle handling method.
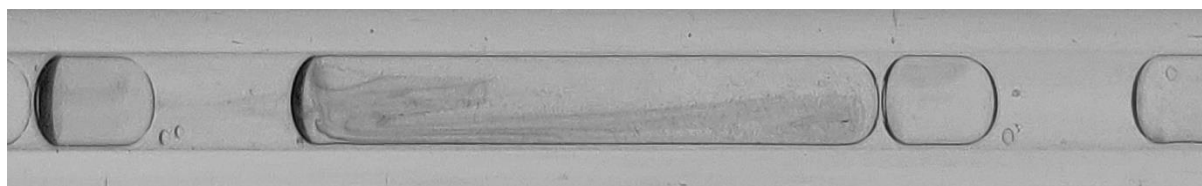
Fig. 3.18. Transport of barium sulphate particles in hydrophobic channels

In our work wall wettability was altered, and the inert liquid phase was used for encapsulating the particles in dispersed phase in segmented flow regime. This is analogous to the third method described in the aforementioned section, but the inert phase was used as the reacting system is single phase here. The capillary wall wettability was altered from hydrophilic to hydrophobic by treating with Octyltrimethoxysilane. Functionalized glass capillaries having hydrophobic walls were used to perform the reaction producing Barium Sulphate particles along with toluene as an inert phase, which resulted in Barium Sulphate particles in dispersed and reacting aqueous phase enclosed in continuous and inert toluene phase, ensuring no or minimal wall interaction (see Fig. 3.18). Fig 3.18 also shows how the particles are recirculated inside the dispersed phase, resulting from Taylor and Laplace vortices formation. This resulted in clogging free flow for hours. Here, from image analysis of the captured images of the segmented flow, the average dead volume was found to be 20 ±5 %, which is a significant improvement in economic terms in comparison to droplet flow.

After this the same reaction was performed in hydrophilic capillary, where toluene worked as spacer dispersed phases. At lower flowrates, small toluene slugs were formed separating the continuous phase at regular intervals (see Fig. 3.19 a-b). The toluene slugs helped in solid transport by formation of shell at the rear and front, pushing the solids in continuous phase as well as enhancing the intensity of internal circulations in continuous phase. At higher flow rates longer toluene slugs are observed and the particles are accumulated mostly at the rear

section of the aqueous phase slugs. Fig 3.19c and 3.19d show the rear and front section of the aqueous phase slug.

(a)

(b)

(c)

(d)
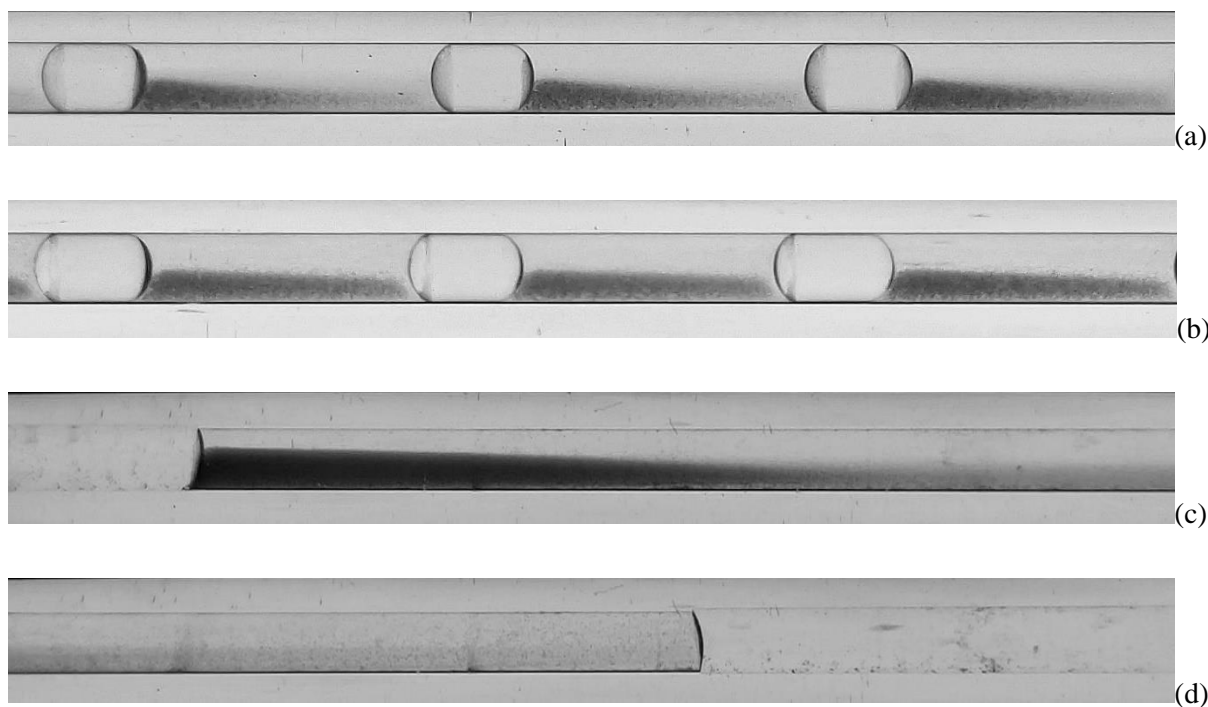
Fig 3.19. Transport of Barium Sulphate particles with toluene as inert phase (a) 0.25 ml/min, (b) 0.5 ml/min, (c) 2 ml/min, (d) 2 ml/min

For the case of indigo synthesis, gas was used as inert phase spacers preventing interaction between the indigo particles in two adjacent liquid segments (see Fig. 3.20a. In addition to that the inert gas segments swept rapidly through the capillary enhancing the transport of rapidly formed indigo particles in the continuous phase slugs. Formation of rear shells on the gas bubbles were clearly visible in at higher flow rates where comparatively longer slugs were observed (see Fig 3.20b).
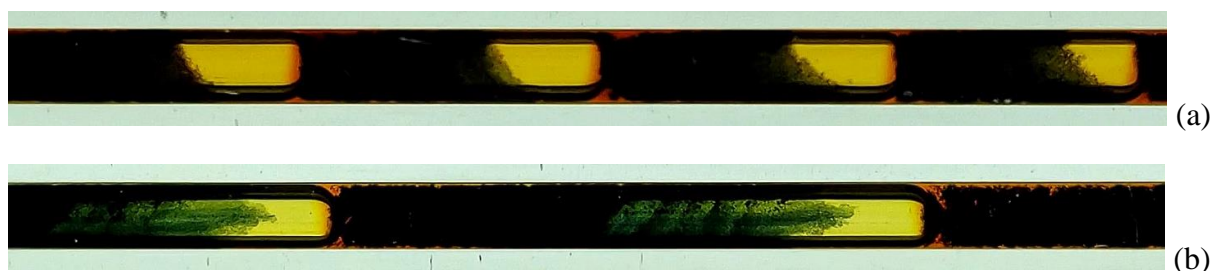
Fig. 3.20. Transport of indigo particles with inert gas phase as spacers.
(a) 0.5 ml/min,(b) 1 ml/min

3.4. Conclusions

In this chapter, we have analyzed the performance of four techniques for understanding the clogging in small straight channels for systems where solid particles are generated. An antisolvent based precipitation system (acetone – salt water) is used for these studies. The methods used for delaying clogging are easy to implement and do not use any external forces. In the first method, inert gas slugs sweep the solid throughout the capillary in helping solid transport. The second method facilitates solid transport by insertion of the immiscible inert liquid slugs escalating the internal circulation in the continuous phase as well as trapping solids in the stagnant zones of inert liquid phase slugs. In the third method, entrapment of the solids in the dispersed phase slugs due to wall wettability change is used for enhanced solid transport. In the fourth method, a multi-injection principle analogous to a semi-batch reactor is used for solid handing by gradually generating the solids in the microcapillary. Furthermore, clogging time measurement experiments were carried out to have a quantitative understanding of the performance of the proposed methods, where liquid insertion methods proved to be most effective. Interestingly, irrespective of the method of delaying clogging and salts, the clogging time scaled almost identically with the residence time. The intercept of the trends was seen to be a strong function of the method itself. Lastly, these strategies were demonstrated for two chemical reactions involving solids. We hope this work will reduce the barrier in implementing flow chemistry methodologies for solid forming reactions to some extent. Though multiphase flow (gas-liquid or liquid-liquid) have been

effectively used to significantly delay clogging, challenges remain for its further development in an industrial scale, both in precise controlling of flow regimes and the complex phenomena of simultaneous mass transfer and chemical reactions.

3.5. Notations

θ_{clog_g} Clogging time with the inert gas phase insertion (s)

θ_{clog_l} Clogging time with the inert liquid phase insertion (s)

θ_{clog_w} Clogging time in capillaries with different wettability (s)

θ_{clog_m} Clogging time in multipoint insertion capillary (s)

θ_{clog_ref} Clogging time without any strategies (s)

Q_T Total flow rate (ml/min)

Re   Reynolds Number (-)

d   Capillary Diameter (mm)

P/P_0 Dimensionless Pressure Drop (-)

τ Residence Time (s)

3.6. References

1.   Hartman, R.L., *Managing Solids in Microreactors for the Upstream Continuous Processing of Fine Chemicals.* Organic Process Research & Development, **2012**. 16(5): p. 870-887.

2.   Sharp, K.V. and Adrian, R.J., *On flow-blocking particle structures in microtubes.* Microfluidics and Nanofluidics, **2005**. 1(4): p. 376-380.

3.   Wyss, H., Blair, D., Morris, J., Stone, H., and Weitz, D., *Mechanism for clogging of microchannels.* Physical Review E, **2006**. 74(6).

4.   Pal, S. and Kulkarni, A.A., *Interfacial precipitation and clogging in straight capillaries.* Chemical Engineering Science, **2016**. 153: p. 344-353.

5.   Dressaire, E. and Sauret, A., *Clogging of microfluidic systems.* Soft Matter, **2017**. 13(1): p. 37-48.

6.   Wu, K. and Kuhn, S., *Strategies for solids handling in microreactors.* Chim. Oggi, **2014**. 32(3): p. 62.

7.   Freitas, S., Hielscher, G., Merkle, H.P., and Gander, B., *Continuous contact-and contamination-free ultrasonic emulsification—a useful tool for pharmaceutical development and production.* Ultrasonics sonochemistry, **2006**. 13(1): p. 76-85.

8.   Berlan, J. and Mason, T.J., *Sonochemistry: from research laboratories to industrial plants.* Ultrasonics, **1992**. 30(4): p. 203-212.

9.   Zhao, C.-X. and Middelberg, A.P., *Two-phase microfluidic flows.* Chemical Engineering Science, **2011**. 66(7): p. 1394-1411.

10.   Kuhn, S., Hartman, R.L., Sultana, M., Nagy, K.D., Marre, S., and Jensen, K.F., *Teflon-Coated Silicon Microreactors: Impact on Segmented Liquid− Liquid Multiphase Flows.* Langmuir, **2011**. 27(10): p. 6519-6527.

11.   Kulkarni, A., Nivangune, N., Joshi, R., and Joshi, R., *Continuous flow multipoint dosing approach for selectivity engineering in sulfoxidation.* Organic Process Research & Development, **2013**. 17(10): p. 1293-1299.

12.   Wang, K., Qin, K., Lu, Y., Luo, G., and Wang, T., *Gas/liquid/liquid three-phase flow patterns and bubble/droplet size laws in a double T-junction microchannel.* AIChE Journal, **2015**. 61(5): p. 1722-1734.

13.   Su, Y., Chen, G., Zhao, Y., and Yuan, Q., *Intensification of liquid–liquid two-phase mass transfer by gas agitation in a microchannel.* AIChE journal, **2009**. 55(8): p. 1948-1958.

14. Assmann, N. and von Rohr, P.R., *Extraction in microreactors: intensification by adding an inert gas phase.* Chemical Engineering and Processing: Process Intensification, **2011**. 50(8): p. 822-827.

15. Aoki, N., Ando, R., and Mae, K., *Gas− liquid− liquid slug flow for improving liquid−liquid extraction in miniaturized channels.* Industrial & Engineering Chemistry Research, **2011**. 50(8): p. 4672-4677.

16. Santos, R. and Kawaji, M., *Developments on wetting effects in microfluidic slug flow.* Chemical Engineering Communications, **2012**. 199(12): p. 1626-1641.

17. Zhao, B., Moore, J.S., and Beebe, D.J., *Surface-directed liquid flow inside microchannels.* Science, **2001**. 291(5506): p. 1023-1026.

18. Gau, H., Herminghaus, S., Lenz, P., and Lipowsky, R., *Liquid morphologies on structured surfaces: from microchannels to microchips.* Science, **1999**. 283(5398): p. 46-49.

19. Haber, J., Jiang, B., Maeder, T., Borhani, N., Thome, J., Renken, A., and Kiwi-Minsker, L., *Intensification of highly exothermic fast reaction by multi-injection microstructured reactor.* Chemical Engineering and Processing: Process Intensification, **2014**. 84: p. 14-23.

20. Klaseboer, E., Gupta, R., and Manica, R., *An extended Bretherton model for long Taylor bubbles at moderate capillary numbers.* Physics of Fluids, **2014**. 26(3): p. 032107.

21. Eain, M.M.G., Egan, V., and Punch, J., *Film thickness measurements in liquid–liquid slug flow regimes.* International Journal of Heat and Fluid Flow, **2013**. 44: p. 515-523.

22. Arsenjuk, L., Kaske, F., Franzke, J., and Agar, D.W., *Experimental investigation of wall film renewal in liquid–liquid slug flow.* International Journal of Multiphase Flow, **2016**. 85: p. 177-185.

23.   Poe, S.L., Cummings, M.A., Haaf, M.P., and McQuade, D.T., *Solving the Clogging Problem: Precipitate-Forming Reactions in Flow.* Angewandte Chemie International Edition, **2006**. 45(10): p. 1544-1548.

Chapter 4

Antisolvent precipitation of Ammonium Perchlorate: Batch to continuous

4. Antisolvent precipitation of Ammonium Perchlorate: Batch to Continuous[3]

In this chapter, a continuous clogging anti-solvent precipitation method was proposed for the safe and rapid preparation ammonium perchlorate (AP) particles, in which water and *n*-butyl alcohol were chosen as solvent and anti-solvent, respectively. The process parameters such as solution and antisolvent temperature, mixing were optimized in batch and continuous capillary reactor for smaller particle size. Optical microscopy and Scanning electron microscopy (SEM) and were used to characterize the particles. The growth kinetics of the precipitated AP particles were also discussed. Clogging issues in continuous operation were addressed by means of ultrasound. In comparison to the conventional batch process, continuous precipitation using a Y-joint and a glass capillary was found to be favourable for obtaining smaller particle size.

4.1. Introduction

Reduction in the particle size enhances its rate of dissolution or reaction, through the enlarged surface area per unit volume [1]. Improvement of drug bioavailability and further scientific interest in micro and nanoparticles owing to their unusual properties lying between the bulk material and molecules is discussed in chapter 1 (section 1.4.1) [2].

Several top-down milling methods for size reduction of different compounds are used for years which are highly energy intensive and often induce a degree of amorphousness, affecting product quality and stability [3]. The several limitations of top-down methods were discussed in chapter 1(section 1.4.2). Due to their poor control over mean particle size, PSD, morphology,

and scalability of the top down methods [4], bottom-up approaches have become popular for micronization of particles in the last two decades. Moreover, grinding is not preferred for temperature sensitive materials and toxic materials handled in this work, due to chances of ignition and toxic dust production. Bottom-up approaches provide advanced control over particle size, morphology and crystallinity in comparison to the top-down methods. Among the different bottom-up approaches such as evaporative precipitation [5, 6], liquid antisolvent precipitation [7-9], spray drying [10, 11], cooling crystallization [12] and supercritical precipitation [13-15], liquid antisolvent precipitation (referred as ASP henceforth) is found to be generally convenient as it operates at atmospheric pressure and does not require expensive equipment. The antisolvent used in this method precipitates the solute molecules by replacing the dissolved solute molecule in the solvent with itself thereby reducing the dissolving power of the solvent for the solute. A wide range of applicability and several advantages of choosing ASP for this work is discussed thoroughly in the introduction chapter.

In the present chapter, Ammonium perchlorate (referred as AP henceforth) is chosen as a case study, and we aim to determine a continuous clogging free method for production of fine AP particles of the desired size. AP is used as a constituent in pyrotechnic compositions and also used as a raw material for the production of perchloric acid and many metallic perchlorates. Previously, Levinthal et al. have used cooling and evaporation of solvents as the driving forces for precipitation of AP in an immiscible two-phase batch system, where AP particles are collected from the non-solvent phase[16]. Recently, Zhenye et al. have used ceramic membrane antisolvent crystallization technique for production of size and morphology controlled particles [17]. Though developing a method of continuous precipitation with control on particle size and PSD is our goal, experiments in the batch process were performed at the beginning for the

identification of optimized solvent /anti-solvent pair and mixing conditions to get the desired AP particle size (~10 µm). A clogging free continuous anti-solvent precipitation method was proposed for the safe and rapid preparation of ammonium perchlorate (AP) particles, in which, water and *n*-butyl alcohol were selected as a solvent and anti-solvent respectively. Growth kinetics of the precipitated AP particles were investigated in the semi-batch process using a focused beam reflectance measurement (FBRM, Mettler Toledo) probe. The effect of processing parameters on the particle size and shape of AP particles such as solution and antisolvent temperature, mixing was investigated. The optimized conditions found in the batch experiments have been utilized in a glass capillary reactor in a continuous manner.

The chapter is organized as follows: the next section details out the experiments and observations, the methods we implemented, and the data processing techniques in this work. Subsequently, optimization of the particle size of AP particles in batch experiments is presented by studying the effect of parameters. Then optimization of continuous experiments was performed, clogging issues were addressed, and finally, the particle size and the PSD obtained in various experimental strategies are compared before summarizing the major findings from this chapter.

4.2. Experimental Section

4.2.1. Materials

Organic solvents such as *n*-butyl alcohol (99.5% pure from Merck Chemicals Ltd, India) and n-propyl alcohol (99.0% pure from Merck Chemicals Ltd, India) have been used as anti-solvents. Ammonium Perchlorate (AP) was obtained in powder form (~ 300-500 micron size). Millipore water is used for making the aqueous solution of AP. These chemicals have been used without any further purification.

4.2.2. Procedure & Analysis

4.2.2.1. Batch Experiments

The batch experiments were performed in a flat-bottomed jacketed glass reactor (50 ml volume) having standard baffles. The reactor was filled with a saturated solution of pure AP at temperatures varying from 30 °C to 80 °C. The temperature of the solution was stabilized to the desired initial temperature using a temperature bath (Julabo, Germany). *n*-propyl alcohol and *n*-butyl alcohol were used as the anti-solvents. Antisolvents were added to the solution at a location close to the magnetic stirrer under constant stirring conditions (900 rpm). The temperature of the anti-solvents was varied from 30°C to -10°C. For another set of experiments in batch mode, a glass reactor of 50 ml volume was immersed in an ultrasonic bath for enhanced micromixing. The temperature in the ultrasound bath was held constant by means of a temperature bath (Julabo, Germany) and two high flow rate peristaltic pumps. Schematic illustrations of the two batch experimental setups are presented in Fig 4.1.

(a)   (b)
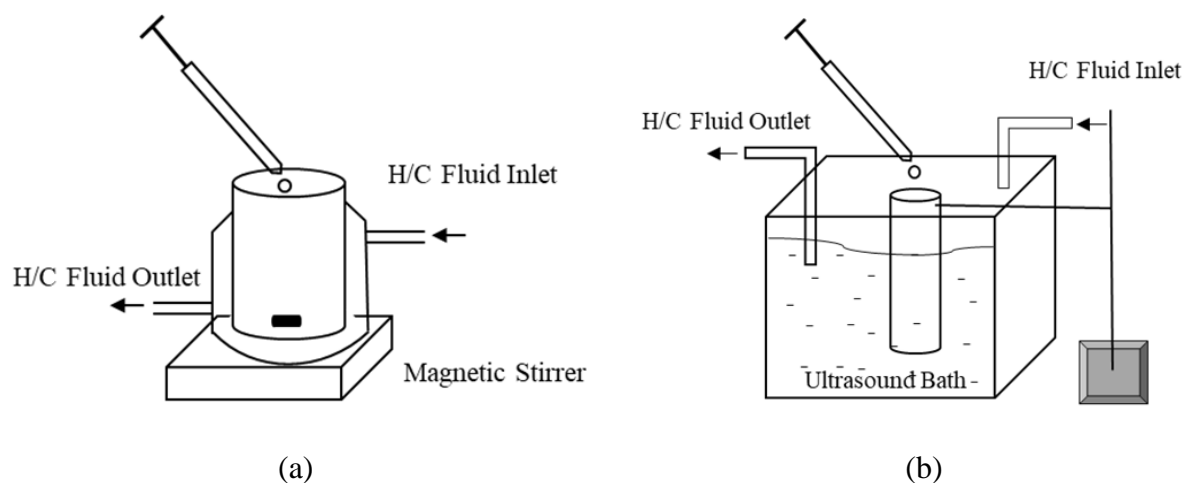
Fig. 4.1. Schematic of experimental setups for precipitation of AP in batch reactor (a) with magnetic stirrer (b) with ultrasound bath

4.2.2.2. Continuous Experiments

For continuous precipitation, both, AP solution and antisolvent (*n*-butyl alcohol) were introduced in a horizontally positioned capillary at equal flow rates using a Y-joint. The solution was kept in a temperature bath and pumped to the capillary inlet using a peristaltic pump (Longer BQ50-1J, China). Antisolvent was pumped to the capillary inlet using a syringe pump (Holmarc, India), followed by a heat exchanger coil connected to a temperature bath (Julabo, Germany) kept at desired antisolvent temperature (See Fig. 4.2). A glass capillary of 2 mm diameter and 20 cm length was used, which provided 23.5 seconds of residence time. A filtration assembly was connected to the capillary outlet which consisted of a Whatman Grade 1 filter paper, Büchner funnel and a vacuum pump (Buchi, Switzerland).
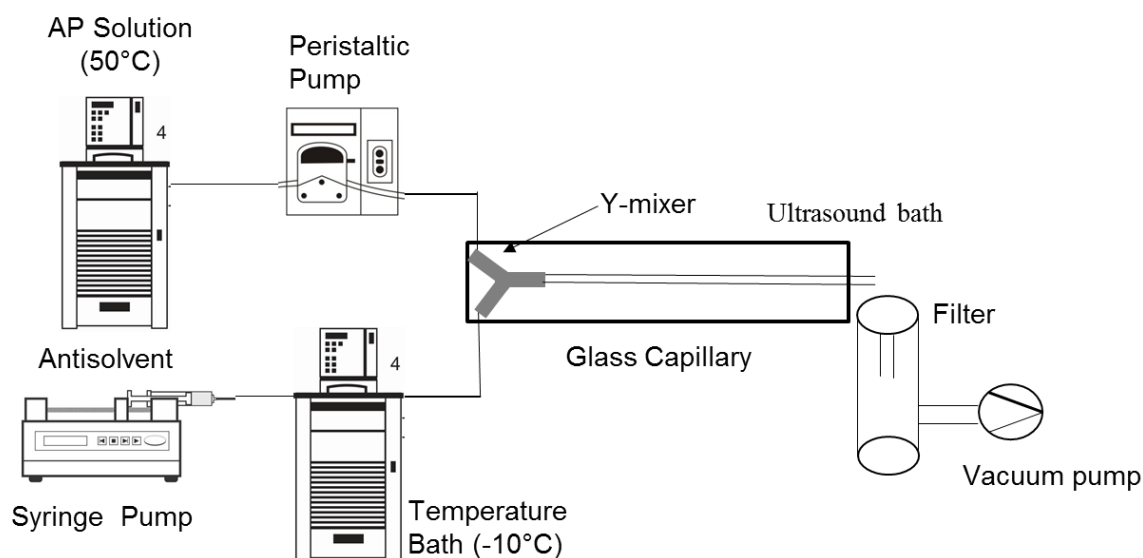
Fig 4.2. Schematic of experimental setups for continuous precipitation of AP in a straight glass capillary

For kinetics, study experiments saturated AP solution is kept in the jacketed batch reactor, and antisolvent is added gradually at -10°C with a syringe pump. The jacketed glass reactor is stirred continuously using an overhead stirrer. A Focused Beam Reflectance Measurement (FBRM, Mettler Toledo) probe was immersed in the solution, which measures in line chord length distribution (CLD) using laser back-scattering principle. The FBRM probe, connected to a data acquisition system was used for online monitoring the mean chord length and chord length distribution for 30 minutes during the precipitation. A schematic of the said system for kinetics study is shown in Fig 4.3.
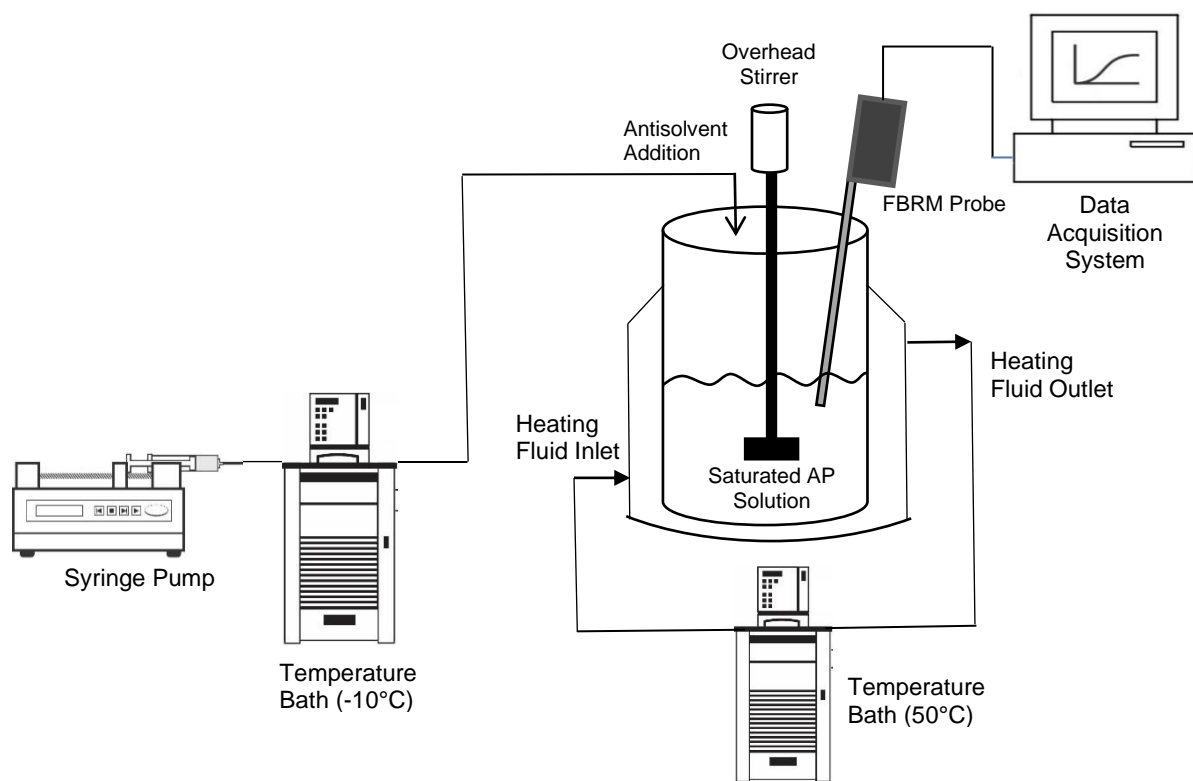
Fig. 4.3. Schematic of the FBRM setup for kinetics study

4.2.2.3. Particle Size Measurement

The precipitated particles were analyzed for the particle size and shape using Optical

Microscopes (Zeiss - Stereo Discovery v20 and Zeiss Primo Star) and Scanning Electron Microscope (E-SEM Quanta 200-3D). Particle size distribution data was obtained by randomly selecting 300 particles in a micrograph, and particle sizes were obtained using ImageJ 1.8 software after doing a suitable calibration. Average particle size, PSD and standard deviation in particle sizes have been estimated using Microsoft Excel and Matlab software.

4.3. Results and Discussion

4.3.1. Selection of solvent and antisolvent

For the identification of the best solvent /anti-solvent pair for preparation of small AP particles, different physical properties of the solvents are compared. Water is chosen as a solvent for AP as the solubility of AP in water is found to be much higher compared to organic solvents. Solvents having low solubility of AP can be used as antisolvent. The experiments are designed to be performed at high temperatures due to the requirement of low processing volume owing to the linear increase of AP solubility with temperature. So the criteria for an antisolvent should be having a higher boiling point and low solubility in AP. *n*-butyl alcohol and *n*-propyl alcohol are selected as anti-solvents for meeting these three criteria. Fig. 4.5b compares boiling points of the different organic solvents while Fig. 4.5c gives the comparison of the solubility of various organic solvents in water. Batch experiments were performed using *n*-butyl alcohol and *n*-propyl alcohol as antisolvents, and the precipitated particles are shown in Fig. 4.4a and b respectively. Initial batch experiments were performed by mixing the aqueous solution and antisolvent using a magnetic stirrer. When *n*-propyl alcohol was used as antisolvent, the solution antisolvent mixture formed a single phase system, but for *n*-butyl alcohol, the solution antisolvent mixture was a multiphase system. For the case of *n*-propyl alcohol, precipitation occurs in the bulk single

phase, and the precipitated particles were susceptible to grow. For *n*-butyl alcohol, solvent and antisolvent phases are intertwined together in the form of emulsion and precipitation occurs at the interface. When stirring was stopped after 1 min, the two phases formed two different layers, and a relatively significant portion of fine particles remains suspended in the antisolvent phase. Relatively coarser particles tend to settle out at the bottom of the reactor which were recycled after separating by decantation. Due to interfacial precipitation, and the particles being in *n*-butyl alcohol phase their growth was subdued. Similar observations have been reported in the literature [16].

(a)   (b)
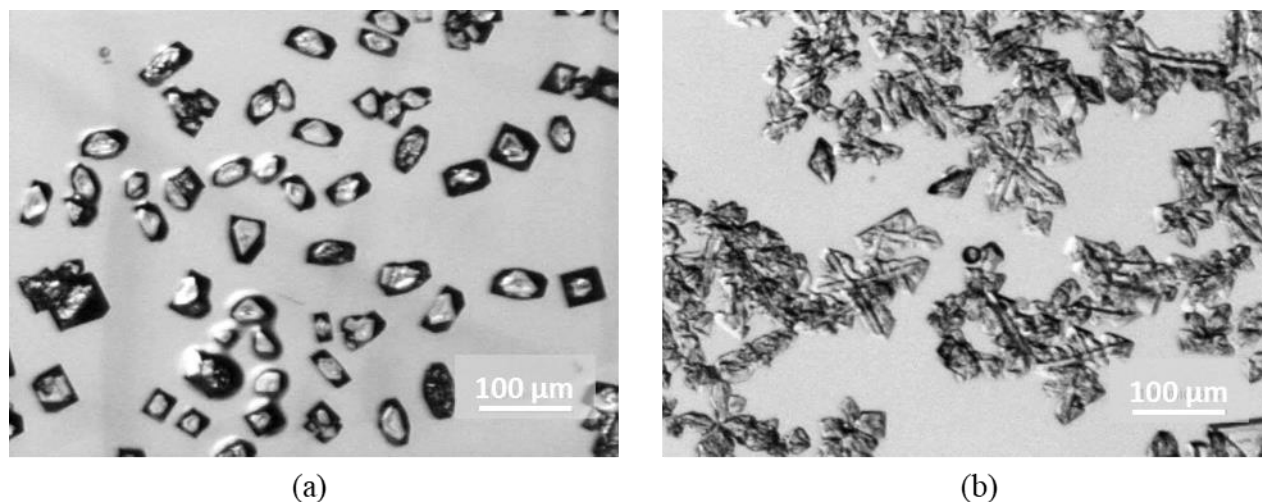
Fig. 4.4. Effect of antisolvents on particle shape. (a) *n*-butyl alcohol, (b) *n*-propyl alcohol

(a)

(b)

(c)
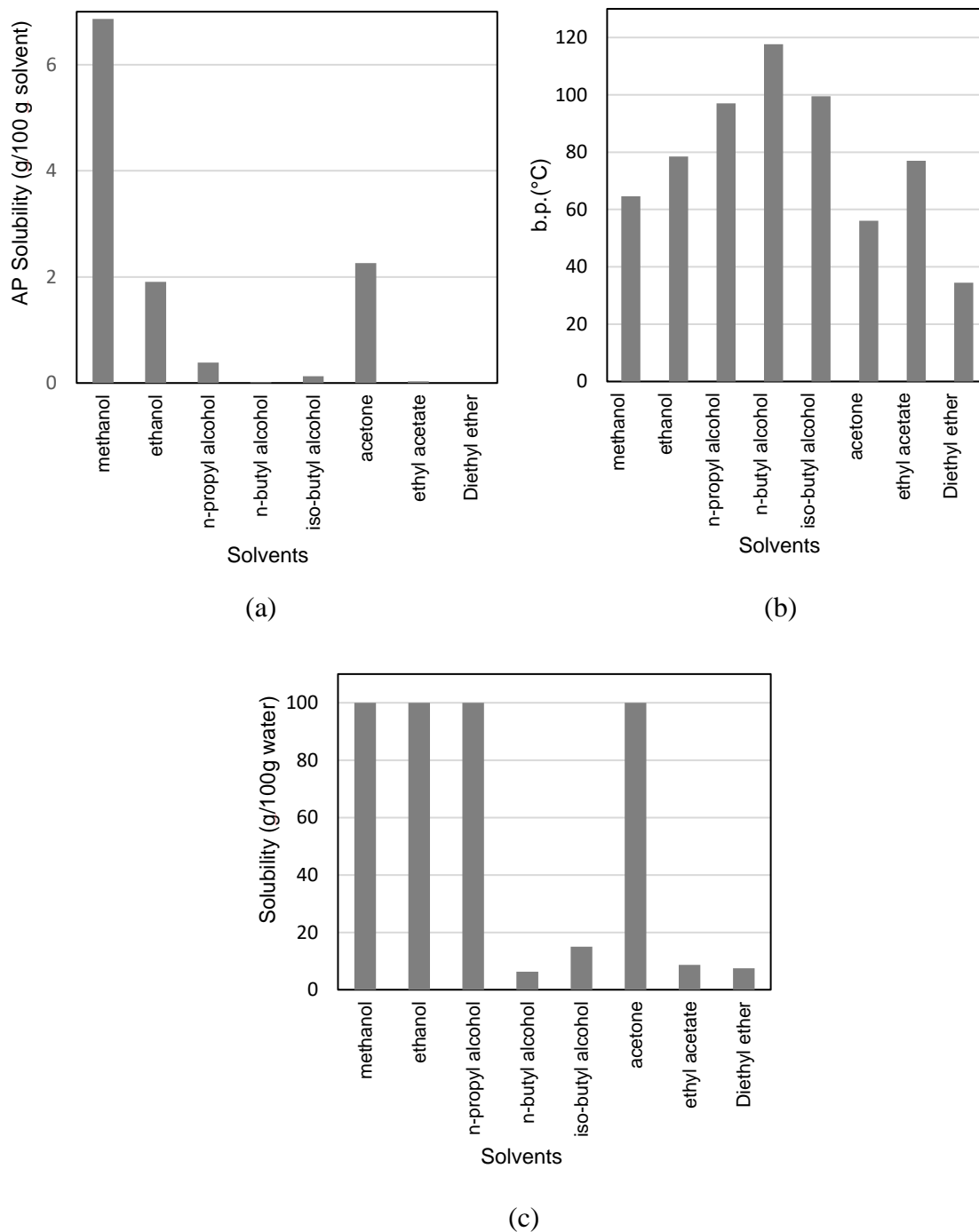
Fig. 4.5. (a) Comparison of solubility of ammonium perchlorate in different organic solvents (g/100g).[18]; (b) Comparison of boiling points of various organic solvents (°C); (c) Comparison of solubility of organic solvents in water (g/100g)

Comparing particle sizes and shapes of the particle images in Fig. 4.4a and b clearly indicate that the antisolvent composition has a strong influence on the shape and size of precipitated particles. The growth of particles in a dendritic structure is observed in the case of *n*-propyl alcohol while for the case of *n*-butyl alcohol a gradual depression on the particle surface from edge toward centre is observed. This is due to the two different growth kinetics in different particle surfaces at the phase interface. Takiyama et al. [19] have reported that the particle surfaces facing the aqueous phase and the organic phase are flat and stepped. It was also observed that *n*-butyl alcohol precipitates more uniform particles in comparison to *n*-propyl alcohol. In addition to this, *n*-propyl alcohol results in a single phase flow in continuous experiments, while *n*-butyl alcohol results in multiphase segmented flow. Precipitation in the segmented flow system (with *n*-butyl alcohol) is limited to the interface. This results in a reduction of the growth of the particles leading to the formation of smaller particles, which is the objective of this work. Hence *n*-butyl alcohol was chosen as the desired antisolvent.

4.3.2. Batch experiments and optimization

4.3.2.1. Effect of the solution and anti-solvent temperature on mean particle size & PSD

Particle formation by the liquid antisolvent process involves two steps - mixing of solution and antisolvent to create supersaturation and then precipitation, which comprises of nucleation and growth of the particles. In the present study, supersaturation is mainly driven by two forces – the anti-solvent effect and solubility decrease due to a temperature reduction of the mixture. Along with anti-solvent addition, the solubility of AP can be further controlled by reducing the temperature resulting from the temperature difference between solution and anti-solvent. This helps to attain higher supersaturation ratio and facilitates the formation of a larger number of nuclei and smaller mean particle size [9]. The classical theory of homogeneous

nucleation also suggests higher nucleation rate results in finer particle size [20]. To understand

the effect of temperature on the precipitation process, experiments were performed at six initial

temperatures of the solution and three different temperatures of the anti-solvent. These effects on

mean particle size are shown in Fig. 4.6 and Fig. 4.7(a-c) represent how the PSD of precipitated

AP particles changes with initial solution temperatures for anti-solvent temperatures of -10°C,

0°C and 30°C respectively.
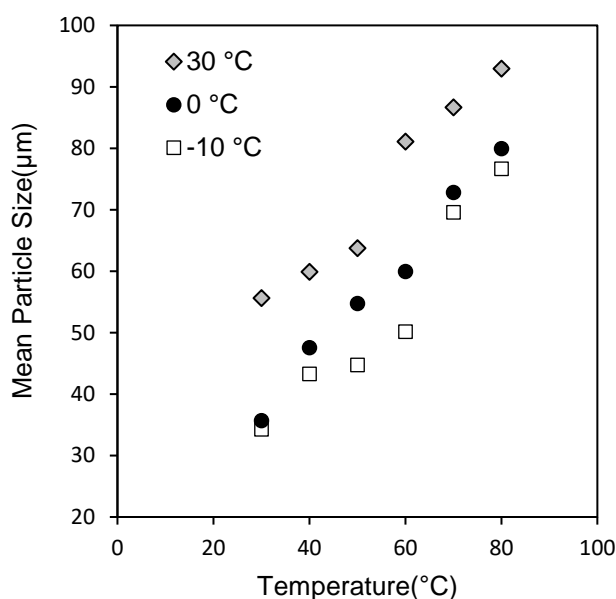
Fig. 4.6. Effect of initial solution temperature and antisolvent temperature on mean particle size
(in the presence of ultrasound-induced mixing)

For anti-solvent addition at a lower temperature, the mean particle sizes obtained were

found to be smaller than higher temperature anti-solvent addition case irrespective of the initial

temperature of AP solution. However, for all antisolvent addition temperature, the mean particle

size increases with initial solution temperature, and the peaks of the particle size distribution

moves towards higher particle sizes. Comparing Fig 4.7a, b and c we can say these movement of

peaks are receded with reducing antisolvent temperature. Fig. 4.7 also shows the peak width at

half height also increases with increasing solution temperature which infers to a wider distribution of particle sizes. The movement of the peaks and entire number fraction distribution to larger sizes can be explained by uncontrolled growth along the particle structure and agglomeration. The measured PSDs are composed of a mixture of single particles and agglomerates. Agglomerates probably dominate in forming the second peak of higher particle size. This could be explained by comparatively a lesser amount of agglomeration that can be achieved using low temperature antisolvent.
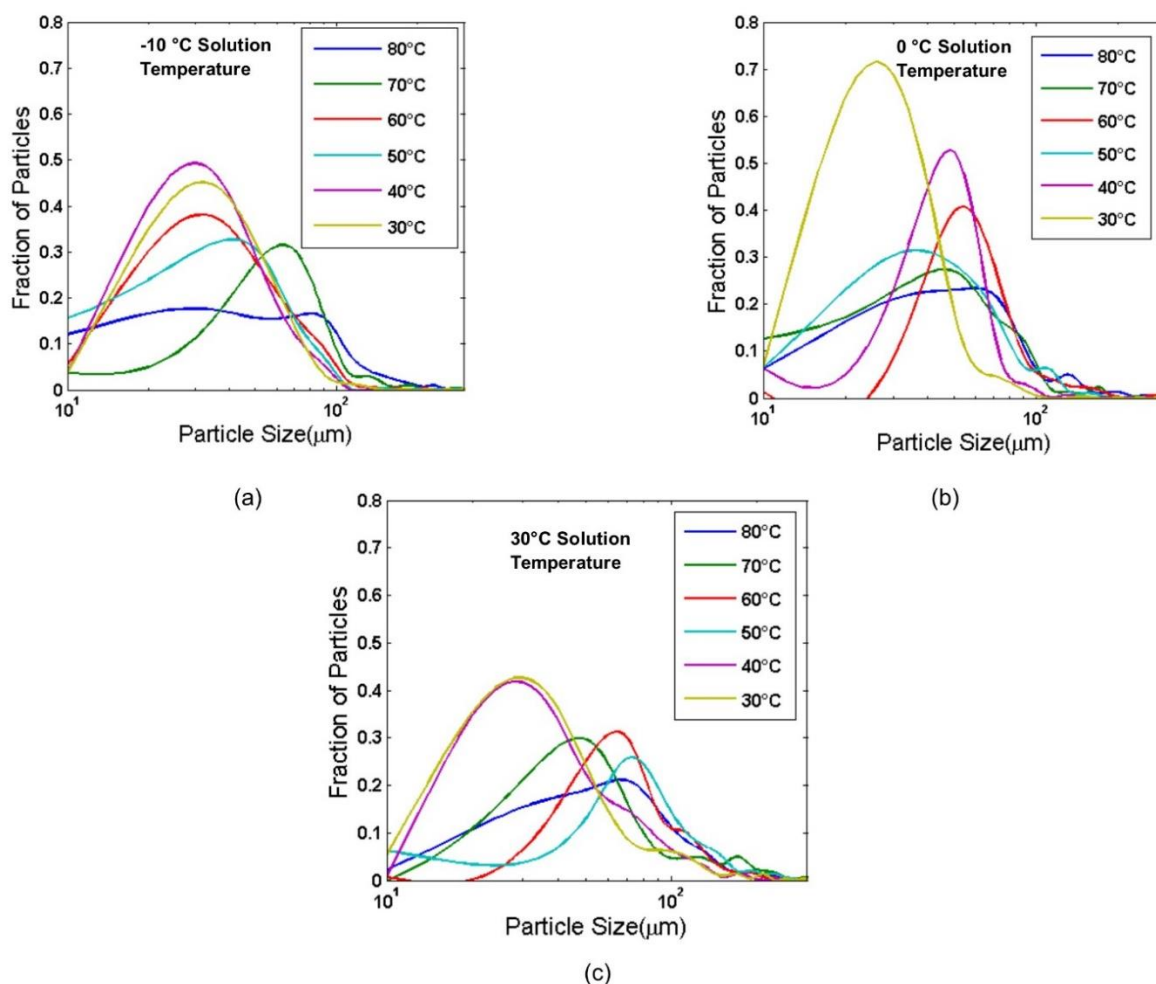
Fig. 4.7. Effect of initial solution temperature and antisolvent temperature on PSD

For the case of combined antisolvent-cooling precipitation, the equilibrium concentration of the solute is a function of both the solvent/antisolvent composition and the temperature (T) in the system. So the supersaturation and nucleation rate depend on both of the factors. Though solvent to antisolvent ratio is kept constant at 1:1, the antisolvent effect enhances at higher temperature scenario as the solubility of antisolvent in the solvent increases with temperature.

Addition of antisolvent at low temperature produces a higher temperature gradient in the system resulting in faster supersaturation, higher nucleation rates and lower particle sizes which are in accordance with experimental data. The level of super saturation can be further increased by keeping the solvent saturated at a higher temperature that helps to generate steeper temperature gradient and should result in lower particle sizes. However, the trends in experimental particle sizes are exactly the opposite. Conversely, higher solution temperature facilitates the growth of the particles as a higher amount of AP is present in the solution compared to lower solution temperature scenarios. The growth of AP particles in aqueous solution is primarily controlled by the diffusion while in the antisolvent phase growth is arrested due to lack of AP in the antisolvent phase. Though the AP particles were collected from the antisolvent phase, vigorous mixing with the solution phase using magnetic stirrer or an ultrasound bath was seen to promote growth and agglomeration.

Fig. 4.8 shows the variation in AP solubility in water and the variation of AP yield with solution temperature. While the solubility of AP in water increases linearly with increasing temperature, the % yield also increases with solution temperature but at a lower rate. So an optimized solution and antisolvent temperature of 50°C and -10°C are chosen respectively based on desired mean particle size and yield.
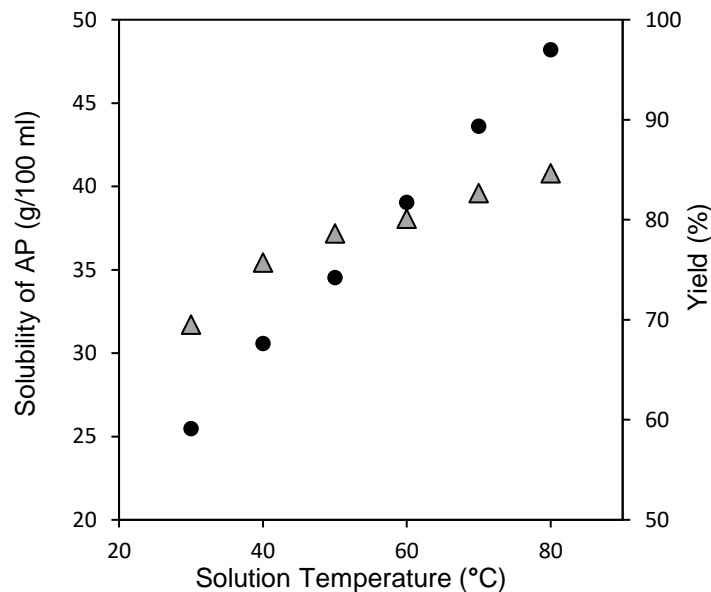
Fig. 4.8. Variation of solubility of AP in water with temperature (°C) and Effect of different solution temperatures on yield (at -10°C antisolvent temperature and ultrasound)

4.3.2.2. Effect of mixing conditions

Uniform mixing conditions in the reactor generate uniform supersaturation in a very short time, eliminating mixing limitation to achieve finer mean particle size with narrow PSD [20]. If the mixing is insufficient in the reactor, it could be inferred that confined elevated supersaturation gets generated locally at the point of anti-solvent addition, which subsequently results in non-uniform supersaturation throughout the reactor. To refrain from such situations to occur and in order to get good control over PSD, an intensified mixing in microscopic level of solution and antisolvent is necessary. One such option is to induce spatially uniform micromixing can be in the form of ultrasonic waves which are known to provide better mixing in precipitation processes of various type of materials [21, 22]. When ultrasound propagates through any liquid generation of cavities throughout the medium (although spatially distributed based on intensity) and their subsequent collapse leads to the formation of microscopic regions of extreme excitations with high temperature and pressure [23]. Along with the collapse of

transient cavitation bubbles, oscillation of stable cavitation bubbles and acoustic streaming also results in the improvement of micromixing [24]. Ultrasound shockwaves are reported to increase the nucleation rate due to an increase in the local concentration of solute molecules in the shock and greater extent of heterogeneous nucleation [25]. Here, an ultrasound bath is used instead of a conventional magnetic stirrer to verify the effect of mixing ensuring rapid and spatially uniform supersaturation. In the rest of this section, we will discuss the effect of ultrasound on the precipitation process. Fig. 4.9a shows the effect of reduced particle size using ultrasound when compared to the conventional magnetic stirrer. It is evident that the ultrasound reduced the mean particle size irrespective of the initial solution temperature when other conditions were kept constant.

In the absence of ultrasound, poor micro-mixing controls the mixing process; hence it becomes hard to attain superior control over particle size [20]. While enhanced micro-mixing attained by the usage of ultrasound produces uniform supersaturation and drastically reduces the mean AP particle size. It has been reported in the literature that the application of ultrasound in ASP diminishes induction times for nucleation as well as the spread of variability in induction times for a constant supersaturation ratio [21]. Comparing the particle images in Fig. 4.9b, it could be inferred that sonication also reduced the degree of agglomeration of precipitated AP particles significantly, however the growth of the single particles is not reduced significantly. This could be due to the fact that the usage of ultrasound is more effective in arresting agglomeration than growth. With cavitation, intensive vibration and uniform distribution of local nuclei population ultrasound is effectively reduces agglomeration. The shock waves, generated by cavitation, curtail the time of contact among particles. As a consequence, after contact the adequate time to bond together is not being provided to the particles resulting in prevention of

particle agglomeration. [23, 26]. On the contrary, growth rates were observed to be of the same order of magnitude for both with and without ultrasound [21, 27].

(a)
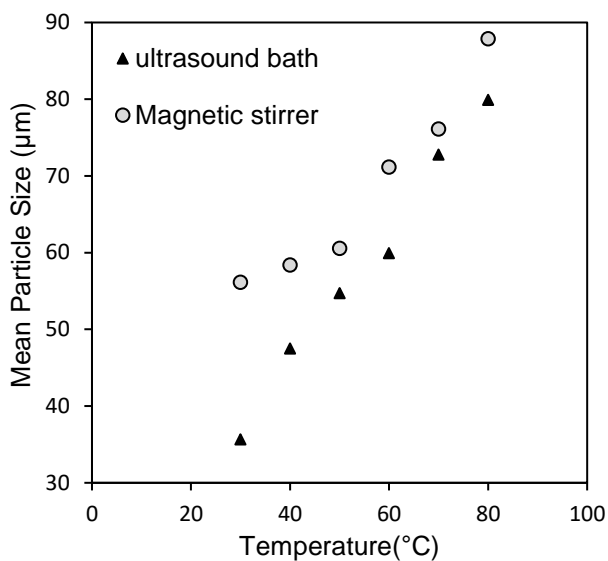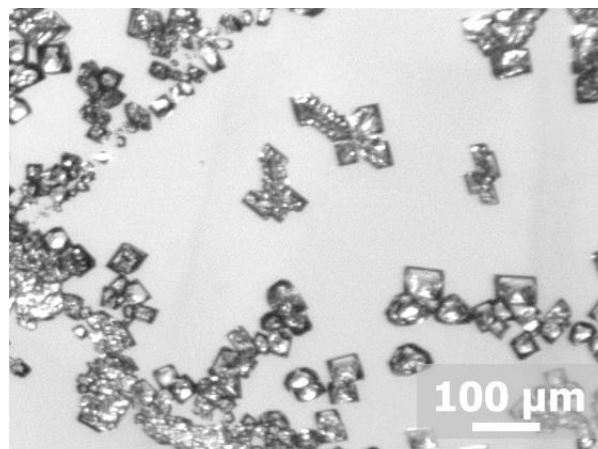
| Magnetic Stirrer | Ultrasound Bath |
| Mean Particle size 69.42 μm | Mean Particle size 47.53 μm |

(b)

Fig. 4.9. (a) Effect of mixing on mean particle size at 0°C antisolvent addition temperature, (b) Effect of Ultrasound on Particle Aggregation (Solution at 40°C, Antisolvent at 0°C)
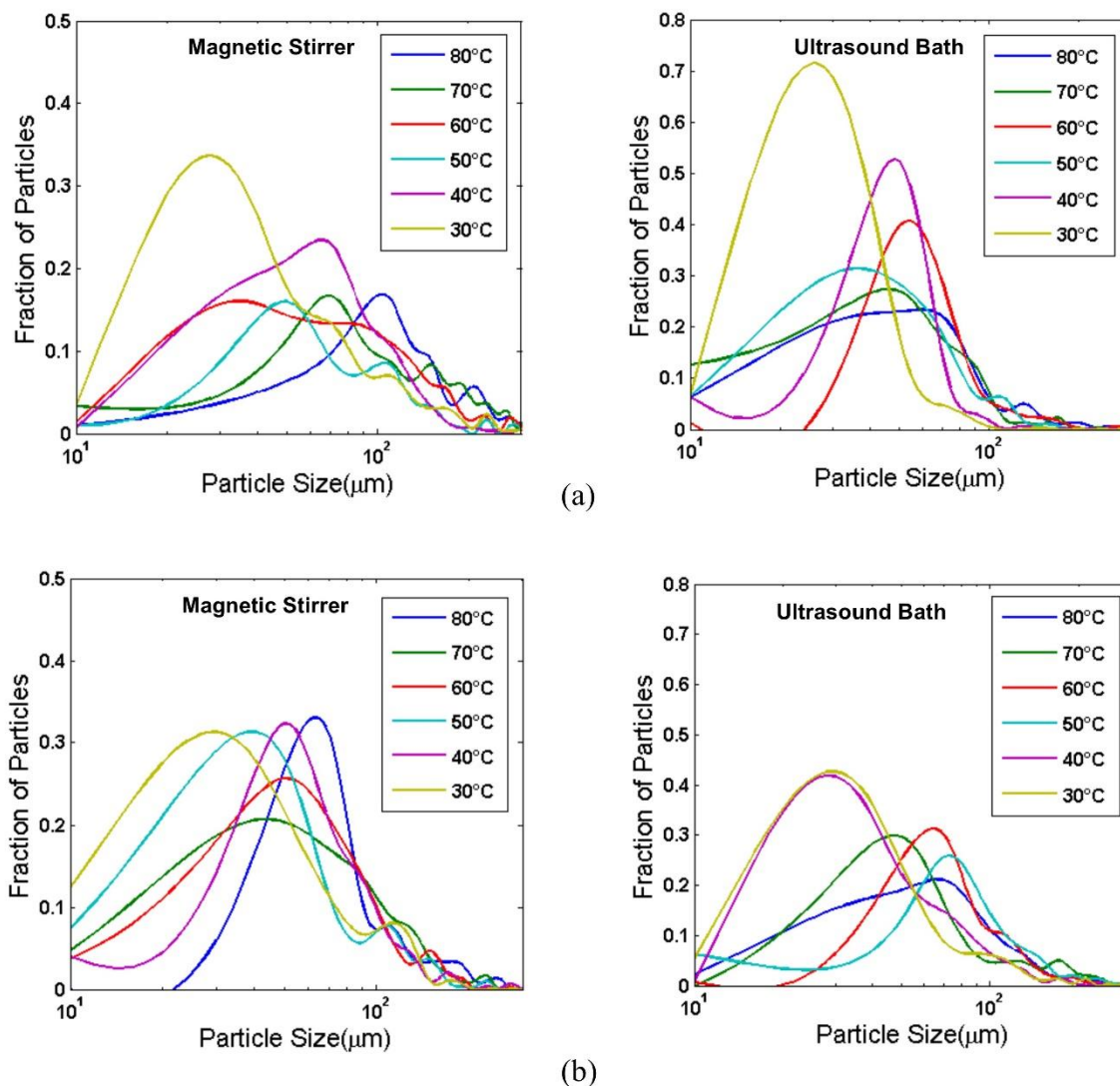
Fig. 4.10. Effect of ultrasound on PSD for Solution temperature of 50°C: (a) Antisolvent at 30°C, (b) Antisolvent at 0°C.

The usage of ultrasound has resulted in a movement of the peaks to lower particle sizes as well as narrower PSD irrespective of temperatures (see Fig. 4.10). Though the usage of ultrasound has shifted the peaks to lower particle sizes, an increase of peak width at half height resulting from wider PSD was observed with increasing initial solution temperature. The occurrence of second peaks in higher particle zones has been decreased significantly due to the

minimal aggregate formation in the presence of the ultrasonic bath. At higher solution temperatures, the reduction in mean particle size reduction is found to be lesser. With increasing temperature, the vapour pressure of the liquid increases, which reduces the intensity of collapse of the cavitation bubbles [28] . This makes the usage of ultrasound less effective in the prevention of agglomeration at higher temperatures resulting in less reduction in the particle size with ultrasonication at higher temperatures (see Fig. 4.9a). It could be concluded that ultrasound could be used as mixing enhancement and agglomeration prevention tool for antisolvent precipitation of AP particles effectively.

4.3.3. Kinetics study

Kinetic studies of a process are typically performed to understand the characteristic time of a system. This knowledge is important while designing a reactor as the mixing time should be lower than the system characteristic time for making the process kinetically dependent rather than mixing dependent. As the reactor size increases mixing time also increases for similar operating conditions which eventually limit the size at which the reactor can be operated. A reactor can be considered perfectly mixed depending on the kinetics of the process [29]. The kinetic data helps to understand the limit of scale-up operations that can be achieved providing the desired outcome.

A precipitation process comprises of three major stages - the development of supersaturation, followed by nucleation, and then growth. Here, for getting small particle sizes in ASP, while performing continuous experiments, the residence time in the reactor was needed to be chosen suitably so that the growth dominated region can be avoided. As the particle formation timescales are very small, a FBRM probe is used for online monitoring the mean chord length, which is a representation of the mean particle size of the population [30]. The mean chord length

is plotted with time in Fig. 4.11, for the optimum experimental conditions found in the batch. After 25 seconds a transition region is observed where the growth of particles suddenly increased, (see Fig. 4.11) for the optimum conditions found previously. A residence time lower than 25 seconds is kept for all continuous flow experiments to suppress the growth of the precipitated particles. Moreover, a trend is clearly apparent that the dotted line can be considered as the transition between nucleation and growth dominated regions. This can be explained by the lamer mechanism which conceptually segregates the nucleation and growth in two steps. A rapid increase in the amount of available solute in the solution initially drives the supersaturation ratio en route to the metastable zone limit. The nucleation rate shoots up to a very higher value on the verge of the metastable zone, and a large population of nuclei are simultaneously born. This considerably lessens the concentration of free solute monomers in the solution. As these nuclei initiate to grow under the control of the diffusion of the solute monomers through the solution, they drive the supersaturation downward again and thereby arresting further nucleation. This starts the growth dominated region subsequently [31, 32] .
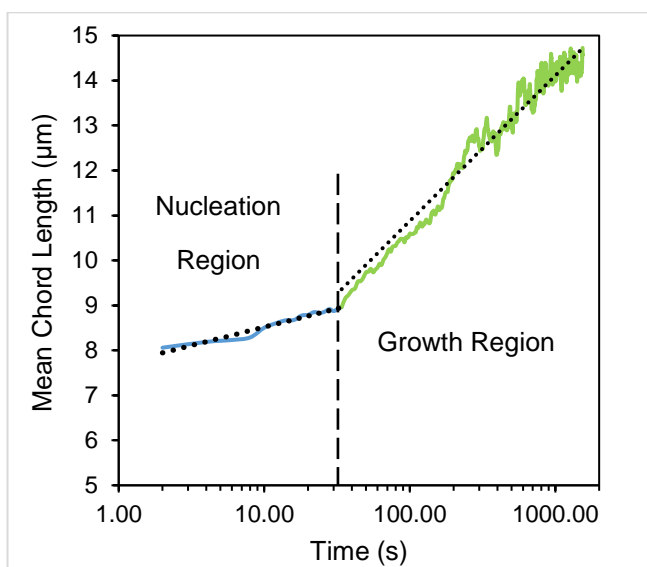
Fig. 4.11. Mean chord length variation with time (50°C solution temperature and -10°C antisolvent temperature)

4.3.4. Continuous precipitation

Continuous experiments were performed in glass capillaries using a Y-joint mixer at similar conditions to batch experiments. The experiments were performed with and without capillary immersion in an ultrasound bath. Solution temperatures were kept at 30 °C to 80 °C while the antisolvent temperature was kept as -10 °C. Without the use of ultrasound bath, experiments could not be performed at higher solution temperatures (more than 50°C) due to clogging problem in the inlet Y-joint and glass capillary. Capillary immersion in the ultrasound bath reduced the clogging problem, but 70°C and 80°C solution temperature still resulted in partial blockage of the capillary. For lower solution temperatures (< 70°C) continuous operation for more than an hour without any clogging could be achieved under sonication. Fig. 4.12a and c shows mean particle size and typical particle images of the precipitated AP particles in batch and continuous mode respectively.

It was observed that at a fixed antisolvent temperature the mean particle size increases with solution temperature in batch mode while in continuous mode it decreases until 50°C and then increases. Hence solution temperature at 50°C is recommended for further experiments as the optimum as it led to uniform sized particles of mean particle size of 14.29 μm and 11.46 μm in the absence and presence of ultrasound respectively. Fig. 4.12b represents the comparison of the obtained PSDs in continuous and batch modes for the solution temperature where the lowest mean particle size is obtained in a continuous flow, i.e. 50°C. The variation in mean particle size with solution temperature is found to be of different fashion compared to batch experiments. For the case of continuous flow, inlet Y-joint provides better mixing than batch experiments using magnetic stirrer. Thus the usage of ultrasound does not drastically improve the mixing performance in a continuous flow.

(a)

(b)

Batch   Continuous

(c)
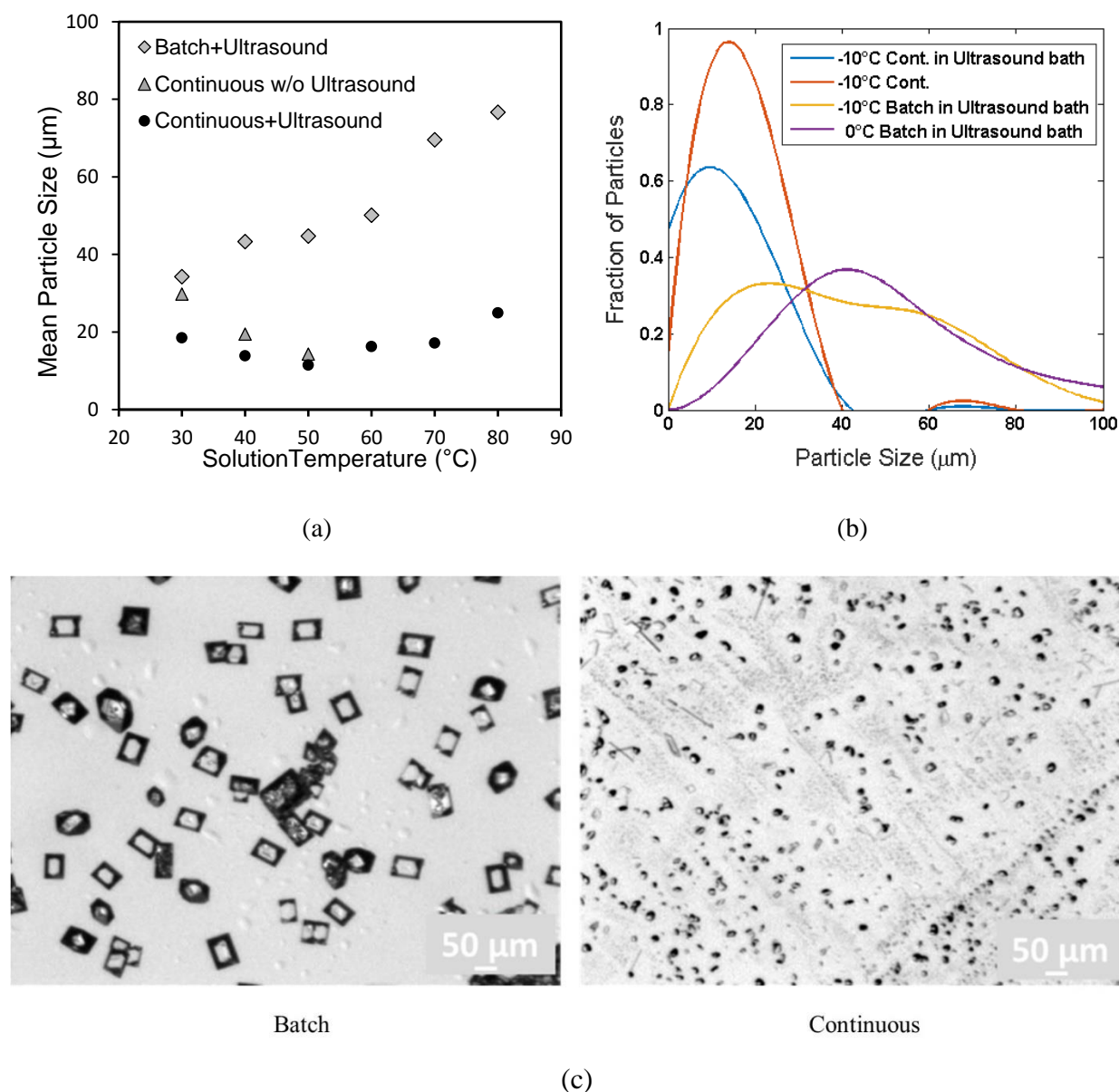
Fig. 4.12. Comparison of between batch and continuous precipitation of AP (Solution at 50°C, Antisolvent at -10°C) (a) Mean particle size, (b) Particle size distribution (c) Optical microscopy images

However, it helps in preventing agglomeration and particle deposition at the mixer and capillary wall. With increasing temperature, the cavitation rate also decreases which results in decreased efficiency[28] of ultrasound in agglomeration prevention, which was observed for solution

temperature above 50°C. Typical SEM images of precipitated AP particles formed at different temperatures are shown in Fig. 4.13.
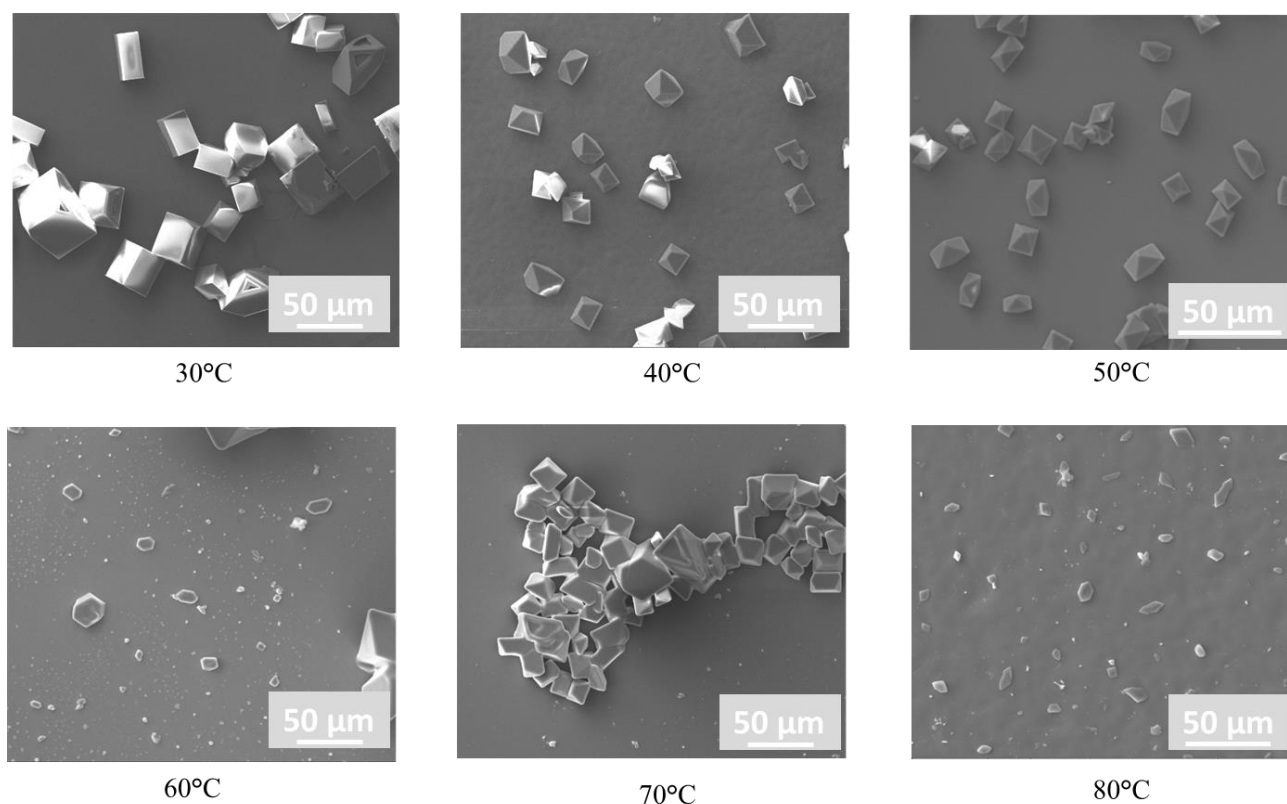
Fig. 4.13. SEM Micrographs of continuously precipitated AP particles at increasing solution temperature (Antisolvent Temperature -10 °C, Ultrasound Bath)

With higher solution temperature, the temperature difference between the solvent and antisolvent increases resulting in higher supersaturation while due to the higher solubility of AP at higher temperatures more AP is available in the system facilitating the growth of the particles. These counteracting effects work simultaneously on mean particle size. As *n*-butyl alcohol and water are partially miscible, multiphase flow is observed in the capillary under continuous operation, and the mass transfer and precipitation occur only at the liquid-liquid interface rather than in bulk. In multiphase flow, precipitation occurs at the liquid-liquid interface, as the organic antisolvent phase only interacts with the aqueous solution phase at the interface. Due to the lack

of AP in the antisolvent system, the tendency for the growth of the particles is lowered. While in the batch process, due to precipitation in the agitated bulk system, the particles were more susceptible to growth with increasing temperatures despite higher supersaturation achieved.

In the continuous process, the higher supersaturation with increasing temperatures dominates tendency to particle growth till 50°C. For higher temperatures due to the huge amount of AP available in the system facilitates growth and it starts to dominate the higher supersaturation effects. For higher temperatures (> 50°C) this resulted in a rise in mean particle size with increasing temperature. Lower residence time in continuous flow system compared to the batch system also helped in reduction of growth resulting in lower mean residence time. Though the precipitated AP particles are close to the desired particle size, the processing capacity of the system was 17g per hour. Increasing flow rates for increasing capacity resulted in clogging of the capillary reactor. In order to avoid clogging and yet have large scale precipitation, usage impinging jet reactors for precipitation is explored in the next chapter.

4.4. Conclusion

A continuous ASP method was optimized for the safe and rapid preparation of ammonium perchlorate (AP) particles. Water and *n*-butyl alcohol found to be best suitable solvent and anti-solvent pair. Precipitation in a batch reactor with and without ultrasound induced mixing, and continuous capillary reactor were studied in order to remove mixing limitations. For batch systems, usage of ultrasound bath for more intensified mixing compared to magnetic stirrer has resulted in a significant decrease in mean particle size. Temperatures of 50°C and -10°C were found as the optimum solution temperature and antisolvent temperature, finding a balance between particle size and yield. In continuous operation in a capillary reactor, interfacial

precipitation was observed in the slug flow regime, where precipitation occurring only at the liquid-liquid interface provides less tendency to the growth of the particles. Continuous flow experiments often lead to clogging at higher solution temperatures. Usage of an ultrasound bath resulted in better mixing as well as clogging free operation for hours, however scalability will remain an issue.

4.5. References

1.   Lince, F., Marchisio, D.L., and Barresi, A.A., *Strategies to control the particle size distribution of poly-ε-caprolactone nanoparticles for pharmaceutical applications.* Journal of colloid and interface science, **2008**. 322(2): p. 505-515.

2.   Horn, D. and Rieger, J., *Organic nanoparticles in the aqueous phase—theory, experiment, and use.* Angewandte Chemie International Edition, **2001**. 40(23): p. 4330-4361.

3.   Chiou, H., Chan, H.-K., Prud'homme, R.K., and Raper, J.A., *Evaluation on the use of confined liquid impinging jets for the synthesis of nanodrug particles.* Drug development and industrial pharmacy, **2008**. 34(1): p. 59-64.

4.   Dalvi, S.V. and Dave, R.N., *Controlling particle size of a poorly water-soluble drug using ultrasound and stabilizers in antisolvent precipitation.* Industrial & Engineering Chemistry Research, **2009**. 48(16): p. 7581-7593.

5.   Chen, X., Young, T.J., Sarkari, M., Williams III, R.O., and Johnston, K.P., *Preparation of cyclosporine A nanoparticles by evaporative precipitation into aqueous solution.* International Journal of Pharmaceutics, **2002**. 242(1-2): p. 3-14.

6.   Kakran, M., Sahoo, N., Li, L., Judeh, Z., Wang, Y., Chong, K., and Loh, L., *Fabrication of drug nanoparticles by evaporative precipitation of nanosuspension.* International journal of pharmaceutics, **2010**. 383(1-2): p. 285-292.

7.   Zhao, H., Wang, J.-X., Wang, Q.-A., Chen, J.-F., and Yun, J., *Controlled liquid antisolvent precipitation of hydrophobic pharmaceutical nanoparticles in a microchannel reactor.* Industrial & Engineering Chemistry Research, **2007**. 46(24): p. 8229-8235.

8.   Zu, Y., Wu, W., Zhao, X., Li, Y., Wang, W., Zhong, C., Zhang, Y., and Zhao, X., *Enhancement of solubility, antioxidant ability and bioavailability of taxifolin nanoparticles by liquid antisolvent precipitation technique.* International journal of pharmaceutics, **2014**. 471(1-2): p. 366-376.

9.   Beck, C., Dalvi, S.V., and Dave, R.N., *Controlled liquid antisolvent precipitation using a rapid mixing device.* Chemical Engineering Science, **2010**. 65(21): p. 5669-5675.

10.   Vehring, R., *Pharmaceutical particle engineering via spray drying.* Pharmaceutical research, **2008**. 25(5): p. 999-1022.

11.   Sansone, F., Picerno, P., Mencherini, T., Villecco, F., D'ursi, A., Aquino, R., and Lauro, M., *Flavonoid microparticles by spray-drying: Influence of enhancers of the dissolution rate on properties and stability.* Journal of Food Engineering, **2011**. 103(2): p. 188-196.

12.   Abbas, A., Nobbs, D., and Romagnoli, J.A., *Investigation of on-line optical particle characterization in reaction and cooling crystallization systems. Current state of the art.* Measurement Science and Technology, **2002**. 13(3): p. 349.

13.   Reverchon, E., Adami, R., Caputo, G., and De Marco, I., *Spherical microparticles production by supercritical antisolvent precipitation: interpretation of results.* The Journal of supercritical fluids, **2008**. 47(1): p. 70-84.

14.   Kawashima, Y. and York, P., *Drug delivery applications of supercritical fluid technology*. **2008**, Elsevier.

15.   Mukhopadhyay, M. and Dalvi, S.V., *Mass and heat transfer analysis of SAS: effects of thermodynamic states and flow rates on droplet size.* The Journal of supercritical fluids, **2004**. 30(3): p. 333-348.

16.   Levinthal, M.L., Allred, G.F., and Poulter, L.W., *Method of making finely particulate ammonium perchlorate*. **1977**, Google Patents.

17.   Ma, Z., Li, C., Wu, R., Chen, R., and Gu, Z., *Preparation and characterization of superfine ammonium perchlorate (AP) crystals through ceramic membrane anti-solvent crystallization.* Journal of Crystal Growth, **2009**. 311(21): p. 4575-4580.

18.   Willard, H. and Smith, G.F., *The Perchlorates of the alkali and alkaline earth metals and ammonium. Their solubility in water and other solvents* Journal of the American Chemical Society, **1923**. 45(2): p. 286-297.

19.   Takiyama, H., Otsuhata, T., and Matsuoka, M., *Morphology of NaCl crystals in drowning-out precipitation operation.* Chemical Engineering Research and Design, **1998**. 76(7): p. 809-814.

20.   Dalvi, S.V. and Dave, R.N., *Analysis of nucleation kinetics of poorly water-soluble drugs in presence of ultrasound and hydroxypropyl methyl cellulose during antisolvent precipitation.* International journal of pharmaceutics, **2010**. 387(1): p. 172-179.

21.   Ruecroft, G., Hipkiss, D., Ly, T., Maxted, N., and Cains, P.W., *Sonocrystallization: the use of ultrasound for improved industrial crystallization.* Organic Process Research & Development, **2005**. 9(6): p. 923-932.

22.   Thorat, A.A. and Dalvi, S.V., *Liquid antisolvent precipitation and stabilization of nanoparticles of poorly water soluble drugs in aqueous suspensions: Recent developments and future perspective.* Chemical Engineering Journal, **2012**. 181: p. 1-34.

23.   Guo, Z., Zhang, M., Li, H., Wang, J., and Kougoulos, E., *Effect of ultrasound on anti-solvent crystallization process.* Journal of Crystal Growth, **2005**. 273(3): p. 555-563.

24.   Jordens, J., Bamps, B., Gielen, B., Braeken, L., and Van Gerven, T., *The effects of ultrasound on micromixing.* Ultrasonics sonochemistry, **2016**. 32: p. 68-78.

25.   Sander, J.R., Zeiger, B.W., and Suslick, K.S., *Sonocrystallization and sonofragmentation.* Ultrasonics sonochemistry, **2014**. 21(6): p. 1908-1915.

26.   De Castro, M.L. and Priego-Capote, F., *Ultrasound-assisted crystallization (sonocrystallization).* Ultrasonics sonochemistry, **2007**. 14(6): p. 717-724.

27.   Bari, A.H., Chawla, A., and Pandit, A.B., *Sono-crystallization kinetics of K2SO4: Estimation of nucleation, growth, breakage and agglomeration kinetics.* Ultrasonics sonochemistry, **2017**. 35: p. 196-203.

28.   Mason, T.J. and Lorimer, J.P., *Applied sonochemistry: uses of power ultrasound in chemistry and processing.* Betz-Druck, Darmstadt, **2002**: p. 3-4.

29.   Paul, E.L., Atiemo-Obeng, V.A., and Kresta, S.M., *Handbook of industrial mixing: science and practice.* **2004**: John Wiley & Sons.

30.   Schöll, J., Vicum, L., Müller, M., and Mazzotti, M., *Precipitation of L-Glutamic Acid: Determination of Nucleation Kinetics.* Chemical engineering & technology, **2006**. 29(2): p. 257-264.

31.   Thanh, N.T., Maclean, N., and Mahiddine, S., *Mechanisms of nucleation and growth of nanoparticles in solution.* Chemical reviews, **2014**. 114(15): p. 7610-7630.

32.   Chu, D.B., Owen, J.S., and Peters, B., *Nucleation and Growth Kinetics from LaMer Burst Data.* The Journal of Physical Chemistry A, **2017**. 121(40): p. 7511-7517.

Chapter 5

Confined Impinging Jet Reactor for Antisolvent Precipitation
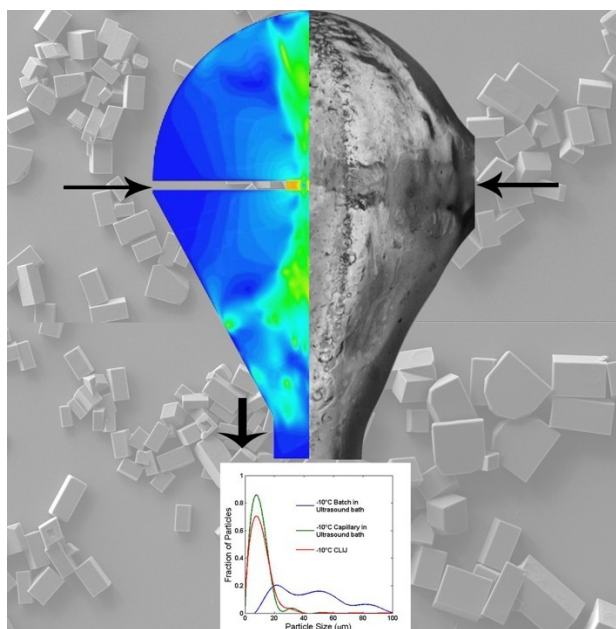
5. Confined Impinging Jet Reactor for Antisolvent Precipitation[4]

A confined impinging jet flow reactor (CIJR) was used for clogging free continuous antisolvent precipitation of ammonium perchlorate (AP) microparticles. The geometry of the CIJR was optimized to achieve excellent mixing with a significant reduction in the particle deposition on walls. The flow in the IJR was explored through computational fluid dynamic simulations. Multiphase VOF simulations were performed to study the formation and fragmentation of liquid sheets formed by two impinging jets. Finally, liquid antisolvent precipitation of AP was performed in a CIJR at optimum process conditions and using water and *n*-butyl alcohol as a solvent and antisolvent system for optimum performance. The performance of CIJR was compared with the experiments in batch mode as well as a continuous capillary reactor. At identical inlet jet velocity of the solution and antisolvent phases that corresponded to $1792 < Re < 7193$ for the saturated aqueous solution of AP and $1135 < Re < 4553$ for the antisolvent butanol phase, 8.98-16.98 µm Ammonium perchlorate particles were attained.

5.1. Introduction

Reduction in the particle size enhances its rate of dissolution or reaction, through the enlarged surface area per unit volume. A clogging free continuous antisolvent precipitation method for AP as a model system was developed in the previous chapter. The capillary microreactor system was limited to 17g/hour due to clogging issue at higher flow rates. Scaling up of the

precipitation system without compromising with the quality of the particles was explored in this chapter. A confined impinging jet reactor (CIJR) was used for this purpose. Impinging jet reactors rapidly mix two jets of liquids impinging at very high velocity (1.0-6.8 m/s in our experiments) and necessitate no external mechanical mixing. As a result of their collision and impingement, high turbulent kinetic energy is generated and then quickly dissipated, inducing very fast mixing compared to traditional continuous stirred tank reactors [1, 2]. Mostly three types of impinging jets are reported in literature – free, submerged and confined [3]. Confined impinging jet reactors (CIJR) are typically used for the case of flash precipitation. CIJR is a single-pass system where smaller characteristic mixing timescales are achieved inside the reactor enclosure, in comparison to the traditional mixing processes. The fundamental kinetics of a process is typically unveiled from the influence of mixing in the system if the fluid structures are mixed on a microscopic level. Comparison of mixing and the process time scale can be obtained from the value of the Damköhler number ($Da = {}^{\tau_{Mixing}}/_{\tau_{Process}}$). For values of Damköhler number $\ll 1$, a process is not influenced by the mixing performance of the system. However, for the case of fast processes, i.e. for higher values of Damköhler numbers, the process becomes dependent on mixing. CSTRs are not capable of fulfilling such high mixing requirement for a very fast process, while due to their high mixing potential, CIJRs can operate in a kinetically controlled regime [2]. Moreover, mixing has a critical role in ASP process, as it regulates the initiation of supersaturation, on which the nucleation and growth rates are governed by. A small increase of supersaturation can result in many order increase in the nucleation rate values but only a small increase in the growth rate. Hence, nucleation is favoured over growth, and small particles are produced at high supersaturation ratios [4-6]. In addition to this, rigorous micromixing throughout the system leads to the same supersaturation for most of the nuclei in the system, resulting in uniform growth and

particle size. On the contrary, inadequate mixing of the system leads to growth disparity among nuclei, resulting in a wider PSD.

CIJRs have been reported to be used in precipitation applications due to its lower characteristic mixing time in the order of milliseconds [7-9]. Several authors have reported that the use of CIJR shows the ability to produce small particles via reactive precipitation [2, 10-12], liquid anti-solvent precipitation [7, 13, 14], supercritical antisolvent precipitation [15, 16] and precipitation polymerization [17]. Though Chiou et al. have reported that this process is not suitable for ASP of all compounds, it can be concluded from their work that in such single-pass process, very fast precipitating systems (i.e. flash precipitation) can only be efficiently operated [13].

The initial geometry of CIJR developed by Prudholmme group[3] was widely used for flow characterization and applications in the literature. In the present work, the aforementioned geometry is modified for removal of wall effects and deposition, and the mixing performance is investigated in both the reactor geometries using computational fluid dynamics (CFD). The turbulence in the CIJR geometry was modelled by the Reynolds-averaged Navier-Stokes (RANS) apporach[18]. Gavi et al. [19] have shown that the flow predicted by RANS k-ε turbulence model with enhanced wall treatment accords well with the large eddy simulation (LES) as well as the experimental results obtained by Johnson and Prud'homme[3]. Studies by several authors [10, 18-24] have shown that a two-layer k–ε model is able to satisfactorily predict the turbulent flow fields in an impinging jet reactor of similar dimensions. As the average Re in our operating conditions resides in the turbulent regime, standard k-ε model [25] with enhanced wall treatment [26] considering the pressure gradient effects in the flow domain was employed to model the flow in the CIJR [27]. Although single-phase simulations have been carried out widely in the literature to

study impinging jets, in the actual experimental condition, two liquid phases impinging with each other to form a thin liquid sheet inside the confined reactor initially filled with quiescent air. In addition to this, in single phase simulations, the hydrodynamic parameters are under-predicted as it accounts for the viscous dissipation. Such a system can only be predicted with the help of multiphase models. Hence it is essential to use multiphase computational models for the study of impinging jets. One of the primary studies using Volume of Fluids (VOF) approach for an oblique impinging water jet system was performed by Inoue et al. [28]. Later, Chen et al. [29] and Arienti et al. [30] have also studied the evolution of liquid sheets formed by the impingement of two single liquid slanted jets, and its subsequent fragmentation into droplets and ligaments using VOF. In the present work, the interaction of the two impinging jets of different liquids is simulated using the VOF model and compared with experimentally captured videos at high speed. The developed impinging jet reactor was used for rapid antisolvent precipitation, which induces uniform and fast mixing in the system, resulting in faster nucleation and smaller particles. The work appears to be the first systematic study in which the mixing performance, impingement dynamics of jets are studied in a CIJR to perform liquid antisolvent precipitation in multiphase flow.

In view of this introduction, the chapter is organized as follows: the next section details out the experimental and the modelling methods we implemented, and the data processing techniques in this work. Subsequently, mixing performance and jet impingement dynamics in our impinging jet reactor is investigated using CFD. This was followed by the observations on particle size and PSD of the AP particles obtained from the impinging jet reactor. Then the particle size and the PSD obtained in various experimental strategies are compared before summarizing the major findings from this work.

5.2. Experimental and modelling

5.2.1. Materials

Organic solvents such as *n*-butyl alcohol (99.5% pure from Merck Chemicals Ltd, India) and n-propyl alcohol (99.0% pure from Merck Chemicals Ltd, India) have been used as anti-solvents. Ammonium Perchlorate (AP) was obtained in powder form (~ 300-500 micron size). Millipore water is used for making the aqueous solution of AP. These chemicals have been used without any further purification.

5.2.2. Experimental Procedure & Analysis

5.2.2.1. Continuous experiments in impinging jets

1 mm diameter nozzles were used to make the collinear alignment of the impinging jets. Glass is used as the reactor material as the reactor is required to be transparent for flow imaging as well as compatible with organic solvents and high working pressure. The jets impinge inside a cavity made out of merging of a half-sphere and a conical section with an outlet. The surrounding glass enclosure of the jets system works as a mixing chamber. The geometry and the dimensions of the impinging jet reactor used in our experiments are shown in Fig. 5.2c and the schematic of the setup is shown in Fig. 5.1. The reservoirs for aqueous AP solution and the antisolvent were maintained at a fixed temperature using constant temperatures baths (Julabo, Germany). Solution and antisolvent are pumped using two peristaltic pumps (Longer, China) with insulated tubings for minimizing heat losses. Experiments were performed at flow rates of 70-322 ml/min of the solution and antisolvent, each. A constant solvent to antisolvent flow ratio of 1:1 is maintained similar to previous experiments. A similar filtration assembly was connected to the outlet of the reactor. Filtered particles were collected and analyzed subsequently. A high-speed camera (Photron Fastcam Mini AX200) was used at 6250 fps for visually capturing the impinging of jets.
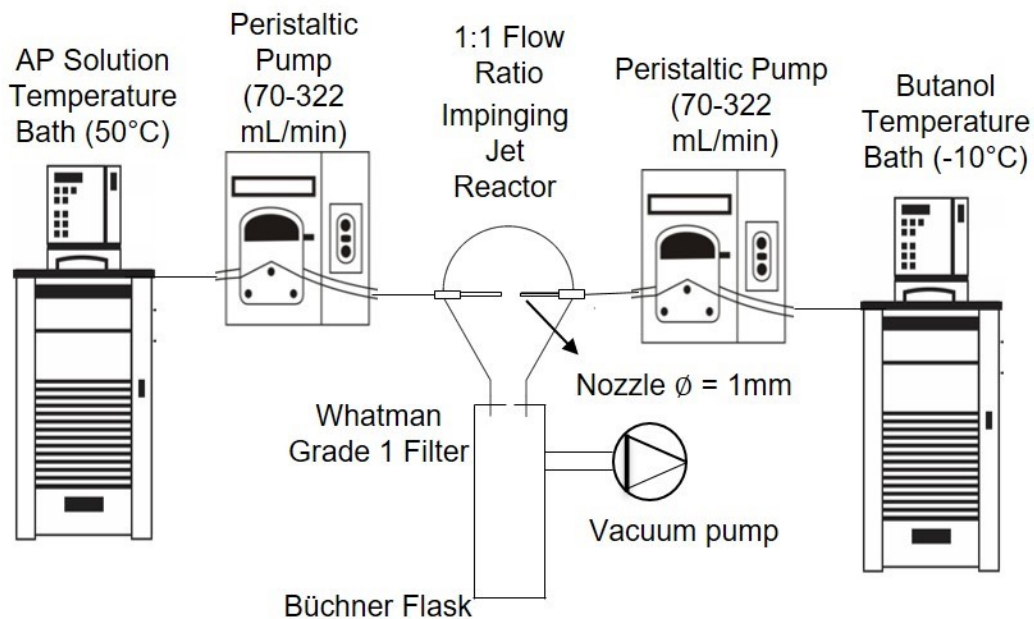
Fig. 5.1. Schematic of the setup for antisolvent precipitation using confined impinging jet reactor setup

5.2.2.2. Particle Size Measurement

The particle size of the precipitated particles was analyzed using Optical Microscope (Zeiss - Stereo Discovery v20 and Zeiss Primo Star) as well as Scanning Electron Microscope (E-SEM Quanta 200-3D). Three hundred particles in a micrograph were randomly selected, and particle sizes were obtained using ImageJ 1.8 software after doing a suitable calibration. Microsoft Excel and Matlab® were used for post-processing of the data.

5.2.3. Computational and Numerical Details

The model Equations

Continuity Equation:
$$\frac{\partial \rho}{\partial t} + \nabla \cdot (\rho \vec{v}) = 0 \tag{5.1}$$

Momentum Equation:
$$\frac{\partial}{\partial t}(\rho \vec{v}) + \nabla \cdot (\rho \vec{v} \vec{v}) = -\nabla p + \nabla \cdot (\bar{\bar{\tau}}) + \rho \vec{g} \tag{5.2}$$

Energy Equation:
$$\frac{\partial}{\partial t}(\rho E) + \nabla \cdot (\vec{v}(\rho E + p)) = \nabla \cdot (k_{eff} \nabla T + \bar{\bar{\tau}}_{eff} \vec{v}) \tag{5.3}$$

where, $\vec{v}$ is the velocity vector (m/s), ρ is the density (kg/m^3), t is time (sec), $\bar{\bar{\tau}}$ is stress tensor, $\rho \vec{g}$ is gravitational body force (N), is pressure in N/m^2, k_{eff} is the effective thermal conductivity which is given by $k+k_t$, k_t being the turbulent thermal conductivity based on the turbulent model employed in this case *k-ε*.

k-ε model equation:

$$\frac{\partial}{\partial t}(\rho k) + \frac{\partial}{\partial x_i}(\rho k u_i) = \frac{\partial}{\partial x_j}\left[\left(\mu + \frac{\mu_t}{\sigma_k}\right)\frac{\partial k}{\delta x_j}\right] + G_k + G_b - \rho \varepsilon \tag{5.4}$$

$$\frac{\partial}{\partial t}(\rho \varepsilon) + \frac{\partial}{\partial x_i}(\rho \varepsilon u_i) = \frac{\partial}{\partial x_j}\left[\left(\mu + \frac{\mu_t}{\sigma_\varepsilon}\right)\frac{\partial \varepsilon}{\delta x_j}\right] + C_{1\varepsilon}\frac{\varepsilon}{k}(G_k + C_{3\varepsilon}G_b) - C_{2\varepsilon}\rho\frac{\varepsilon^2}{k} \tag{5.5}$$

$$\mu_t = \rho C_\mu \frac{k^2}{\varepsilon} \tag{5.6}$$

where k is the turbulent kinetic energy (m^2/s^2), ε is the dissipation rate (m^2/s^3), u_i is the velocity vector (m/s), G_k is the generation of turbulence kinetic energy due to mean velocity gradient, G_b is the generation of turbulence kinetic energy due to buoyancy, while α_k and α_ε are the inverse effective Prandtl numbers for k and ε and μ_t is the turbulent viscosity. The values of $C_{1\varepsilon}, C_{2\varepsilon}, C_\mu$, σ_k and σ_ε (constants) were kept 1.44, 1.92, 0.09, 1.0, and 1.3 respectively.

For simulating mixing following species transport equation was used to simulate

$$\tag{5.7}$$

multispecies flow in the CLIJ
$$\frac{\partial}{\partial t}(\rho m_i) + \nabla \cdot (\rho \vec{v} m_i) = -\nabla \cdot \vec{J_i}$$

where m_i is the mass fraction of species k and $\vec{J_i}$ is the mass diffusion in the turbulent

flow given by $\quad \vec{J_i} = -\left(\rho D_{i,m} + \frac{\mu_t}{Sc_t}\right)\nabla m_i - D_{T,i}\frac{\nabla T}{T}$ (5.8)

where Sc_t is the turbulent Schmidt Number, μ_t is the turbulent viscosity, $D_{i,m}$ is the mass diffusion

coefficient of the species i in the mixture. $D_{T,i}$ is the thermal diffusion coefficient. The density and

kinematic viscosity of the fluid and mass diffusivity of tracer in mixture were considered as

constant. Explicit VOF (Volume of Fluid) model with explicit formulation was used to simulate

multiphase flow in the CLIJ taking into consideration the surface tension and wall adhesion. For

the qth phase the equation has following form:

$$\frac{\partial \alpha_q}{\partial t} + \nabla \cdot \left(\alpha_q \vec{v}_q\right) = 0 \qquad (5.9)$$

The density and viscosity of the fluid in the multiphase simulation used in the above equation are

those of a mixture and are given by $\rho = \sum \alpha_q \sigma_q$ and $\mu = \sum \alpha_q \mu_q$ [27]

The governing equations (5.1-5.9) of continuity, momentum, turbulence, species transport were

numerically solved using commercial CFD code FLUENT (Ansys Inc., version 17.0) which is

based on the finite volume method. The 3D computational mesh (see fig 5.2B & 5.2D) used for a

numerical solution was generated in ICEM CFD using O-grid blocking technique. The blocks were

strategically split and associated, ensuring high quality mesh in the entire fluid domain. Refined

(Fine) mesh was used near wall/critical regions, and course mesh was employed in the other

regions. 1.2 growth ratio was used for the inflation of the mesh from fine to course. To capture the

boundary layers, it was ensured that the mesh at the wall was fine, and the growth ratio from the

wall was kept 1.1 to ensure smooth growth. Key mesh properties like orthogonal quality, aspect

ratio, Jacobean and the skewness were kept within limits and maintained according to standards

[31]. The total cells in the domain are 8 million. The inlet section was resolved by 600 grids. The

grid independence was tested with different mesh sizes, and the mesh with the highest refinement was employed to ensure the accuracy of the solution with minimum possible fluxes. No slip boundary conditions were applied at the wall, and the flow was treated as incompressible. The influence of gravity was taken into consideration in the direction of the outlet. Initially, single phase simulations were performed which is well known in the literature for quantification of mixing in the geometries. Multiphase VOF simulations were performed thereafter to understand jet impingement dynamics. Details for single and multiphase simulations performed are presented subsequently.

(C)

(D)
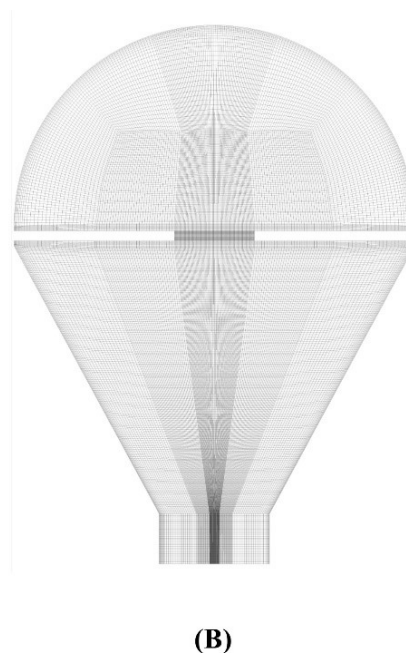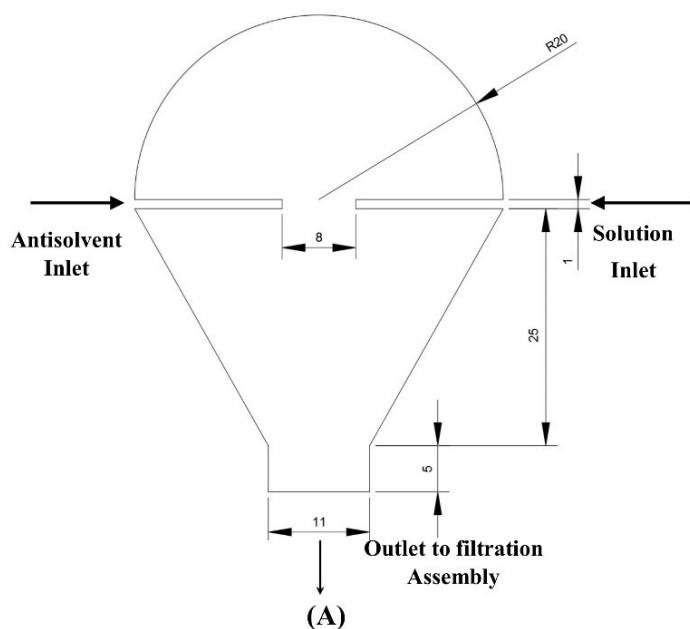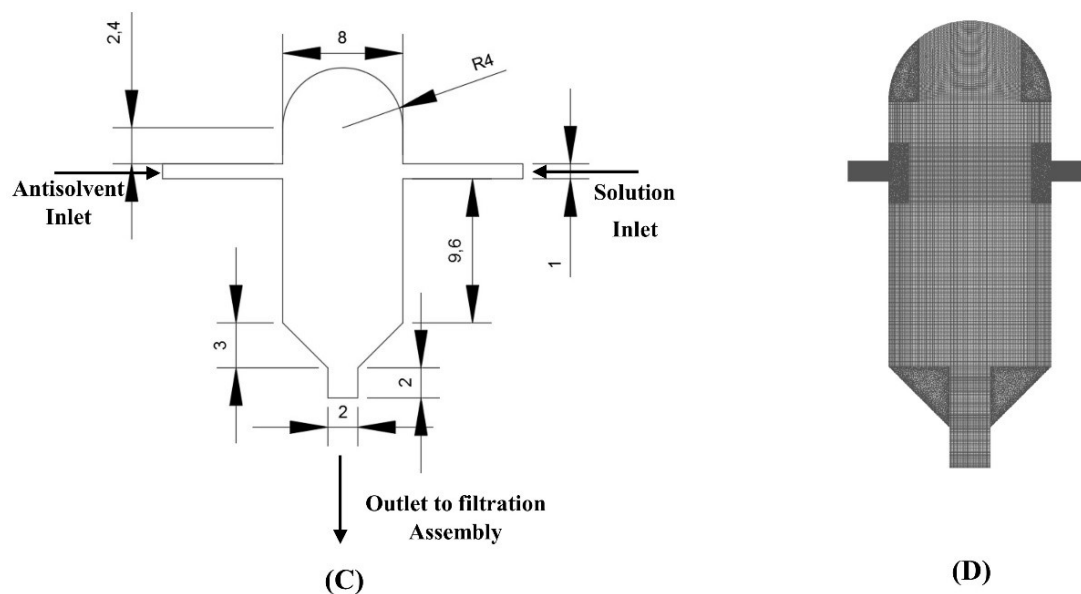
Fig. 5.2. (A) Schematic of the modified CIJR geometry (all the dimensions are in mm), (B) Computational mesh for modified CIJR geometry. (C) Schematic of the conventional CIJR geometry (all the dimensions are in mm), (D) Computational mesh for conventional CIJR geometry (The minimum orthogonal quality is 0.85 and the maximum aspect ratio is 12)

5.2.3.1. Single Phase Flow, Species Transport and estimation of Mixing Performance

Single phase flow and species transport were solved for steady state. Water (ρ =1000 kg/m^3 and μ = 0.001 Ps) was used as a working fluid from both the inlets. The inlet boundary condition was velocity inlet (3 m/s), and the outlet boundary condition was pressure outlet (P=0). The pressure velocity coupling was performed by SIMPLE algorithm. The parameters: Momentum, turbulent kinetic energy and turbulent dissipation rate were spatially discretized with second-order upwind scheme. Pressure was spatially discretized by using PRESTO scheme. The equations were iteratively solved till the convergence criteria of 10^{-6} were achieved for all the parameters. The solution was initialized using the hybrid scheme.

To quantify mixing intensity in the CIJR, water along with a tracer (having similar properties that of water) was used to solve the species transport equation along with turbulence. Water was injected from one inlet and the tracer was injected from the other inlet. The mixing

intensity is based on the obtained time history of the mass tracer and defined by the Danckwerts' intensity of segregation [32, 33]. Mixing intensity (I_m) is defined as:

$$I_m = 1 - \sqrt{I_s} = 1 - \sqrt{\frac{\sigma^2}{\sigma_{max}^2}} \quad \text{where} \quad \sigma^2 = \frac{1}{V} \int_V (c - \overline{c})^2 dV \qquad (5.10)$$

Where, $\overline{c}$ denotes the mean value of the concentration field c, σ^2 and σ_{max}^2 are variance and maximum possible variance, V is the volume of the selected computational domain.[33, 34]

3.2. Multiphase Volume of fluid simulations (VOF)

Explicit VOF (Volume of Fluid) model [35] was used to simulate multiphase flow in the confined impinging jet reactor (CIJR) taking into consideration the surface tension and wall adhesion. Three Eulerian phases consisting of air (ρ=1.2kg/m^3 and μ=1.78x10^{-5} Ps), water and *n*-butyl alcohol (ρ=810kg/m^3 and μ=0.00107 Ps) were used as working fluids for modelling multiphase flow in CIJR. Explicit VOF formulation was employed with volume fraction cutoff of 10^{-6} and Courant number cutoff of 0.25. Surface tension was computed as a body force based on CSF (Continuum Surface Force model) along with the wall adhesion term [36]. Momentum, Turbulent kinetic energy and turbulent dissipation rate was spatially discretized by using the second order upwind scheme. Pressure was discretized using the QUICK scheme[37], and the volume fraction was discretized using the geometric reconstruction scheme which uses the piecewise-liner approach [38]. The convergence criteria of 10^{-6} were kept for all the parameters except for continuity that was kept at 10^{-4}, to save computing time. The time step of 10^{-6} was sufficient to maintain the Courant number between 0.01-0.1 well within acceptable limits[39, 40]. Maximum of 20 iterations per time step, proved to be optimum to achieve the set convergence criteria. The solution was initiated with air as the working fluid to simulate the actual experimental

condition. Inlet velocity of water and *n*-butyl alcohol was kept at 3m/s. Iso-Surface of 0.5 volume fraction with respect to air was monitored in the fluid domain for every 0.5 milliseconds of flow time, and subsequently, volume rendering technique was employed to visualize the multiphase flow in CIJR.

5.3. Results and Discussion

5.3.1. Computational fluid dynamics study of impinging reactor based geometry

5.3.1.1. Flow and mixing in CIJR

In a typical CIJR, two liquid jets collide with each other and intensify the momentum, heat, and mass transfer in the impinging region. Conversion of the kinetic energy of the liquid jets into pressure energy and flow redirection, thereby achieving a significant energy dissipation in a very short volume (15-1500 W/Kg for 70-300 mL/min flowrate)[41]. Impinging region of the CIJR comprises of high TKE which intensifies turbulent transfer and enhances the mixing efficiency. As mentioned earlier, jet inlets in the conventional geometry open on reactor wall [3, 19, 41-44] (see fig. 5.2a). In this case, liquid jets are susceptible to Coanda effect to some extent [45], which is the tendency to affix to the nearby mixing chamber surface. Such an effect results in a partial circumvention of the impingement area comprising of highest magnitude of TKE[20] and wall deposition. To avoid the circumvention and wall deposition caused by Coanda effect, the jet inlets was stretched further into the reactor enclosure in our modification of the geometry. This is intended to enhance concentrated jet impingement with higher TKE as jet's emerging from flat orifices have relatively lower energy than the tapered orifices that help carry more energy with the jet. The reactor enclosure is also tweaked with a conical bottom section and significantly larger outlet to prevent deposition of any solids on the reactor surface and clogging problem.

Computational flow modelling is performed to visualize and study the impingement of the jets, mixing and high kinetic energy zones in the conventional and the modified geometry of CIJRs.

Figure 5.4 (a-b) compares the turbulent kinetic energy at the cross-section plane (see Fig. 5.3 for a visual illustration of cross-section plane) along the inlet of the jets, for the conventional and the modified geometry respectively. The maximum turbulent kinetic energy and the distribution of kinetic energy in the conventional and modified geometry are comparable for same boundary conditions. Mixing intensity was used for quantifiying mixing in CIJR, which was estimated by using equations 5.10 . Performed simulations clearly indicate that both the geometries provide a 99% mixing intensity. These comparisons of turbulent kinetic energy and mixing intensity clearly indicate that the modified geometry performs similarly in terms of availability of fluid energy at the impinging section and mixing performance while removing the wall effects.
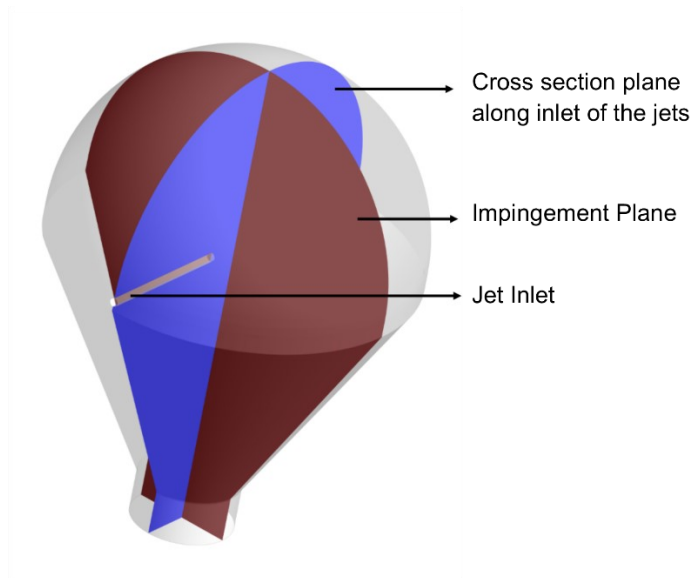
Fig. 5.3. Section planes of the Confined liquid impinging jet geometry.

<div align="center">(a)   (b)</div>
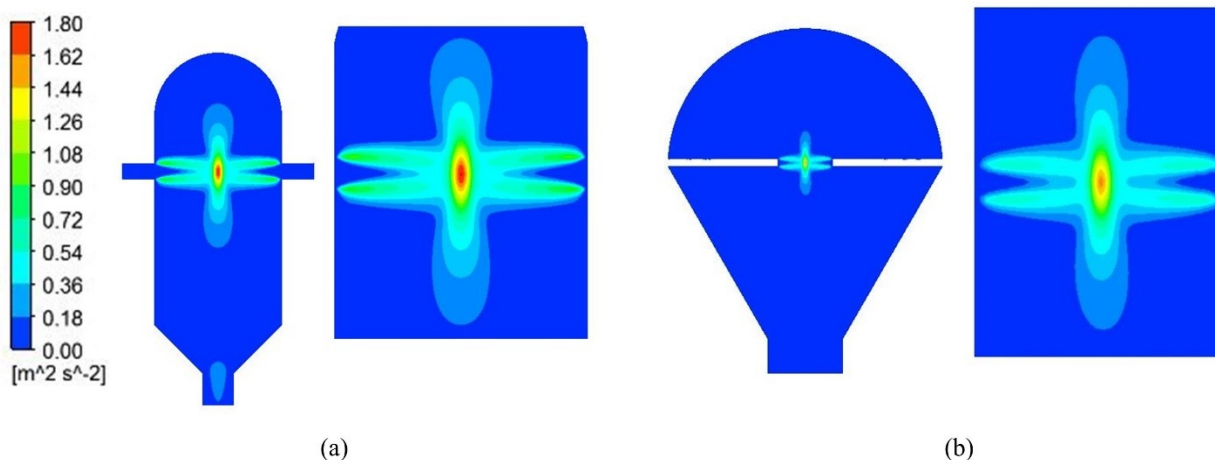
Fig. 5.4. Distribution of Turbulent Kinetic Energy at the crossection plane in (a) conventional Geometry and (b) modified Geometry.

5.3.1.2. Impingement dynamics of jets in CIJR

When two co axial liquid jets collide, they form a circular expanding sheet in the perpendicular plane to the jet inlets [46]. The sheet thickness decreases radially as it grows from the point of jet impingement and eventually disintegrates. At lower values of jet Reynolds number (Re < 2000), the breakup of sheets is dominated by capillary instability and smooth or ruffled sheets are observed. For the case of jet Reynolds number>2000, Kevin Helmholtz instability becomes prominent due to the interaction (velocity shear) of the sheet with the surrounding air [47]. The upstream part of the sheet becomes very unstable, and a fully developed sheet ceases to exist. The impact waves arising from hydrodynamic instabilities generate disturbances of higher amplitude causing the breakup of the sheet to liquid ligaments and droplets [29]. Li et al. have experimentally monitored the transition from the laminar closed rim to open rim and then to turbulent regime liquid sheets [47]. The angle between axes of the two jets, which is referred to as impinging angle is 60°-120° in their experiments. The transition Reynolds numbers for different angles are represented in table 5.1.

Table 5.1. Variation of transition Reynolds Number with impinging angle (Li et al. [47])

Impinging Angle	60°	90°	120°
Transition Re (Open Rim)	2369	2155	2053
Transition Re (Turbulent)	3429	2989	2876

It is evident from table 5.1 with increasing impingement angle the transition Re decreases for open rim as well as turbulent jets [47]. In the geometries under consideration in this chapter, the jets collided at an impinging angle of 180°. 141 ml flow rate of each jet results in ~3 m/s velocity and Re = 2488; our experimental conditions should result in a turbulent regime [47]. The purpose of the present study was to study the interaction of the impinging jets of solution, and antisolvent phase numerically and explore the usefulness of the conditions to design experiments for high throughput antisolvent precipitation of AP as a model system.

A high-speed camera was used to experimentally capture the jet impingement in our CIJR reactor. Fig. 5.5a and b show that the sheet formation by impingement of liquid jets that can be seen in from the predictions in VOF simulations actually exists when seen using a high-speed camera. The film formed due to impingement undergoes break-up and eventually forms a large number of satellite drops. This transient phenomenon is shown in Fig 5.5c. Volume rendering techniques were used to track the transition in the flow field. After the impact of the two liquid phases, the sheet forms and grows in a radial direction. Then instability wave arises on the sheet, and the sheet disintegrates into ligaments and droplets. The ligaments were formed in a pattern of waves similar to the impact waves observed in the ruffled sheet regime. The size of the droplets and ligaments decrease radially outward from the jet core/axis. Furthermore, it has also been

observed that once the drops hit the wall, they agglomerate and forms bigger droplets on the inner walls of the CIJR.

(a)   (b)

2.5 ms   3.5 ms   6.5 ms   10.5 ms   14.5 ms

(c)
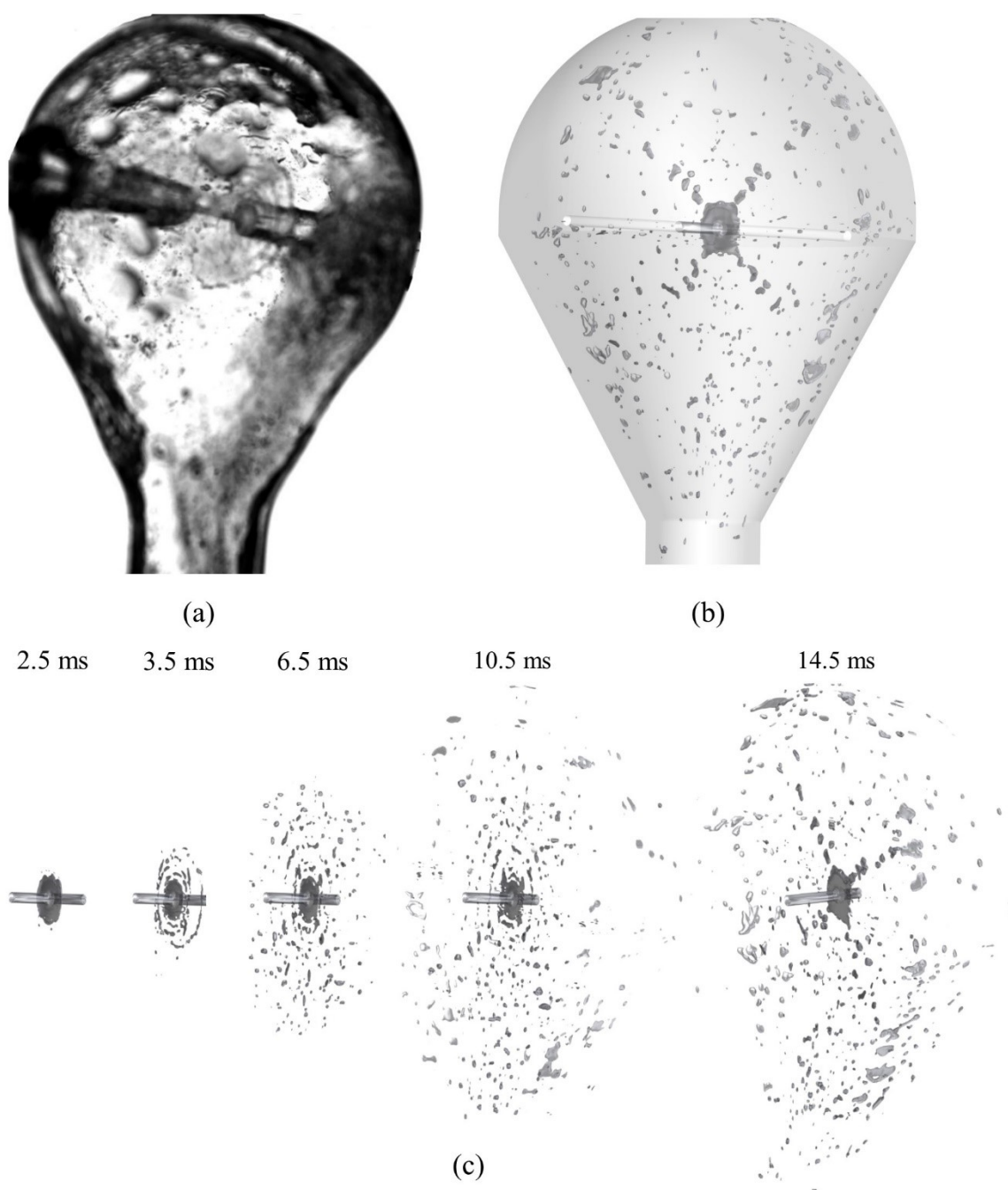
Fig. 5.5. Sheet formation by jet impingement (a) experimental, (b) VOF simulation; (c) Interaction of impinging jets with time (CFD simulations)

Further to impingement, mixing in the CIJR also depends on the subsequent droplet interaction of the two phases. Fig. 5.6 shows both water and *n*-butyl alcohol phases inside the CIJR at 80ms. The green colour represents the aqueous solvent phase, and the blue colour represents the organic antisolvent phase. It can be observed from the figure 5.6 that both water and n-butanol phases are intertwined together in the form of ligaments and droplets and they do remain isolated. Though droplet breakup from liquid sheet was reported in previous VOF studies in literature, it was based on single liquid phase. This interwinted nature of the droplets and ligaments of two different phases were first reported in the current study. Such small-scale interaction between the two phases results in increasing the effective interfacial area, which contributes to the enhanced performance of the CIJR in terms of mixing and mass transfer.
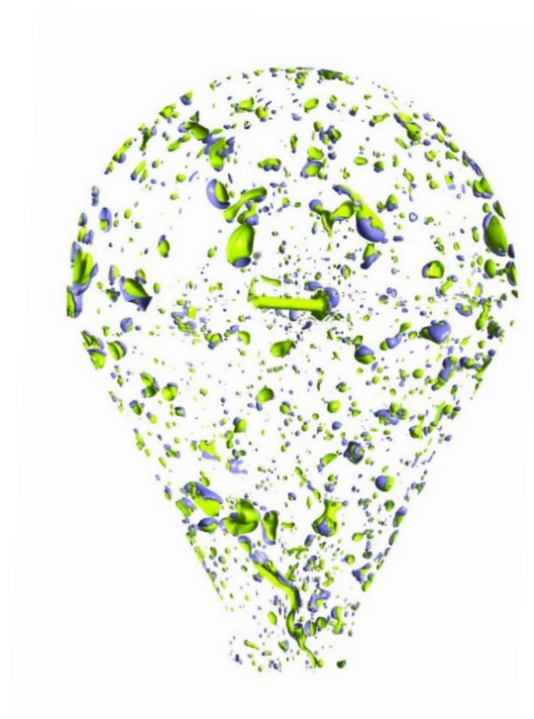
Fig. 5.6. Droplets of Water and *n*-butyl alcohol in the CIJR (at 80ms from the moment both jets comes out of the nozzle)

The active regions in the fluid domain wherein the water and n-butyl alcohol phase are interacting are shown in Fig 5.7 and 5.8. The figures also showcases the transient location of the sheet for three different velocities of the liquid jets. Before the two-phases entered the domain, it was filled with stagnant air (initialization of the solution with air at zero velocity). For very low velocities of the liquid jets (1 ms^{-1}), sheet formation is heavily influenced by gravity and liquid bulbs were found to detach from the sheet after 32 ms. With increasing velocities of the jet, the sheet formation is observed to be symmetric in nature and less influenced by gravity. The location of the liquid sheet is also found to be shift towards the antisolvent inlet side with time as the density of water is more than that of n-butyl alcohol irrespective of jet velocity (see Fig. 5.8).
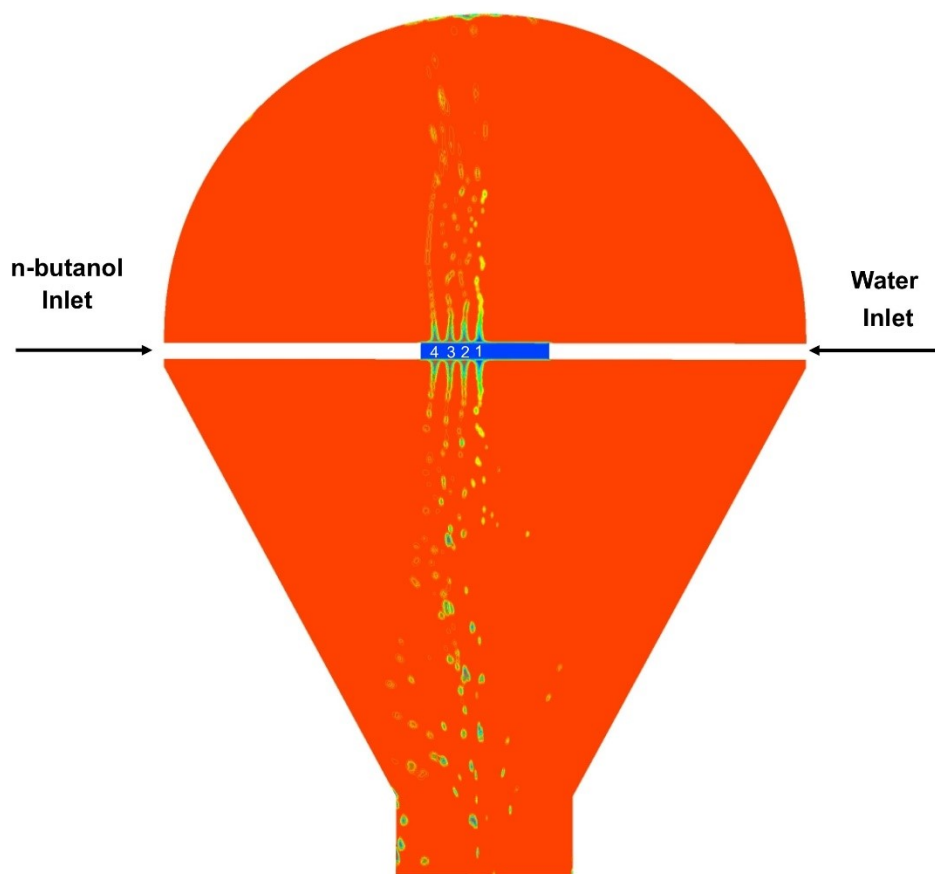
Fig. 5.7. Movement of liquid sheet along the impingement axis to equilibrium position for 5 ms^{-1} jet velocity. (1) 2.5 ms, (2) 7.5ms, (3) 12.5 ms, (4) 22.5 ms
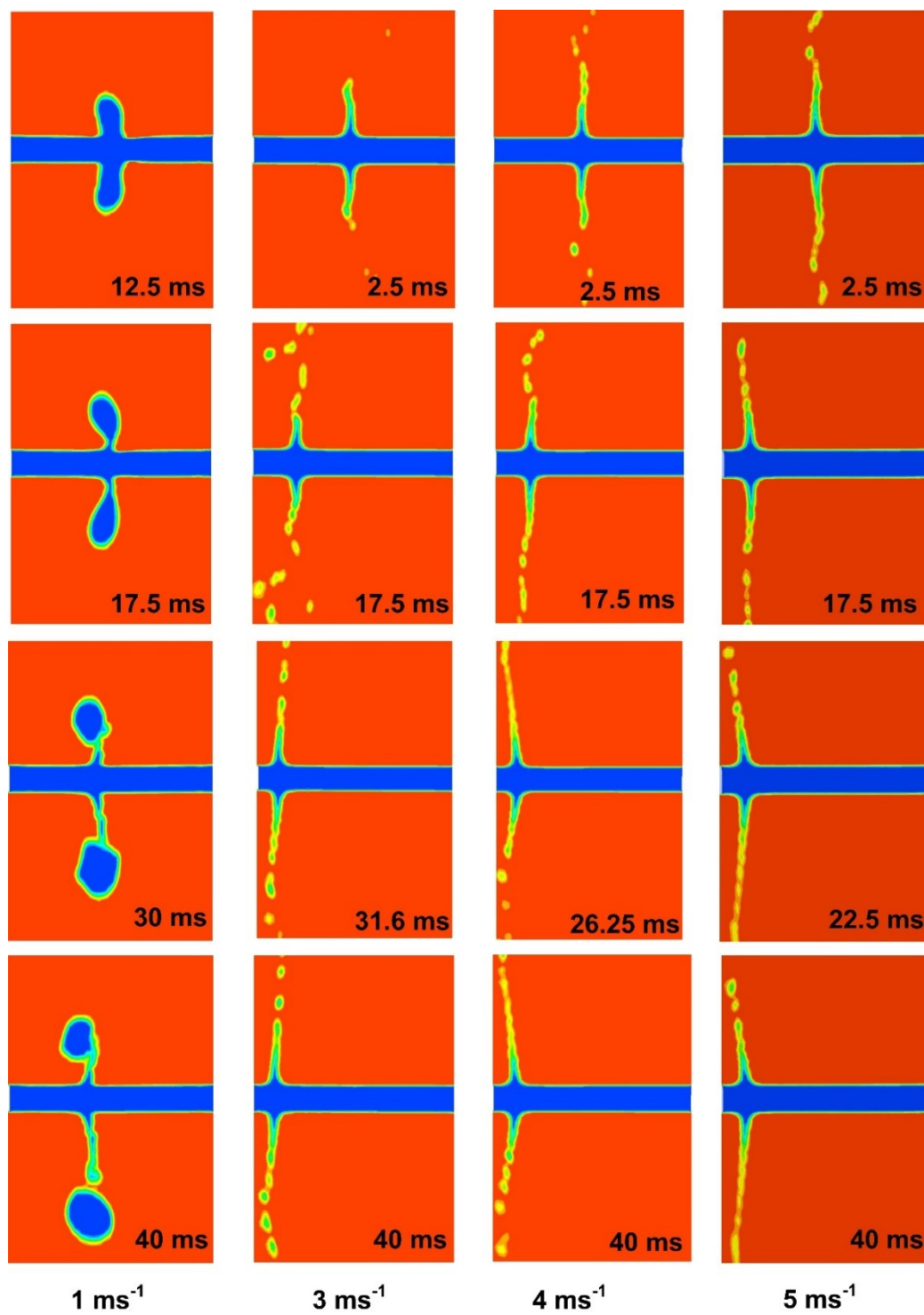
Fig. 5.8. Evolution of liquid sheet for different jet velocities

5.3.2. Continuous precipitation of AP in modified CIJR geometry

In the previous chapter, antisolvent precipitation of AP was optimized in batch and continuous capillary reactor. Water and *n*-butyl alcohol were found to be optimized solvent-antisolvent pair. 50°C and -10°C were found to be solution and antisolvent temperature respectively for optimized particle size and yield. These optimized conditions were followed while carrying out continuous antisolvent precipitation in the modified geometry of CIJR proposed and characterized in the previous section of the chapter. Flow rates are varied from 70 ml/min to 322 ml/min providing a handling capacity of 1.45-6.67 kg/hour. The precipitated particles were found to be in the range of 8.98-16.98 µm mean diameter. Fig. 5.8a shows the variation in precipitated particle size with total *Re* of the impinging jets. Here very high average jet *Re* $1.46 \times 10^3 - 5.87 \times 10^3$ indicates intensified mixing which subsequently results in the production of small particles. Initially, a decrease in the AP particle size is observed with increasing jet Reynolds number, which reaches a plateau.

(a)   (b)

(c)   (d)
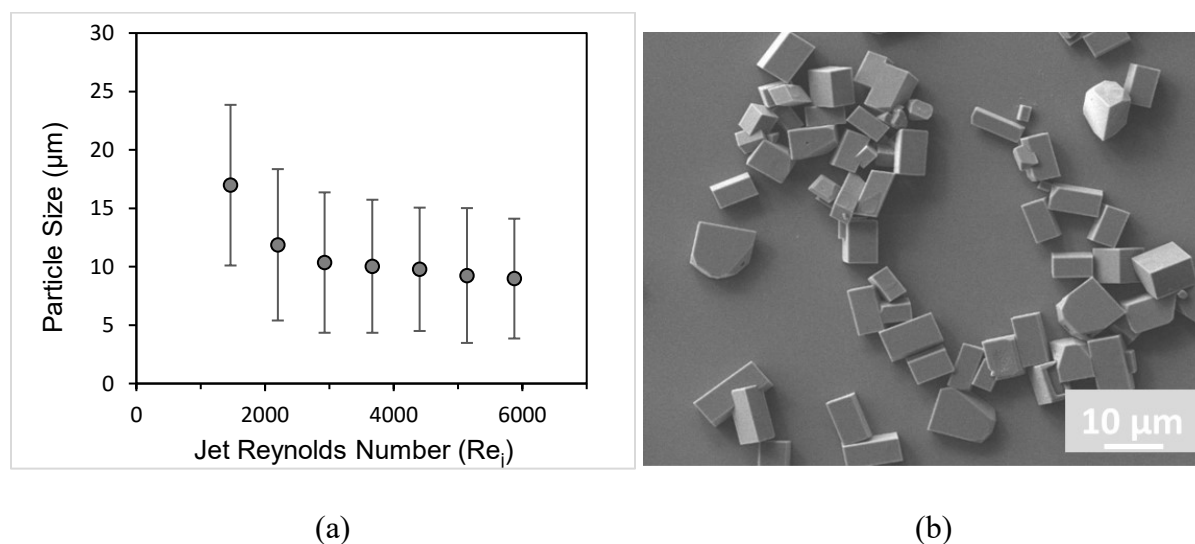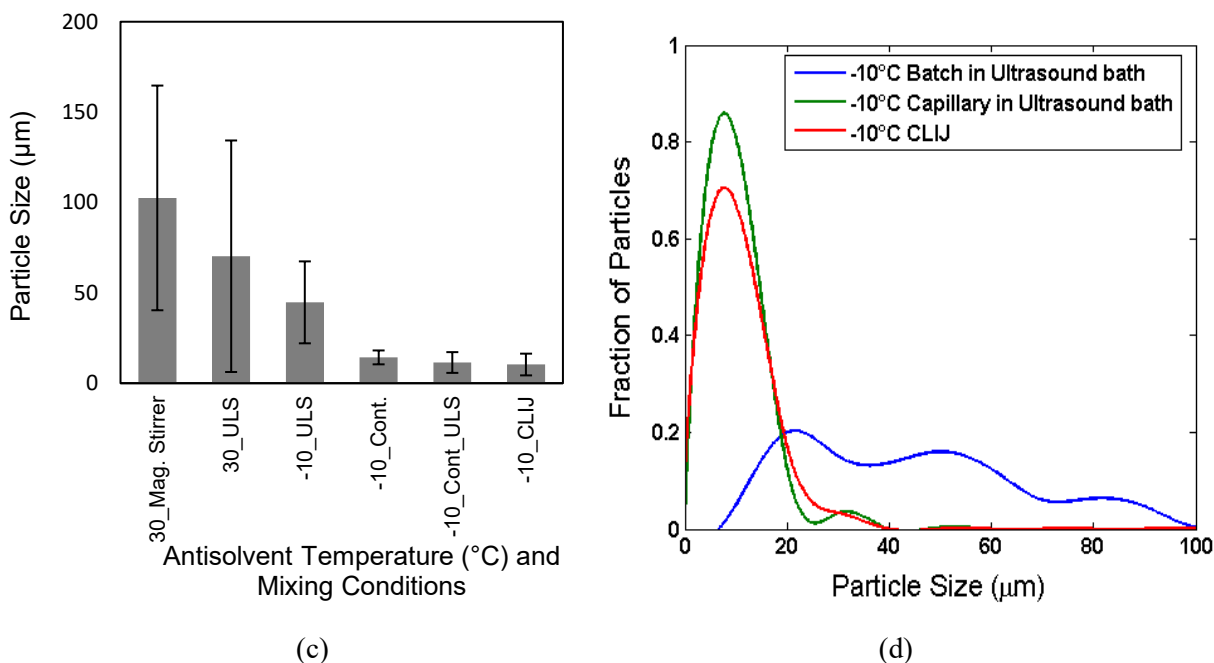
Fig. 5.9. (a) Effect of Reynolds number on AP particle size, (b) SEM images of AP particles (mean particle size 10.35 µm) precipitated using impinging jet reactor (141 ml/min flow rate of solution and antisolvent, 50°C solution temperature and -10° antisolvent temperature), (c) Mean particle Sizes, (d) PSD of AP particles in different processes at a 50°C solution temperature. (ULS – Ultrasound bath, Cont. – Continuous capillary reactor)

This results from the gradual mixing quality enhancement with increasing jet Reynolds number (Re_J) [9, 48]. The average sheet thickness when two jets collide is observed to decrease with increasing Re_J. The sheet becomes ruffled and finally turbulent in nature [47]. With decreasing sheet thickness, smaller drops are formed at the edge of the sheet. For higher jet Reynolds number ($Re_J > 3000$) particle sizes no longer depended on Re_J. Similar observations of particle sizes reaching a plateau have been reported by several authors for antisolvent [49] and reactive precipitation [43, 50]. Moreover, most of the studies have reported a plateau in process performance as the Reynolds number is increased in impinging jets [3, 8, 51]. Images of the precipitated AP particles at optimum conditions in an impinging jet reactor are shown in Fig. 5.8b. The comparison of AP particle sizes and PSD obtained in various conditions and reactors are

presented in Fig. 5.9c and 5.9d respectively. Comparing the mean particle size and particle size distribution of various processes in Fig. 5.9c and 5.9d respectively, it can be concluded that impinging jet reactor gives a performance similar to a capillary microreactor as described in the previous chapter but at 40-400 times higher capacity making it a scaled-up option.

5.4. Conclusion

Mixing performance and jet impingement dynamics have been studied in our modified CIJR geometry and compared with the conventional design. It was found that the modified geometry prevents the wall effects and wall deposition while performed similarly in terms of mixing and utilization of the fluid energy available at the impinging area. The dynamics of liquid sheet formation, movement along the impingement axis and fragmentation is predicted using the VOF method. On impingement, the liquid sheet is found to shift towards the lower density liquid inlet and becomes stable after reaching an equilibrium position. Formation of interwinted droplets and ligaments of two different phases after sheet fragmentation results in increasing the effective interfacial area, contributing to the enhanced mixing and mass transfer performance of the CIJR. The modified geometry of CIJR was applied to perform scaled up experiments in optimized conditions found from the previous batch and continuous flow experiments. 8.98-16.98 µm AP particles were achieved in the Reynolds number range of 1792–7193 for the saturated aqueous AP solution stream and 1135 – 4553 for the antisolvent *n*-butyl alcohol stream. With increasing jet Reynolds number *(Re$_J$)*, increase in the mixing performance due to the higher kinetic energy, formation of smaller droplets, reduction in sheet thickness results in smaller particle size. More studies on the effect of impinging angle, inlet velocities of both the fluids, jet diameter, configurations of jets, etc. need to be studied separately to achieve a reliable scale-up methodology.

5.5. Notations

$I_m =$ Mixing intensity (-)

$I_s =$ Intensity of segregation (-)

$\sigma^2 =$ Variance of concentration (mol²/l²)

$\sigma_{max}^2 =$ Maximum possible variance of concentration (mol²/l²)

$\overline{c} =$ Mean value of the concentration field c (mol/l)

$V =$ Volume of the selected computational domain (l)

5.6. References

1. Lince, F., Marchisio, D.L., and Barresi, A.A., *Strategies to control the particle size distribution of poly-ε-caprolactone nanoparticles for pharmaceutical applications.* Journal of colloid and interface science, **2008**. 322(2): p. 505-515.

2. Metzger, L. and Kind, M., *On the transient flow characteristics in Confined Impinging Jet Mixers-CFD simulation and experimental validation.* Chemical Engineering Science, **2015**. 133: p. 91-105.

3. Johnson, B.K. and Prud'homme, R.K., *Chemical processing and micromixing in confined impinging jets.* AIChE Journal, **2003**. 49(9): p. 2264-2282.

4. Gavi, E., Marchisio, D., and Barresi, A., *On the importance of mixing for the production of nanoparticles.* Journal of Dispersion Science and Technology, **2008**. 29(4): p. 548-554.

5. Marchisio, D.L., Rivautella, L., and Barresi, A.A., *Design and scale-up of chemical reactors for nanoparticle precipitation.* AIChE Journal, **2006**. 52(5): p. 1877-1887.

6. Dalvi, S.V. and Dave, R.N., *Controlling particle size of a poorly water-soluble drug using ultrasound and stabilizers in antisolvent precipitation.* Industrial & Engineering Chemistry Research, **2009**. 48(16): p. 7581-7593.

7. D'Addio, S.M. and Prud'homme, R.K., *Controlling drug nanoparticle formation by rapid precipitation.* Advanced drug delivery reviews, **2011**. 63(6): p. 417-426.

8. Mahajan, A.J. and Kirwan, D.J., *Micromixing effects in a two-impinging-jets precipitator.* AIChE Journal, **1996**. 42(7): p. 1801-1814.

9. Krupa, K., Nunes, M.I., Santos, R.J., and Bourne, J.R., *Characterization of micromixing in T-jet mixers.* Chemical Engineering Science, **2014**. 111: p. 48-55.

10. Lince, F., Bolognesi, S., Marchisio, D.L., Stella, B., Dosio, F., Barresi, A.A., and Cattel, L., *Preparation of poly (MePEGCA-co-HDCA) nanoparticles with confined impinging jets reactor: Experimental and modeling study.* Journal of pharmaceutical sciences, **2011**. 100(6): p. 2391-2405.

11. Hacherl, J.M., Paul, E.L., and Buettner, H.M., *Investigation of impinging-jet crystallization with a calcium oxalate model system.* AIChE journal, **2003**. 49(9): p. 2352-2362.

12. Siddiqui, S.W., Unwin, P.J., Xu, Z., and Kresta, S.M., *The effect of stabilizer addition and sonication on nanoparticle agglomeration in a confined impinging jet reactor.* Colloids and Surfaces A: Physicochemical and Engineering Aspects, **2009**. 350(1-3): p. 38-50.

13. Chiou, H., Chan, H.-K., Prud'homme, R.K., and Raper, J.A., *Evaluation on the use of confined liquid impinging jets for the synthesis of nanodrug particles.* Drug development and industrial pharmacy, **2008**. 34(1): p. 59-64.

14. Han, J., Zhu, Z., Qian, H., Wohl, A.R., Beaman, C.J., Hoye, T.R., and Macosko, C.W., *A simple confined impingement jets mixer for flash nanoprecipitation.* Journal of pharmaceutical sciences, **2012**. 101(10): p. 4018-4023.

15. Calvignac, B. and Boutin, O., *The impinging jets technology: A contacting device using a SAS process type.* Powder Technology, **2009**. 191(1-2): p. 200-205.

16.   Careno, S., Boutin, O., and Badens, E., *Drug recrystallization using supercritical anti-solvent (SAS) process with impinging jets: Effect of process parameters.* Journal of Crystal Growth, **2012**. 342(1): p. 34-41.

17.   Zhang, C., Pansare, V.J., Prud'Homme, R.K., and Priestley, R.D., *Flash nanoprecipitation of polystyrene nanoparticles.* Soft Matter, **2012**. 8(1): p. 86-93.

18.   Wilcox, D.C., *Turbulence modeling for CFD.* Vol. 2. **1993**: DCW industries La Canada, CA.

19.   Gavi, E., Marchisio, D.L., and Barresi, A.A., *CFD modelling and scale-up of confined impinging jet reactors.* Chemical Engineering Science, **2007**. 62(8): p. 2228-2241.

20.   Liu, Y., Olsen, M.G., and Fox, R.O., *Turbulence in a microscale planar confined impinging-jets reactor.* Lab on a Chip, **2009**. 9(8): p. 1110-1118.

21.   Woo, X.Y., Tan, R.B., and Braatz, R.D., *Modeling and computational fluid dynamics− population balance equation− micromixing simulation of impinging jet crystallizers.* Crystal Growth and Design, **2008**. 9(1): p. 156-164.

22.   Gavi, E., Marchisio, D.L., Barresi, A.A., Olsen, M.G., and Fox, R.O., *Turbulent precipitation in micromixers: CFD simulation and flow field validation.* Chemical Engineering Research and Design, **2010**. 88(9): p. 1182-1193.

23.   Da Rosa, C.A. and Braatz, R.D., *Multiscale Modeling and Simulation of Macromixing, Micromixing, and Crystal Size Distribution in Radial Mixers/Crystallizers.* Industrial & Engineering Chemistry Research, **2018**. 57(15): p. 5433-5441.

24.   Liu, Y. and Fox, R.O., *CFD predictions for chemical processing in a confined impinging-jets reactor.* AIChE Journal, **2006**. 52(2): p. 731-744.

25. Launder, B.E. and Spalding, D.B., *Mathematical models of turbulence*. **1972**: Academic press.

26. Chen, H. and Patel, V., *Near-wall turbulence models for complex flows including separation.* AIAA journal, **1988**. 26(6): p. 641-648.

27. *Ansys Inc. FLUENT Theory Guide 17.0* **2016**.

28. Inoue, C., Watanabe, T., and Himeno, T. *Study on atomization process of liquid sheet formed by impinging jets*. in *44th AIAA/ASME/SAE/ASEE Joint Propulsion Conference & Exhibit*. **2008**.

29. Chen, X., Ma, D., Yang, V., and Popinet, S., *High-fidelity simulations of impinging jet atomization.* Atomization and Sprays, **2013**. 23(12).

30. Arienti, M., Li, X., Soteriou, M.C., Eckett, C.A., Sussman, M., and Jensen, R., *Coupled level-set/volume-of-fluid method for simulation of injector atomization.* Journal of Propulsion and Power, **2012**. 29(1): p. 147-157.

31. Thompson, J.F., Soni, B.K., and Weatherill, N.P., *Handbook of grid generation*. **1998**: CRC press.

32. Danckwerts, P., *The definition and measurement of some characteristics of mixtures.* Applied Scientific Research, Section A, **1952**. 3(4): p. 279-296.

33. Bothe, D., Stemich, C., and Warnecke, H.-J., *Fluid mixing in a T-shaped micro-mixer.* Chemical Engineering Science, **2006**. 61(9): p. 2950-2958.

34. Lobasov, A. and Minakov, A., *Analyzing mixing quality in a T-shaped micromixer for different fluids properties through numerical simulation.* Chemical Engineering and Processing: Process Intensification, **2018**. 124: p. 11-23.

35.   Hirt, C.W. and Nichols, B.D., *Volume of fluid (VOF) method for the dynamics of free boundaries.* Journal of computational physics, **1981**. 39(1): p. 201-225.

36.   Brackbill, J., Kothe, D.B., and Zemach, C., *A continuum method for modeling surface tension.* Journal of computational physics, **1992**. 100(2): p. 335-354.

37.   Leonard, B.P., *A stable and accurate convective modelling procedure based on quadratic upstream interpolation.* Computer methods in applied mechanics and engineering, **1979**. 19(1): p. 59-98.

38.   Youngs, D.L., *Time-dependent multi-material flow with large fluid distortion.* Numerical methods for fluid dynamics, **1982**.

39.   Courant, R. and Hilbert, D., *Methods of mathematical physics [Methoden der mathematischen Physik, engl.] 1*. **1965**: CUP Archive.

40.   Courant, R., Friedrichs, K., and Lewy, H., *On the partial difference equations of mathematical physics.* IBM journal of Research and Development, **1967**. 11(2): p. 215-234.

41.   Siddiqui, S.W., Zhao, Y., Kukukova, A., and Kresta, S.M., *Characteristics of a confined impinging jet reactor: energy dissipation, homogeneous and heterogeneous reaction products, and effect of unequal flow.* Industrial & Engineering Chemistry Research, **2009**. 48(17): p. 7945-7958.

42.   Marchisio, D.L., *Large eddy simulation of mixing and reaction in a confined impinging jets reactor.* Computers & Chemical Engineering, **2009**. 33(2): p. 408-420.

43.   Zhu, Z., Anacker, J.L., Ji, S., Hoye, T.R., Macosko, C.W., and Prud'homme, R.K., *Formation of block copolymer-protected nanoparticles via reactive impingement mixing.* Langmuir, **2007**. 23(21): p. 10499-10504.

44.   Valente, I., Celasco, E., Marchisio, D., and Barresi, A., *Nanoprecipitation in confined impinging jets mixers: Production, characterization and scale-up of pegylated nanospheres and nanocapsules for pharmaceutical use.* Chemical engineering science, **2012**. 77: p. 217-227.

45.   Khalde, C.M., Pandit, A.V., Sangwai, J.S., and Ranade, V.V., *Flow, mixing, and heat transfer in fluidic oscillators.* The Canadian Journal of Chemical Engineering, **2019**. 97(2): p. 542-559.

46.   Taylor, G., *Formation of thin flat sheets of water.* Proc. R. Soc. Lond. A, **1961**. 259(1296): p. 1-17.

47.   Li, R. and Ashgriz, N., *Characteristics of liquid sheets formed by two impinging jets.* Physics of fluids, **2006**. 18(8): p. 087104.

48.   Li, W.-f., Wei, Y., Tu, G.-y., Shi, Z.-h., Liu, H.-f., and Wang, F.-c., *Experimental study about mixing characteristic and enhancement of T-jet reactor.* Chemical Engineering Science, **2016**. 144: p. 116-125.

49.   Chow, S.F., Sun, C.C., and Chow, A.H.L., *Assessment of the relative performance of a confined impinging jets mixer and a multi-inlet vortex mixer for curcumin nanoparticle production.* European Journal of Pharmaceutics and Biopharmaceutics, **2014**. 88(2): p. 462-471.

50.   Shen, H., Hong, S., Prud'homme, R.K., and Liu, Y., *Self-assembling process of flash nanoprecipitation in a multi-inlet vortex mixer to produce drug-loaded polymeric nanoparticles.* Journal of Nanoparticle Research, **2011**. 13(9): p. 4109-4120.

51.   Liu, Y., Cheng, C., Prud'homme, R.K., and Fox, R.O., *Mixing in a multi-inlet vortex mixer (MIVM) for flash nano-precipitation.* Chemical Engineering Science, **2008**. 63(11): p. 2829-2842.

Chapter 6

Ultrasound-Assisted Batch and Continuous Flow Process for Antisolvent

Precipitation of Metformin Hydrochloride Microparticles

6. Ultrasound-Assisted Batch and Continuous Flow Process for Antisolvent Precipitation of Metformin Hydrochloride Microparticles[5]

In this chapter, small sized particles of the antidiabetic drug metformin hydrochloride (MHC) were precipitated via liquid antisolvent technique in a clogging free inverted jet reactor (IJR). This was used as a small passive mixer in which intensified turbulent mixing of the solution and the antisolvent occurred under controlled conditions. Initially, the optimized conditions for antisolvent precipitation (ASP) were investigated by studying the effect of solute concentration, antisolvent to solvent ratio and antisolvent temperature in batch systems. The ability of the ASP process to generate small sized MHC particles using a simple and scalable setup provides a pathway to manufacturing MHC for formulations at a higher scale.

7.1. Introduction

In recent years, synthesis of inorganic or hybrid (organic-inorganic) nano and micro particles had made a mark in particle technology because it shows unique properties than their bulk counterparts [1]. Organic microparticles are becoming popular in colloidal chemistry due to their applications in the electronics, nano-medicine [2], and food industry [3]. Small sized organic particles play an essential role in making the stable formulation of active pharmaceutical ingredients (APIs). Hence, micronization of APIs is required to be established for obtaining homogeneous small sized particles with desired properties. Though, significant efforts have been taken into the direction towards the lab scale synthesis of small-sized organic particles in the

recent year's high throughput synthesis for industrial applications are still in development[4]. Liquid antisolvent precipitation (ASP) is becoming widely used for the production of small sized organic particles of wide varieties. In the ASP, precipitation of solute is accomplished by diminishing the power of the solvent for the solute dissolved in the solution. A non-solvent for solute called as antisolvent is added to the solution [5]. Operating at standard conditions without the involvement of sophisticated instrumentation and other advantages of ASP over other top-down and bottom- up approaches has been discussed in chapter 1.

As the size and shape of organic particles are highly sensitive to synthesis conditions which determine the properties of particles (stability of dispersion, dissolution, compressibility, compaction and the flowability of APIs). To obtain the desired shape and size of APIs particles, it is important to understand elementary steps (viz. nucleation and growth) of particle synthesis with respect to the changes in process parameters. As ASP is a solvent exchange method, mixing of solvents plays a vital role to produce smaller size particles [6]. The solvent exchange is a diffusion limited phenomenon [7], where fast and efficient mixing can result in small size monodisperse particles [8, 9]. Slow and inefficient mixing results in locally non-uniform nucleation and growth rates leading to poly-dispersed particles. Typically, ASP has been carried out in a classical batch reactors. This batch synthesis is limited to low production rate, poor reproducibility and wider particles size distribution owing to poor mixing and dead time. In the classical batch method, processing large volume and controlled the addition of reagent to achieve homogeneous mixing becomes very difficult. Currently, large size continuous stirred tank reactor or homogenizers have been used for high throughput production of organic particles, but their mixing timescales are usually not smaller than the precipitation time scales. Moreover, achieving spatial homogeneity in large reactors is challenging [10].

In the last decade, micro and mini reactors and confined impinging jet reactors evolved for the production of well controlled micro/nanoparticles which is highly reproducible and scalable [11-13]. Micro and mini reactors often encountered clogging issue after precipitation due to deposition of particles on the wall of the reactor while confined impinging jet reactors were limited to flash precipitation scenarios [14]. To resolve the aforementioned issues, alternative method is demonstrated in the present work for high throughput continuous ASP of organic particles using inverted jet reactor (IJR) which provides comparatively higher residence time. Furthermore, ultrasound is used to provide superior micromixing in ASP to diminish induction times for nucleation and provide a constant supersaturation ratio [15, 16]. In the current work, a systematic study is performed for optimization of the batch precipitation conditions and the batch process is translated to the continuous inverted jet reactor. As a case study, we chose metformin hydrochloride (MHC) API for this purpose. MHC is a biguanide group drug molecule which is an antidiabetic/hypoglycemic agent that acts predominantly by inhibiting hepatic glucose release [17, 18]. Although MHC is a water-soluble API, the objective was to produce small size MHC particles which in future could be homogeneously dispersed, easily encapsulated or formulated which could be used for controlled drug delivery in an aqueous environment.

6.2. Experimental Section

6.2.1. Chemicals and Materials

Metformin Hydrochloride (MHC) powder supplied by *Abhilash Chemicals & Pharmaceuticals Pvt. Ltd* and used as received for the experiments. Organic solvents such as *n*-butyl alcohol (99.5% pure from *Merck Chemicals Ltd,* India) and *n*-propyl alcohol (99.0% pure from *Merck Chemicals Ltd,* India) were used as anti-solvent. Milli-Q water was used for making the aqueous solution of metformin hydrochloride (MHC). Histidine was purchased from *HiMedia Laboratories Pvt. Ltd.* India These chemicals were used without any further purification.

6.2.2 Batch ASP of MHC

Batch experiments were performed in 30 ml glass vials. Aqueous solutions of MHC at different concentrations were prepared as mentioned in Table 1. The antisolvent mixture was prepared by mixing *n*-propyl alcohol and *n*-butyl alcohol in 50% v/v proportion and kept at the desired temperature using a temperature bath (*Julabo, Germany*). A glass vial containing 15 ml of antisolvent was partially submerged into an ultrasound bath (*Equitron, India*) operating at 53 KHz, 100% power at room temperature. 1 ml of aqueous MHC solution was immediately injected into antisolvent with continuous sonication. After a minute, a drop of the precipitate was placed on a glass slide for determination of particle size. The 1 ml solution of precipitate was dispersed in 4 ml of *n*-butyl alcohol, and a drop is casted on a glass slide to capture an image. The precipitate was separated by vacuum filtration using Whatman paper 1 and dried at room temperature.

Table 6.1. MHC concentration in water

Sr. No.	Solute concentration (%)	Amount of MHC (g/10 ml)
1	100	4.120
2	95	3.914
3	90	3.708
4	85	3.502
5	80	3.296

6.2.3 Continuous flow ASP of MHC in the inverted jet reactor (IJR)

The inverted jet reactor (IJR) was immersed in an ultrasound bath as shown in the schematic representation of the experimental setup in Fig. 6.1. The bell-shaped device having three inlets of 1 mm I.D. was used for continuous precipitation. Two jet inlets were directed opposite to each other, and the third inlet was kept perpendicular to the two opposing inlets from the bottom of the reactor. Two peristaltic pumps were used to flow the antisolvent (*n*-propyl alcohol: *n*-butyl alcohol, 50% v/v) through two side inlets of IJR using insulated silicon tubing at a flow rate of 30 ml/min. A syringe pump (Longer Pumps, China) was used to flow the metformin hydrochloride solution from the central inlet of the reactor. These two streams of antisolvent along with the third stream of MHC solution underwent rapid mixing (at a flow rate of 4 ml/min) under sonication. A filtration assembly was connected to the IJR outlet which consisted of a Whatman Grade 1 filter paper, Büchner funnel and a vacuum pump (Buchi, Switzerland). Filtered particles were collected and analyzed subsequently.
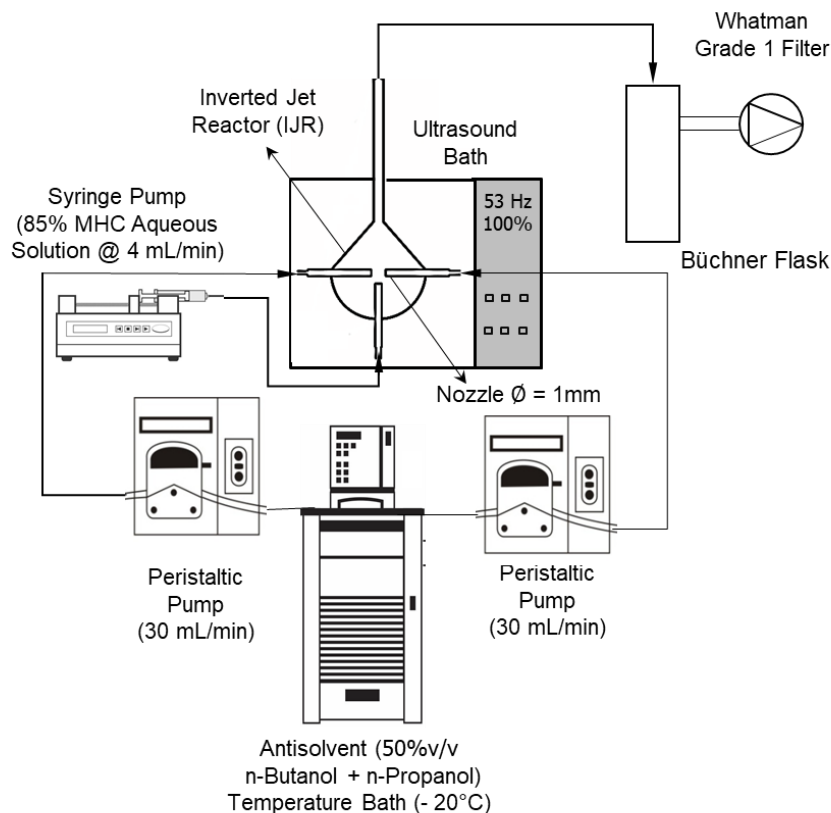
Fig. 6.1. Schematic of the experimental setup for continuous flow synthesis of MHC particles

6.2.4 Particle Size Measurement

Length of the precipitated particles was considered as size and was analysed for the particle size using an optical microscope (Zeiss Primo Star). Particle size distribution was generated by randomly selecting 300 particles in a micrograph and size of the particles was measured using ImageJ 1.8 software. Average particle size, PSD and standard deviation in particle sizes were estimated using Microsoft Excel and Matlab® software.

6.3. Results and Discussion

The approach for finding the ways to precipitate MHC particles started with a selection of a favourable solvent and antisolvent pair. The key requirements to obtain fine API particles by

ASP are i) antisolvent should be miscible with solvent and ii) API should have low solubility in antisolvent. In this work, water was used as the solvent because of the high solubility of MHC in water. *n*-propyl alcohol and *n*-butyl alcohol were both used in pure form as antisolvent. Due to high solubility of MHC in methyl and ethyl alcohol, they were not used as antisolvents. It was observed that *n*-propyl alcohol took longer time (6.5 min) to start precipitation and produced particle of higher size (48 μm) while *n*-butyl alcohol took comparatively smaller time for precipitation to start (20 s) and produced smaller particles (30 μm). In addition to this, *n*-propyl alcohol is miscible with water while *n*-butyl alcohol is partially soluble. Due to the limited solubility of *n*-butyl alcohol in water, it formed a two-phase system resulting in lower yields of the precipitate. To address this issue, we used a mixture of *n*-propyl alcohol: *n*-butyl alcohol (50% v/v) as antisolvent which was completely miscible with water. A white coloured precipitate was observed in a short time when an aqueous solution of MHC injected into *n*-propyl alcohol and *n*-butyl alcohol mixture. Here, we would like to summarize that mixture of *n*-propyl alcohol: *n*-butyl alcohol (50% v/v) act as efficient antisolvent due to its miscible nature with water and low solubility of MHC..

6.3.1 Effect of MHC concentration

The driving force for precipitation is the supersaturation created by mixing the API solution and the antisolvent [8]. Variation in size and shape of the particles depends upon nucleation and growth which can be tuned by the degree of supersaturation in the system. The degree of supersaturation relies on the concentration of solute and the amount of antisolvent. Here, we studied the effect of the concentration of solute (MHC) on the particles size of MHC for a fixed antisolvent ratio. MHC solutions of varied solute concentration from 100% to 80 % of the

saturated concentration was prepared and injected into the 15 ml antisolvent under sonication. After the solvent exchange, precipitate yielded MHC particles of elongated and cubic morphology which are depicted in Fig. 6.2. Optical micrographs show a large number of bigger sized rod-shaped particles were observed at 95% solute concentration compared to low concentration systems (see Fig 6.2d). MHC particles precipitated at 85% solute concentration was found to be of small size particles of cubes, rods and needle-shape (see Fig. 6.2b).
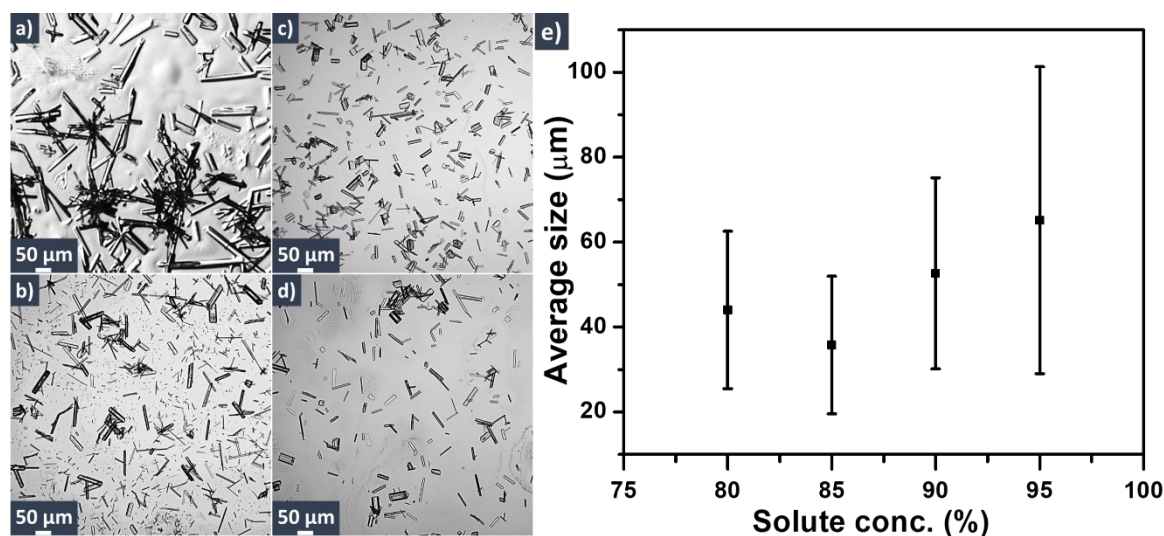
Fig. 6.2. Optical micrographs of MHC particles prepared at different % solute concentration (Solution Temperature 25°C, Ultrasound Bath); (a) 95%, (b) 90%, and (c) 85%, (d) 80%, (e) Effect of solution saturation on the MHC particle size

It was expected that increase in the solute concentration of MHC would yield smaller particles due to reaching a higher degree of supersaturation. In contrary to this, the particle size of MHC was found to be larger for high MHC concentration (95%, 65 μm) compared to the low MHC concentration (80%, 44 μm) (see the Fig. 6.2e). At a higher concentration, though a larger number of nuclei were formed after mixing of the solution and the antisolvent, it also leaded to

the enhanced growth of the nuclei due to higher availability of monomers in the solution. By lowering the solute concentration (85%), nucleation of particles was dominated over growth due to less availability of monomers which resulted into a smaller size of MHC particles (36 μm). For further reduction of concentration (80%) decreased supersaturation and nucleation rate that resulted into a smaller number of nuclei. Despite the reduction in concentration, a sufficient number of monomers were present in solution ramified growth and that resulted in an increase in the size of MHC particles. This kind of sensitivity analysis is known in batch mode crystallization where limited number of seeds when added to even a less saturated solution gives large size of particles over longer time. The aforementioned result can be summarized as 85% concentration of MHC is the optimum concentration to obtain small size particles where nucleation event is predominated over growth.

6.3.2 Effect of antisolvent to solvent (AS/S) ratio

Effect of antisolvent to solvent (AS/S) ratio on particles size was studied for a range of temperatures, and it was observed that AS/S ratio played a vital role in deciding the size of the particle. Fig. 6.3 indicates that variation in AS/S ratio causes significant variation in the size of particles. As the AS/S ratio increased from 5 to 15, particles of MHC became smaller in size (see Fig. 6.3a). This was due to an increase in the degree of supersaturation which produced a large number of smaller nuclei at increased AS/S ratio up to 15. At the AS/S ratio of 15, the maximum amount of MHC formed the nuclei, and a small amount of monomer in the solution caused further growth of particles which resulted in smaller sized MHC particles. The high degree of supersaturation also resulted into narrow particle size distribution (PSD) at AS/S ratio 15 (see Fig. 6.3b). On the other hand, a further increase in AS/S ratio from 15 to 25 reflected into an

increase in the particle size and decrease in total number of particles. This can be explained by the solubility of MHC in the antisolvent mixture. MHC has way higher solubility in *n*-propyl alcohol (2.7 mg/ml) in comparison to *n*-butyl alcohol (0.3 mg/ml). As a result, with increasing AS/S ratio the amount of *n*-propyl alcohol in the solution–antisolvent mixture was increased which in turn reduced the efficacy of the antisolvent mixture. Therefore, AS/S ratio 15 was chosen to be optimum value for producing smaller sized MHC particles.

Optical microscopy images display the morphology of MHC particles (see the Fig. 6.4) prepared using different AS/S exhibits anisotropic structure such as needle, rods and cubes. In most of the cases, the MHC particles grew along the length which can be attributed to the monoclinic crystal structure of MHC, which led to needle and rod shape growth. At AS/S ratio = 5, the shape of particles was decided by the growth of the specific planes and hence the particles grew into needle shape (see Fig. 6.4). When AS/S ratio was increased from, the transition of particle shape can be observed from needles to the rod and eventually to cubes (see Fig. 6.4).
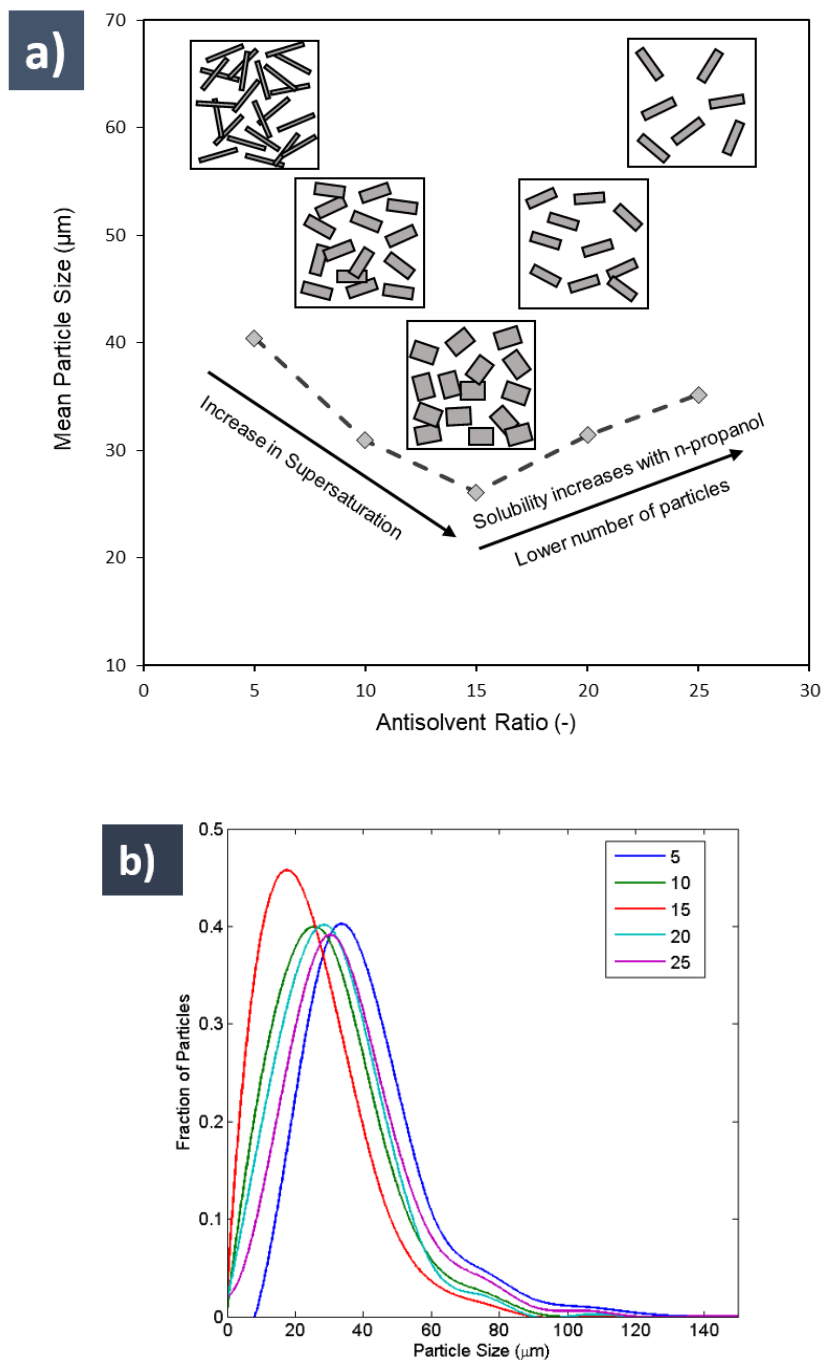
Fig. 6.3. (a) Variation in average particle size with the antisolvent ratio, (b) Variation of PSD with AS/S ratio (at 25 °C)
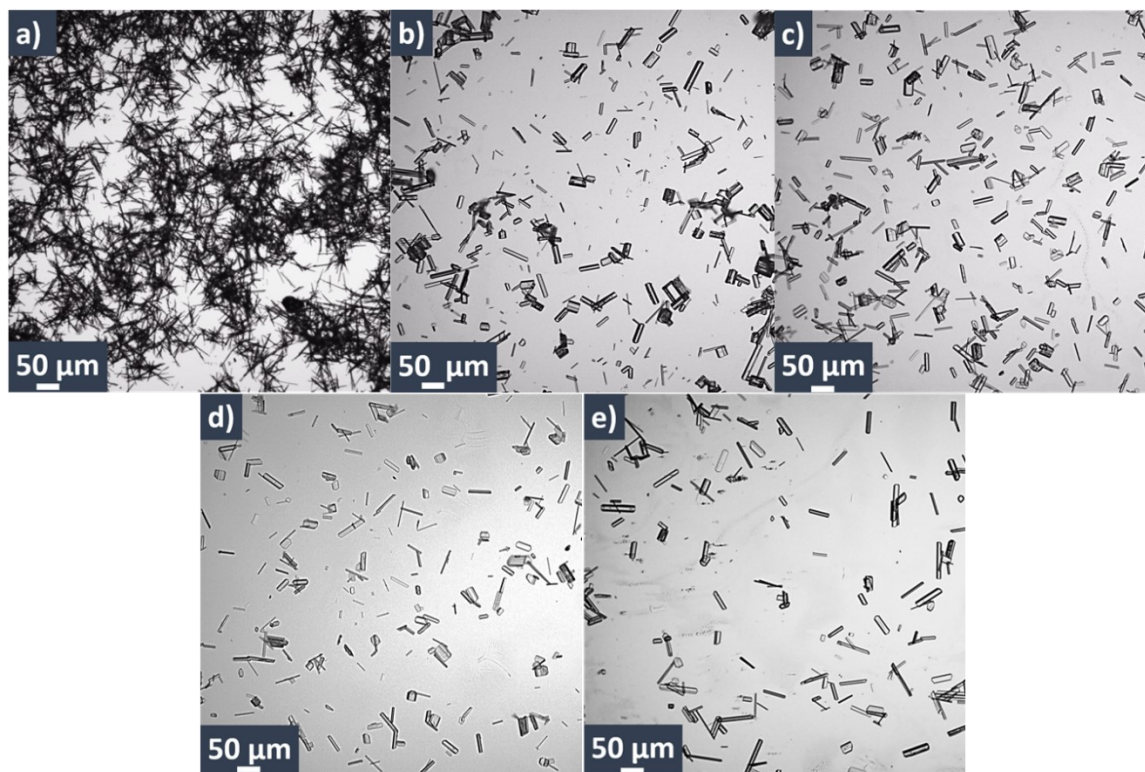
Fig. 6.4. Optical micrographs of MHC particles prepared at different AS/S ratios (Solution Temperature 25°C, Ultrasound Bath); (a) AS/S = 5, (b) AS/S = 10, (c) AS/S = 15, (d) AS/S = 20, and (e) AS/S = 25.

6.3.3 Effect of antisolvent temperature

In liquid antisolvent precipitation, the temperature reduction arising from the difference of temperature between antisolvent and solution works as a driving force in attaining supersaturation along with the antisolvent effect. Here, we systematically investigated the effect of temperature on particle size. A significant reduction in precipitation time was observed with the decrease in AS temperature. It was noted that 24 s, 32 s, 35 s, and 51 s were the precipitation time required at -20°C, -15°C, -10°C and -5°C respectively. As a consequence of lowering

temperature, precipitation occurred relatively faster compared to a higher temperature which could produce small size particles. Optical microscope images depict the change in particle size and morphology as the temperature of antisolvent decreases from -5ºC to -20ºC (see Fig. 6.5). Majority of the particles obtained at -5ºC are found to be rod shapes (see Fig. 6.5a). However, particle obtained at -20ºC found to be a mixture of smaller sized cubes as well as rod shape (see Fig. 6.5d). Due to a technical limitation of thermostat we were not able to experiment below -20 ºC temperature. Size and aspect ratio of MHC particles was determined using images analysis.
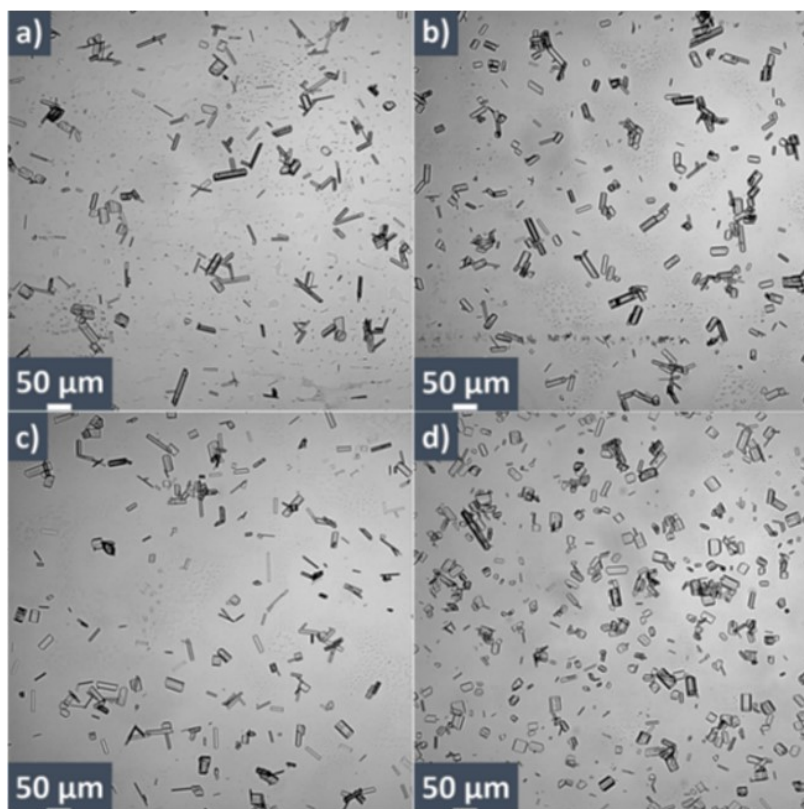

Fig. 6.5. Optical micrographs of MHC particles prepared at different temperatures (Solution Temperature 25°C, Ultrasound Bath); (a) -5ºC, (b) -10ºC, (c) -15 ºC, and (d) -20ºC.
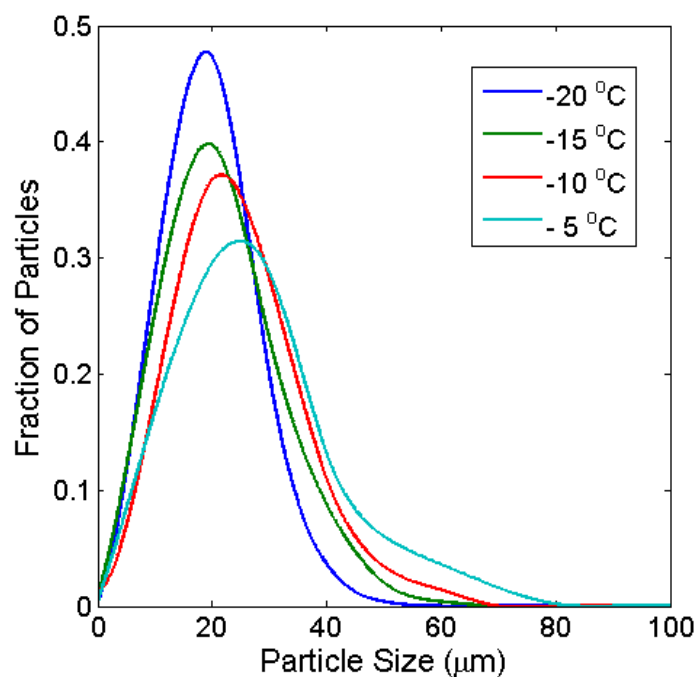
Fig. 6.6. Effect of antisolvent temperature on particle size distribution
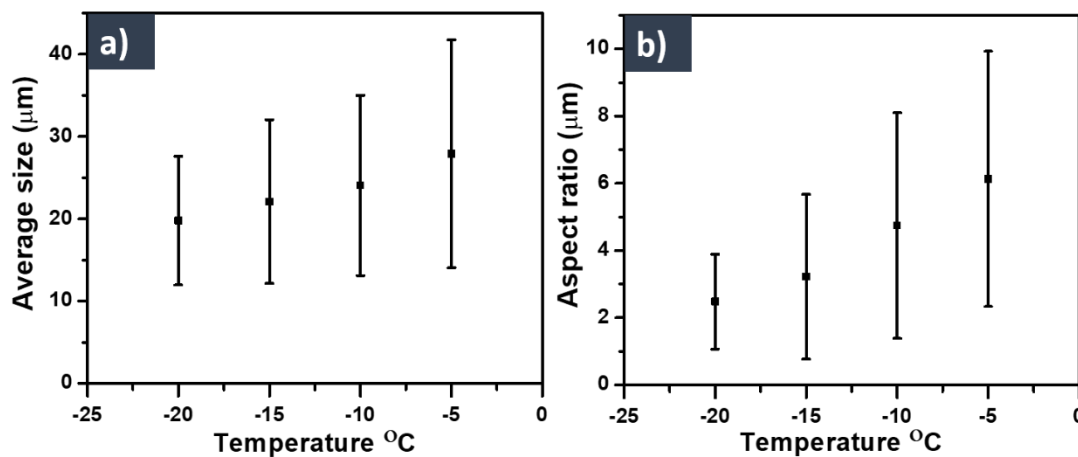

Fig. 6.7. Effect of antisolvent temperature on (a) particle size, and (b) aspect ratio

It can be observed that the reduction in the antisolvent temperature results in more uniform and smaller size MHC particles (-20 °C, 19.8 µm, see Fig. 6.7a). The aspect ratio of the

precipitated particles was also observed to reduce with decreasing antisolvent temperature (see Fig 6.7b). In Fig. 6.6, the particle size distribution curve shows the effect of temperature on the degree of supersaturation that results in narrow particles size distribution (PSD). The rise in the peak height and movement of peaks to the smaller particle size were observed with decreasing temperature (see Fig. 6.6). The main reason behind this was the lowering of the antisolvent temperature that resulted in higher degree supersaturation ratios leading to the formation of a larger number of smaller size nuclei in a short span. On the other hand, precipitation of MHC is diffusion limited phenomenon. Due to a decrease in the temperature, the viscosity of antisolvent increased (~56 % increase from 0°C to -20 °C) [19, 20], which results in the slow diffusion of smaller nuclei/particle [21]. Hence, further particle growth was not possible at low temperature by coalescence and aggregation because of the slow diffusion. Antisolvent temperature played an important role to achieve a high degree of supersaturation which limited the growth of the particles due to the increase in viscosity. Finally, -20°C is selected as the optimum antisolvent temperature producing smaller size MHC particles having 19.8 µm average size and 2.48 aspect ratio.

6.3.4. Continuous precipitation

Initial continuous flow experiments were performed in a co-flow capillary reactor as the optimised antisolvent to solution ratio for the batch experiments was very high. Parallel flow was observed for a different range of flow rates, which was not able to provide adequate mixing performance for precipitation. Submerging the co-capillary system into an ultrasound bath resulted in better mixing leading to precipitation but the particle size observed was quite high (~ 55 µm) compared to the optimum batch conditions (see Fig. 6.7e). This was due to the severe

growth of the particles at the stable interface between the two phases in parallel flow. In addition to the above observations, clogging of the capillary channel was observed which is attributed to the solid deposition on the capillary wall. It was inferred that the co-capillary approach was not be suitable for continuous operation.

Confined liquid impinging jet reactors were reported to provide excellent mixing performance and could run continuously at higher capacity [22] . Chiou et al. [14] studied the feasability and limitation of such a single-pass process and concluded it is suitable for very fast precipitation, where precipitation should occur during impinging For the slowly diffusing antisolvents followed by slow growth of particles one pass conversion or yield from such systems will be very less. In our work, the precipitation initiation times in batch was found to be in the range of 30 s to 60 s which was quite higher than the typical residence times of confined impinging jet reactors. The antisolvent to solvent flow ratio was also higher for liquid sheet formation which is responsible for the enhanced mixing performance in a confined impinging jet reactor. To overcome these difficulties, an inverted jet reactor having three inlets was developed to use the improved mixing conditions attained from the kinetic energy of impingement of the jets but in a submerged state which provided a higher residence time for the precipitation (see Fig. 6.1).

Experimental parameters optimised for ASP in batch at -20˚C were considered for continuous flow antisolvent precipitation in the IJR. Optical microscope image of MHC particles displays that MHC particles are rod and cube shape (see Fig. 6.8a and b). The particles size was determined from the optical images was 18.6 μm which was smaller than particle obtained in batch (19.8 μm) and co-capillary (55 μm). Reduction in size using IJR is attributed to efficient

mixing. Although, mixing of antisolvent and solvent played an important role to achieve faster supersaturation which ensured small sized MHC particles, the addition of additive would inhibit the growth of MHC particles during ASP. To arrest the growth of particle, 1.0 mass % histidine was added while preparing MHC solution. A further reduction in the particle size was observed with the addition of histidine (see Fig. 6.8c) through the particle morphology remained the same. The particle sizes obtained in various experimental conditions are compared in Fig. 6.8c. An overall yield of 85% MHC particles was achieved at optimised continuous flow conditions in IJR.
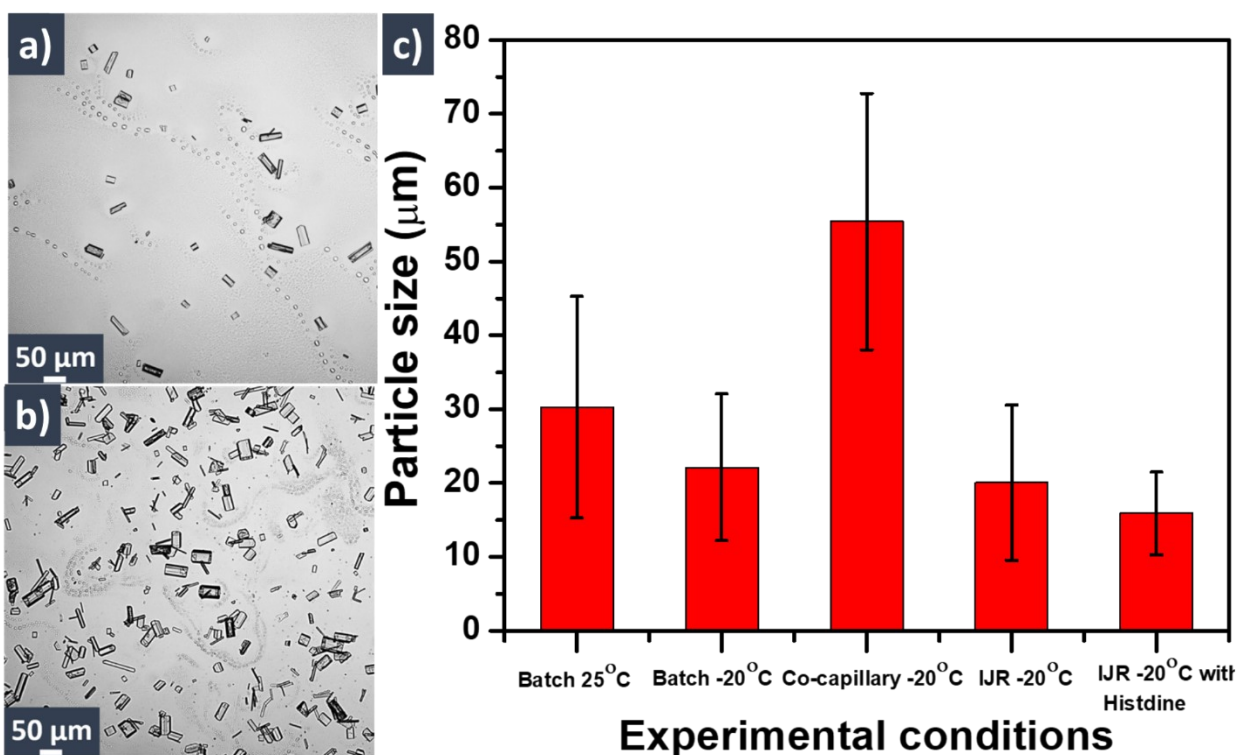
Fig. 6.8. Optical microscope images of MHC particles prepared in flow a) without additive in the inverted jet reactor (Average particle size, 18.6 μm), (b) with additive in inverted jet reactor (Average particle size, 15.8 μm), and (c) Particle size of MHC by ASP from different experimental conditions

Above result could be summarised as ASP process in continuous IJR yield small size MHC particles due to efficient mixing and addition of additive hinder the growth of MHC particle leading to small size particles. Although, particles prepared by changing experimental conditions show different morphology but the PXRD patterns were found to be identical which was ascribed to the monoclinic crystal structure of MHC (see Fig. 6.9). MHC particles prepared using batch, capillary reactor and IJR show similar PXRD patterns and peaks from each pattern exactly match with each other. Hence, PXRD analysis clearly reveals that no other crystal structure or polymorphs were present in MHC particles prepared using different reactors or by changing precipitation condition. Using an inverted IJR was essential for the cases such as MHC as the precipitation time is relatively longer than other salts [22] and longer residence time is needed.
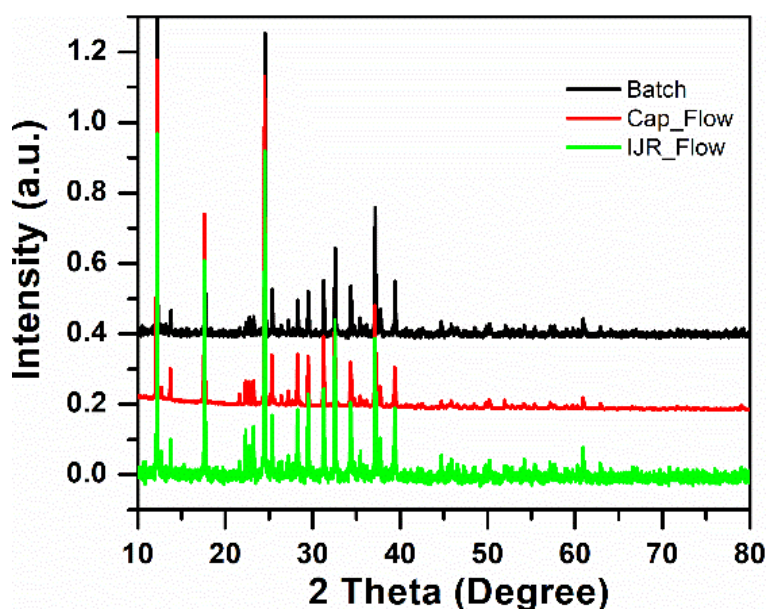
Fig.6.9. PXRD patterns of MHC particles produced in batch, capillary reactor and IJR

6.4. Conclusions

An antisolvent precipitation based continuous flow process was demonstrated for production of small sized MHC particles with higher production rate compared to classical batch process. Enhanced mixing from the integration of ultrasound and IJR helped to yield small sized particles. In the current work, we systematically investigated the effect of process parameters viz. AS/S ratio, the concentration of solute, antisolvent temperature and mixing on ASP to obtain the optimized conditions for smaller sized MHC particles. At -20 °C, AS/S ratio of 15 and 85% solute concentration was found to be the best optimized condition producing small sized (19.8 μm) MHC particles. Adoption of batch ASP process into continuous flow process successfully achieved using an inverted jet reactor. Continuous flow process was adopted to produce small-sized MHC particles in large quantity and reproducible manner. L-histidine was used as a biocompatible additive to suppress growth and agglomeration of the MHC particles. 15 μm sized MHC particles were obtained in a continuous and clogging free manner via antisolvent precipitation in the IJR.

6.5 References

1. Ghosh Chaudhuri, R. and Paria, S., *Core/shell nanoparticles: classes, properties, synthesis mechanisms, characterization, and applications.* Chem. Rev., **2011**. 112: p. 2373-2433.

2. Silva, A.S., Tavares, M.T., and Aguiar-Ricardo, A., *Sustainable strategies for nano-in-micro particle engineering for pulmonary delivery.* J. Nanopart. Res., **2014**. 16: p. 2602.

3.　　Sanguansri, P. and Augustin, M.A., *Nanoscale materials development–a food industry perspective.* Trends Food Sci. Technol., **2006**. 17: p. 547-556.

4.　　Dendukuri, D. and Doyle, P.S.J.A.M., *The synthesis and assembly of polymeric microparticles using microfluidics.* **2009**. 21(41): p. 4071-4086.

5.　　Acton, Q.A., *Advances in Nanotechnology Research and Application: 2012 Edition.* Scholarly Editions, **2012**.

6.　　Matteucci, M.E., Hotze, M.A., Johnston, K.P., and Williams, R.O., *Drug nanoparticles by antisolvent precipitation: mixing energy versus surfactant stabilization.* Langmuir, **2006**. 22: p. 8951-8959.

7.　　Heyer, H., *Kinetics of Precipitation. Von AE Nielsen. International Series of Monographs on Analytical Chemistry. Haupt-Herausg. R. Belcher und L. Gordon. Vol. 18. Pergamon Press, Oxford-London-Edinburgh-New York-Paris-Frankfurt 1964. 1. Aufl., X, 153 S., zahlr. Abb., mehrere Tab., geb.£ 2.0. 0.* Angew. Chem. Int. Ed., **1965**. 77: p. 745-745.

8.　　Zhao, H., Wang, J.-X., Wang, Q.-A., Chen, J.-F., and Yun, J., *Controlled liquid antisolvent precipitation of hydrophobic pharmaceutical nanoparticles in a microchannel reactor.* Ind. Eng. Chem. Res., **2007**. 46: p. 8229-8235.

9.　　Horn, D. and Rieger, J., *Organic nanoparticles in the aqueous phase—theory, experiment, and use.* Angew. Chem. Int. Ed., **2001**. 40: p. 4330-4361.

10.　Hartman, R.L., McMullen, J.P., and Jensen, K.F., *Deciding whether to go with the flow: evaluating the merits of flow reactors for synthesis.* Angew. Chem. Int. Ed., **2011**. 50: p. 7502-7519.

11.   Karnik, R., Gu, F., Basto, P., Cannizzaro, C., Dean, L., Kyei-Manu, W., Langer, R., and Farokhzad, O.C., *Microfluidic platform for controlled synthesis of polymeric nanoparticles.* Nano letters, **2008**. 8(9): p. 2906-2912.

12.   Lim, J.-M., Swami, A., Gilson, L.M., Chopra, S., Choi, S., Wu, J., Langer, R., Karnik, R., and Farokhzad, O.C., *Ultra-high throughput synthesis of nanoparticles with homogeneous size distribution using a coaxial turbulent jet mixer.* ACS nano, **2014**. 8(6): p. 6056-6065.

13.   Kumar, D.R., Prasad, B., and Kulkarni, A., *Impinging jet micromixer for flow synthesis of nanocrystalline MgO: role of mixing/impingement zone.* Ind. Eng. Chem. Res., **2013**. 52(49): p. 17376-17382.

14.   Chiou, H., Chan, H.-K., Prud'homme, R.K., and Raper, J.A., *Evaluation on the use of confined liquid impinging jets for the synthesis of nanodrug particles.* Drug Dev. Ind. Pharm., **2008**. 34(1): p. 59-64.

15.   Thorat, A.A. and Dalvi, S.V., *Liquid antisolvent precipitation and stabilization of nanoparticles of poorly water soluble drugs in aqueous suspensions: recent developments and future perspective.* Chem. Eng. J., **2012**. 181: p. 1-34.

16.   Jordens, J., Bamps, B., Gielen, B., Braeken, L., and Van Gerven, T., *The effects of ultrasound on micromixing.* Ultrasonics sonochemistry, **2016**. 32: p. 68-78.

17.   Setter, S.M., Iltz, J.L., Thams, J., and Campbell, R.K., *Metformin hydrochloride in the treatment of type 2 diabetes mellitus: a clinical review with a focus on dual therapy.* Clin. Ther., **2003**. 25: p. 2991-3026.

18.   Klepser, T.B. and Kelly, M.W., *Metformin hydrochloride: an antihyperglycemic agent.* Am. J. Health Syst. Pharm., **1997**. 54(8): p. 893-903.

19.   Pang, F.-M., Seng, C.-E., Teng, T.-T., and Ibrahim, M., *Densities and viscosities of aqueous solutions of 1-propanol and 2-propanol at temperatures from 293.15 K to 333.15 K.* Journal of Molecular Liquids, **2007**. 136(1-2): p. 71-78.

20.   Bravo-Sánchez, M.G., Iglesias-Silva, G.A., Estrada-Baltazar, A., and Hall, K.R., *Densities and Viscosities of Binary Mixtures of n-Butanol with 2-Butanol, Isobutanol, and tert-Butanol from (303.15 to 343.15) K.* Journal of Chemical & Engineering Data, **2010**. 55(6): p. 2310-2315.

21.   Pieper, M., Aman, S., Hintz, W., and Tomas, J., *Optimization of a continuous precipitation process to produce nanoscale BaSO4.* Chem. Eng. Technol., **2011**. 34(9): p. 1567-1574.

22.   Pal, S., Madane, K., and Kulkarni, A.A., *Antisolvent based Precipitation of Ammonium Perchlorate: Batch, Capillary flow reactor and Impinging Jet Reactor.* Chemical Engineering Journal, **2019**.

Chapter 7

Summary of Conclusions and Recommendations for Future Work

7. Summary of Conclusions and Recommendations for Future Work

The ability to handle solids involving processes in a continuous microfluidic framework offers a huge opportunity, especially in the field of flow chemistry and material science. Continuous methods to perform chemical reaction involving solids, crystallization is considered relevant on an industrial scale as well. The current thesis explores the flow of solid particles in multiphase flow systems to develop methodologies of solid handling with a view on improving the feasibility of micro and millifluidic clogging free particle handling platforms. Impinging jet reactors are also explored as a potential continuous particle handling platforms.

7.1. Conclusions

Chapter 1 reviewed key efforts that were undertaken to handle solid particles in a microfluidic framework. They could be categorized into chemical, active, passive and alternative methodologies. Despite some recent efforts such as pulsed ultrasound and crystal engineering, the approach has been mostly curated to solve a specific chemistry problem. The reported methods are still not being practised on industrially available automated microreactor platforms, because of inadequate understanding of crucial factor such as clogging dynamics influencing their performance.

Chapter 2 covered the understanding of clogging in a multiphase system with a specific focus on clogging time. Effect of relevant parameters such as flow regimes, channel diameters, flow rates was explored. In the segmented flow, the particles were found to travel to the rear stagnation zone, forming shells or hemispherical caps. Subsequently, the detached shells undergo associative growth forming clusters and settled on the channel wall surface. This was observed to

be mainly responsible for clogging in segmented flow regime. But formation of stable shells throughout the capillary length was found to be favourable for enhanced particle transport delaying clogging. The relative rates of interfacial mass transfer, precipitation and the flow govern the clogging time, which shows a near power law behaviour with total flowrates. The mass transfer model provides insights such that crystal formation, growth and agglomeration takes significantly longer time in comparison to interfacial mass transfer.

Strategies to handle solid particles without using external forces was developed in Chapter 3. The particles are controlled inside the channels by means of manipulating the flow in a relatively simple and easy to implement way without modifying the reactor configuration. These are useful for exploring precipitation as well as chemical reactions involving solids in continuous flow. Inert liquid and gas insertion was identified to act the most efficient strategy to suppress clogging in capillaries, thus making the system easy to handle for longer operating hours. While only a proof-of-principle at this stage, the methodologies can be easily optimized from system to system and operated by a single end-user, offering a potential solution to handle solids in flow. Such a system could also help continuous manufacturing to a great extent, and provide a strategy to replace batch manufacturing of solids.

In chapter 4, we develop a framework for the batch to continuous flow optimization of an antisolvent precipitation process for safe and rapid preparation of ammonium perchlorate (AP) particles. From the selection of antisolvents, mixing conditions and temperatures of solvent and antisolvent were optimized keeping a balance between desired particle size, yield and clogging issues. The segmented flow regime in the continuous approach allows precipitation to occur only at the interface, providing less tendency to the growth of the particles.

The continuous flow process developed in the previous chapter was scaled up to 400 times in chapter 5 by means of confined impinging jet reactor (CIJR). CFD simulations and high-speed imaging experiments were performed to investigate mixing performance and impinging dynamics in the turbulent regime. A modified CIJR reactor was proposed, which is superior in terms of mixing and utilization of the fluid kinetic energy available at the impinging area. Smaller particle sizes are obtained with higher jet Reynolds number of the CIJR.

In chapter 6, a novel inverted jet reactor concept was presented for continuous precipitation systems where the precipitation time is in the order of minutes, unlike flash precipitation studied in the previous chapter. This reactor concept is able to utilize the kinetic energy of the liquid impinging jets, provide residence time in order of minutes and operate in a continuous manner. Parametric optimization was first performed in batch, and the optimized process was adopted in continuous flow IJR in a scaled up fashion. L-histidine was used as a biocompatible additive to suppress growth and agglomeration of the MHC particles.

This thesis provides a number of new insights on the ways of handling particles in continuous flow processes. Batch to continuous methodologies for antisolvent precipitation systems is also manifested. The overall approach, the developed particle handling techniques in microchannels and impinging jet reactors in this dissertation will provide a foundation for further research and utilization of solid involving processes in continuous flow to a greater extent.

7.2. Recommendations for Future Work

The following recommendations are proposed for future work. We hope that the published results will serve as useful precedents in motivating future efforts in these directions.

1) Clogging of microchannels is a very stochastic phenomena depends on several interrelated processes such as hydrodynamics, mass transfer, process kinetics, nucleation and growth models. Though each of these has been explored theoretically and several models are available in the literature, integration of these models are necessary to estimate clogging time in microchannels.

2) Most of the work in the thesis was performed, keeping the flow ratio as unity resulting in mostly segmented flow regimes. For the case of flow ratios away from unity, other flow regimes apart from the segmented flow are dominant. Clogging dynamics in such cases needs to be further investigated.

3) Passive methodologies for particle manipulation demands further enhancement, which is resistant to flow regimes irregularities arising from reactive systems. Forcing targeted flow regimes by means of passive forces such as electrohydrodynamic forces and usage of superhydrophobicity could be explored in this regard,

4) As active methodologies are comparatively robust in handling solids and not susceptible to irregular flow regime, systems with low energy footprint are required to be developed in which the intrinsic kinetics are not being altered.

5) Multiphase chemistries are quite abundant such as hydrogenation which involves immiscible liquids, gas and solid catalysts in high pressure. While the literature on organic synthesis in gas-liquid and liquid-liquid segmented flow is widespread, there are no reports on the feasibility of performing such complex chemistries in segmented flow.

In such systems, the local concentration and temperature gradients will result in varying physical properties affecting the hydrodynamics of the flow. It is necessary to quantify these effects and explore such systems since it segmented flow solves the effect of wall deposition/fouling and also provides enhanced mixing.

6) For the development of end to end systems curated for industrial applications, efficient post-processing of microparticles needs further improvement such as fast drying and coating process to suppress agglomeration.

7) Though impinging jet can be used for scale-up for flash precipitation and inverted jet systems are demonstrated for continuous precipitation where the residence time is in the range of minutes, continuous scale-up methodologies for crystallization systems requiring very high residence time such as co-crystallization is necessary.

8) Many compounds in the field of chemistry, material science and biology are attractive candidates for future scale-up technologies. However, considering the demand of the industry for particulate systems, whether its high-cost and low-quantity or low-cost and high-quantity, further optimization must be carried out in order to meet the required demands. Recently, process intensification and integration of unit operations for an end to end continuous manufacturing have resulted in the state of art platforms in the size of shipping container sized units. Further research and integration of active, passive as well as alternative methods of particle handling can fuel the development of such platforms for solids which can be considered as a more practical platform for industries to adopt.

Appendix –I

Important instruments used

Optical microscopy: Capillaries are places under stereo microscope (Zeiss Discovery V20) for flow visualization. A drop of the solution containing precipitate place on glass slide and examined under compound microscope (Zeiss Primo Star).

Scanning Electron Microscopy: SEM images of samples were recorded using scanning electron microscope (E-SEM Quanta 200-3D) operated at 20kV

High speed camera: High speed camera (Photron Fastcam Mini AX200) was used flow visualization in microcapillaries and impinging jet reactors

Appendix – II

General list of abbreviations

ASP	Antisolvent Precipitation
XRD	X-Ray Diffraction
SEM	Scanning Electron Microscopy
CIJR	Confined Impinging Jet Reactor
IJR	Inverted Jet Reactor
AP	Ammonium Perchlorate
MHC	Metformin Hydrochloride
PSD	Particle Size Distribution

AS	Antisolvent
VOF	Volume of Fluid
Re	Reynolds Number
We	Weber Number
Ca	Capillary Number
Bo	Bond Number
Pe	Peclet Number
θ_{clog}	Clogging time
k_La	Overall mass transfer coefficient
ρ	Density
μ	Viscosity
C	Concentration of species
γ	Interfacial/Surface Tension
τ	Residence time

Appendix – III

List of publications

- **S. Pal**, K. Madane, A.A. Kulkarni, Antisolvent based Precipitation: Batch, Capillary flow reactor and Impinging Jet Reactor, **Chemical Engineering Journal** 369 (2019) 1161-1171

- **S. Pal**, A.A. Kulkarni, Quantitative Comparison of Strategies to Delay Clogging in Straight Capillaries, (2019), **Chemical Engineering Science** 199 (2019) 88-99

- **S. Pal**, A.A. Kulkarni, Interfacial precipitation and clogging in straight capillaries, **Chemical Engineering Science** 153 (2016) 344-353.

- **S. Pal**, A.V. Nikam, A.A. Kulkarni, Antisolvent Based Ultrasound-Assisted Batch and Continuous Flow Precipitation of Metformin Hydrochloride Particles, **Journal of Flow Chemistry**, (2020)

- **S. Pal**, K. Madane, M. Mane, A.A. Kulkarni, Impingement Dynamics of jets in Confined Impinging Jet Reactor, **Industrial Engineering Chemistry Research**, (2020)

- C. Sampat, **S. Pal,** A.A. Kulkarni, Effect of wettability on hydrodynamics and mass transfer in small capillaries, **Chemical Engineering Research and Design**, (2020) (First two authors have equal contribution)

- C.A. Shukla, **S. Pal**, A.A. Kulkarni, Hydrodynamics and Selectivity Engineering of Multipoint Dosing Reactor, **Industrial Engineering Chemistry Research** 58, 51 (2019) 22866-22874 (First two authors have equal contribution)

- **S. Pal,** A.A. Kulkarni, Universal Behaviour of Settling and spreading of particle clusters in quiescent fluids in confined vessels, Preprint in **Physics arXiv,** arXiv:2003.03111 [physics.flu-dyn], Under revision in **Experiments in Fluids**

Sayan Pal

Senior Research Fellow

C/O Dr. Amol Kulkarni, Microfluidics & Flow
Chemistry Laboratory, Chemical Engineering &
Process Intensification Department, CSIR-NCL, Pune -
411008

Mobile: +91 7768980933/ +447832621873

E-mail: pal.sayan3@gmail.com

EDUCATION

Ph.D. – Chemical Engineering Sciences 2013-2019

Chemical Engineering & Process Development Division,
CSIR-National Chemical Laboratory, Pune, Maharashtra,
India

Research Topic: Understanding flow of solids in continuous flow
reactors

Supervisor: Dr. Amol Kulkarni, CSIR-NCL

Bachelor of Technology (B.Tech.) – Chemical Engineering
National Institute of Technology, Durgapur, West Bengal, India, 2008-2012

AWARDS & HONORS

- Received CSIR–GATE Fellowship for Doctoral Research 2014-2019
- Received International Travel Support (ITS) from 2017
  Science and Engineering Research Board (SERB), Govt. of India
  to attend the Flow 17 Conference in Paris, France
- Dr. B.D. Kulkarni Award for publication with highest impact 2020
  factor in 2019 in the Engineering Sciences Division, CSIR-NCL

RESEARCH AREA

- Multiphase Microfluidics
- Clogging Dynamics & Particle Handling in flow
- Antisolvent Precipitation
- Confined Impinging Jet Reactors
- Synthesis of micro and nanoparticles in continuous flow

PUBLICATIONS

- **S. Pal**, K. Madane, A.A. Kulkarni, Antisolvent based Precipitation: Batch, Capillary flow reactor and Impinging Jet Reactor, Chemical Engineering Journal 369 (2019) 1161-1171
- **S. Pal**, A.A. Kulkarni, Quantitative Comparison of Strategies to Delay Clogging in Straight Capillaries, Chemical Engineering Science 199 (2019) 88-99
- **S. Pal**, A.A. Kulkarni, Interfacial precipitation and clogging in straight capillaries, Chemical Engineering Science 153 (2016) 344-353.
- K. Anupam, J. Sikder, **S. Pal**, G. Halder, Optimizing the cross-flow nanofiltration process for chromium (VI) removal from simulated wastewater through response surface methodology, Environmental Progress & Sustainable Energy 34 (2015) 1332-1340.
- C.A. Shukla, **S. Pal**, A.A. Kulkarni, Hydrodynamics and Selectivity Engineering of a Multipoint Dosing Reactor, Industrial & Engineering Chemistry Research 58, 51 (2019) 22866-22874.
- **S. Pal**, A.V. Nikam, A.A. Kulkarni, Antisolvent Based Ultrasound-Assisted Batch and Continuous Flow Precipitation of Metformin Hydrochloride Particles, Journal of Flow Chemistry, (2020)
- **S. Pal**, K. Madane, M.Mane, A.A. Kulkarni, Impingement dynamics of Jets in Confined Impinging jet Reactor, Industrial Engineering Chemistry Research, (2020)
- C. Sampat, **S. Pal,** A.A. Kulkarni, Effect of wettability on hydrodynamics and mass transfer in small capillaries, Chemical Engineering Research & Design, (2020)
- **S. Pal,** A.A. Kulkarni, Universal Behaviour of Settling and spreading of particle clusters in quiescent fluids in confined vessels, Preprint in Physics arXiv, arXiv:2003.03111 [physics.flu-dyn], Under revision in Experiments in Fluids

Conferences

- Presented poster in Flow 17 Conference, held in Pierre and Marie Curie University, Paris, France
- Presented oral talk at the Conference on Process Intensification for Fine and Specialty Chemicals, in CSIR-NCL Pune, India in 2015.
- Presented poster at Indo German Conference held in IIT Guwahati, India in 2016.
- Presented posters on each "National Science day" at CSIR-NCL, Pune, India in 2015, 2016 and 2017

SKILLS & EXPERTISE

- Experimentation   Particle Handling in microreactors
  Optimization of particle size in synthesis of micro and nanoparticles
- Flow Visualization   Optical Microscopy, High Speed Imaging
- Modelling and Data Analysis   Fluent, MATLAB, Origin
- Office and publishing   MS office, Mendeley, Endnote

INDUSTRIAL EXPERIENCE

- Deputy Manager in ACC Limited, Chaibasa Cement Works, Chaibasa, Jharkhand, India, June-October, 2012
- Industrial Training in Naptha Cracker Unit in Haldia Petrochemicals (HPL), Haldia, West Bengal, India, May-June, 2011

PERSONAL DETAILS

- Nationality : Indian
- Language: English, Hindi, Bengali
- Date of Birth: 13th June, 1990
- Marital status: Single

REFERENCES

Dr. Amol Kulkarni, (Advisor) Senior Principal Scientist
Chemical Engineering and Process Development Division, CSIR-NCL, Pune, India
E-mail: aa.kulkarni@ncl.res.in

Dr. Ashish Orpe, Principal Scientist,
Chemical Engineering and Process Intensification Department, CSIR-NCL, Pune.
Email: av.orpe@ncl.res.in

Prof. Rajnish Kumar, Associate Professor,
Chemical Engineering Department, Indian Institute of Technology, Madras.
Email: rajnish@iitm.ac.in

Dr. Rahul Bhambure, Scientist,
Chemical Engineering and Process Intensification Department, CSIR-NCL, Pune.
Email: rs.bhambure@ncl.res.in